METABOLISM IN SUBTROPICAL LOWLAND RIVERS

By

LILY KIRK

A DISSERTATION PRESENTED TO THE GRADUATE SCHOOL
OF THE UNIVERSITY OF FLORIDA IN PARTIAL FULFILLMENT
OF THE REQUIREMENTS FOR THE DEGREE OF
DOCTOR OF PHILOSOPHY

UNIVERSITY OF FLORIDA

2020

To Mommy

ACKNOWLEDGMENTS

First and foremost, I thank my husband Matt for “crewing” on my long PhD journey. It definitely could not have happened without his sacrifice and daily logistical support. I am blessed to have a creative, funny, loyal, and beautiful partner in life.

I thank my mother for taking care of me and instilling good habits for life. I thank my brother Grant for believing in me. I thank my mother and father-in-law for their willingness to help in all situations.

I thank my son Silas, too. He was born in the middle of this endeavor, and while I cannot say things got easier, he brightens my days and continues to be my motivation.

I thank many folks in Gainesville for welcoming and looking after our little family. I have not yet found another place with so much community. A special thanks to my friend Sara, who epitomizes the spirit of this town.

I thank Carlos, Paul, Bobby, Kenyon, Jenny, Josefin, Nelson, Jing, Olivia, Sarah, Lauren, Josh, Rachel, Jake, Subodh, Brett, Julianne, Chad, and Yu-seung for building our lab community. I fondly remember trivia nights, canoe trips, bike rides, cook-outs, and the surprise baby shower you all threw me. I thank Larry for guiding so many of us with his wry humor and wisdom. I loved being a graduate student because of this lab.

I thank many folks in SFRC, SNRE, and other departments who make the University of Florida an excellent place to learn and grow. Austin Cary Memorial Forest holds a special place in my heart. I thank my committee members for their encouragement and always making me feel that I was more important than any data.

Finally, I thank my advisor Matt for his confidence in my abilities, his optimism and humor, and for his friendship.

TABLE OF CONTENTS

page

LIST OF TABLES

LIST OF FIGURES

LIST OF ABBREVIATIONS

ANR	Anaerobic respiration
AR	Aerobic respiration
CO_2	Carbon dioxide
DO	Dissolved oxygen
DOC	Dissolved organic carbon
ER	Ecosystem respiration
fCO_2	CO_2 reaeration flux
fDOM	Fluorescent dissolved organic matter
GPP	Gross primary production
LUE	Light use efficiency
NEP	Net ecosystem production
PAR	Photosynthetically active radiation
q_L	Lateral groundwater inflow
RIP	Lateral CO_2 flux from the riparian corridor
RQ	Respiratory quotient
TER	Lateral CO_2 flux from the terrestrial uplands

Abstract of Dissertation Presented to the Graduate School
of the University of Florida in Partial Fulfillment of the
Requirements for the Degree of Doctor of Philosophy

METABOLISM IN SUBTROPICAL LOWLAND RIVERS

By

Lily Kirk

August 2020

Chair: Matthew J. Cohen
Major: Interdisciplinary Ecology

Ecosystem metabolism is an integrated measure of all biological activity in a system. In aquatic systems, its two fluxes – gross primary production (GPP) and ecosystem respiration (ER) – are usually extracted from dissolved gas (oxygen and carbon dioxide) signatures. In flowing waters, recent advances in sensor technology and metabolism modeling have made continuous, open-water metabolism measurements in many locations possible, enabling development of a coherent framework for explaining the variation of stream metabolism in space and time. More broadly, as a major flux that contributes to stream CO_2 evasion, riverine metabolism plays a significant role in global carbon cycling and deserves special attention during this era of climate change.

This dissertation interrogated light's control of GPP in streams, the community respiratory quotient (RQ) and anaerobic respiration (ANR) rates, and the river corridor's contribution to CO_2 evasion. I found that benthic (i.e. streambed) light – *not* the commonly measured stream surface light – was essential to characterize accurately light available for photosynthesis and to predict GPP. Furthermore, contrary to previously reported literature values, benthic light constrains light use efficiencies

across diverse streams and rivers in north-central Florida so that values converge with those of terrestrial systems. At point scales, I measured community RQ (moles of CO_2 biologically produced/moles of oxygen consumed) and found they were lower than the commonly assumed unity and influenced by processes in addition to the quality of organic matter respired. With RQ values during water column anoxia, I was able to estimate riverine ANR. Finally, I found that most stream CO_2 evasion originates within the river corridor, either from internal respiration of allochthonous organic matter or evasion of CO_2 dissolved in lateral groundwater inflows that come from riparian wetlands. This is contrary to the common attribution of CO_2 from lateral inflows to the terrestrial landscape. By exploring some of the widespread assumptions related to lotic metabolism, I hoped to improve our understanding of stream and river ecosystem processes and global carbon cycling.

CHAPTER 1
CONTEXT AND SCOPE OF DISSERTATION

Ecosystem science studies the flow of energy and matter through biotic communities and the abiotic components of an environment. Often ecosystem ecologists will draw a black box around a particular system, then measure and model the fluxes of energy and matter into and out of that system. The activity of the biotic component of the system can be summed into ecosystem metabolism which is essentially two processes: gross primary production (GPP) and ecosystem respiration (ER). GPP converts sunlight into reduced organic carbon compounds, thus powering the ecosystem. ER oxidizes the organic carbon compounds to release energy for work or growth, thus allowing life. The quantification of metabolism developed in parallel to ecosystem science, first emerging in aquatic (marine) systems with bottle incubation in the 1920s, then becoming readily available to aquatic ecologists with the open water diel curve technique in the late 1940s (Staehr and others 2012). By contrast, terrestrial ecologists had only begun to measure ecosystem metabolism with the eddy covariance method (terrestrial analog to the open water diel curve technique) in the 1950s.

The technique for measuring ecosystem metabolism in flowing waters using the open water diel curve technique was developed at Silver Springs, FL (Odum 1956). Metabolism is theoretically easy to measure in rivers and streams due to the continual mixing of water and unidirectional transport of that water carrying the dissolved oxygen (DO) and CO_2 imprints of metabolism. During the day, photosynthesis increases DO and depletes CO_2, which subsequently returns to a nighttime baseline, thus creating a dissolved gas “heartbeat” that is captured downstream, from which we can extract rates of GPP and ER. And like a human heartbeat, metabolism is a convenient tool to assess

the health of a river or stream (Hornberger and others 1976; Fellows and others 2006). Stream metabolism integrates all organisms and habitats existing in the river and reflects landscape, corridor, upstream, and internal processes. Yet despite a long history of ecosystem metabolism measurements in flowing waters, a coherent framework for predicting metabolism in space and time has so far eluded stream ecologists (Bernhardt and others 2018).

Recent advances in DO sensor technology and metabolism modeling have paved the way for unprecedented measurement and understanding of stream metabolism. Until the 2010s, most metabolism studies have been based on limited DO measurements, first with the laborious Winkler titration of water grab samples and later with cumbersome membrane DO sensors. As a result, DO measurements were consigned to baseflow during the warmest months of the year (Hoellein and others 2013) in a few well-studied, iconic systems (e.g. Hubbard Brook, Sycamore Creek, Silver Springs). Recent low-maintenance optical DO sensors have allowed the measurement of DO at high frequency over annual time scales and in diverse locations (e.g. Appling and others 2018b; data.streampulse.org) to capture the dynamic nature and spatial heterogeneity of lotic environments (e.g. Meyer 1990). Concurrent advances in stream metabolism inverse modeling allow estimation of GPP and ER rates from DO time-series data despite limited empirical measurement of gas exchange and uncertainty in reaeration rates (Appling and others 2018a).

Moreover, the development of *in situ* CO_2 sensors within the last decade now allows metabolism to be studied with both DO and CO_2. In water, CO_2 is part of a complicated carbonate system where some dissolved CO_2 may speciate into

bicarbonate or carbonate depending on pH and other environmental conditions or dissolved CO_2 may be locked into keeping alkalinity in solution (Drever 1988). Previously, free dissolved CO_2 was almost always calculated from pH and alkalinity, but those calculated values can differ greatly from actual measurements (Abril and others 2015). Now infrared gas analyzer (IRGA) technology not only allows more accurate, direct, and continuous CO_2 measurement (Johnson and others 2010), but also simultaneous CO_2 measurement with high-frequency DO measurement. The coupling and un-coupling of these two gases sheds insights into ecosystem metabolism processes and assumptions.

In the larger picture, stream metabolism plays a significant role in global carbon cycling. Streams and rivers are supersaturated with CO_2 compared to atmospheric concentrations (Cole and Caraco 2001) and are often net sources of CO_2 to the atmosphere. Not only is stream autotrophy a large component of CO_2 efflux (Minshall 1978), but streams respire a large proportion of the organic matter exported by their terrestrial surroundings, contributing to CO_2 evasion (Del Giorgio and Pace 2008). While high groundwater concentrations of CO_2 can outgas once in contact with stream surface waters, a large proportion CO_2 efflux is still tied to ecosystem metabolism (Hotchkiss and others 2015). Hence, a more thorough understanding of stream metabolism is critical to predicting evasion of the main greenhouse gas causing climate change.

My dissertation aims to enhance our understanding of stream and river metabolism at various scales through both DO and CO_2 measurement. Chapter 2 is a test of the metabolic regimes prediction that stream GPP is constrained by light availability when disturbance is minimal (Bernhardt and others 2018). Our north-central

Florida streams and rivers were ideal test sites for this due to their infrequent bed-moving flood disturbances (lowland waters) and natural gradients in stream width and dissolved color (both facilitating attenuation of incident light). In order to accurately represent light available to the autotrophic community, I modeled benthic (i.e. streambed) light availability for our stream reaches by successively attenuating open sky light through the riparian canopy and water column. Then I tested how well benthic light predicted stream GPP (modeled from DO) as opposed to open sky or stream surface light. Moreover, with accurate benthic light and GPP, I was able to calculate light use efficiency (LUE) for our study reaches. By adjusting LUE for autotrophic light capture ability (i.e. denser autotrophic communities would capture more incident light than sparser communities), I was able to compare LUE across our sites, literature values from other aquatic and terrestrial systems, and theoretical values. I found convergence of LUE values in flowing waters, thus allowing prediction of a maximum GPP envelope. The efforts behind modeling riparian canopy attenuation of light became part of a paper lead by Phil Savoy and in review at Freshwater Science. The modeling of water column light attenuation, evaluation of GPP predicted from benthic light, and analysis of LUE (the bulk of Chapter 2) was reviewed by *Ecosystems* and pending minor revisions.

Chapter 3 tests the accuracy of the commonly assumed community respiratory quotient (RQ) through point-scale experiments in *in situ* mesocosms. In shaded benthic chambers to eliminate primary production to focus only on respiration, I compared DO and CO_2 dynamics in sugar treatments to controls. We chose to conduct this experiment at Ichetucknee Springs, FL, a well-studied chemostatic riverine system. Until benthic

chambers reached hypoxia, I was able to calculate community RQ (mols CO_2 produced/mols O_2 consumed) utilizing natural DOC heterogeneity (control) and regulated DOC composition (sugar treatments). The combined results allowed me to infer the major processes controlling community RQ. After benthic chambers became anoxic, I was still able to observe community RQ due to reaeration in our benthic chambers and thus estimate ANR. The empirical measurement of community RQ that differs greatly from assumed values has major consequences for converting reach and network-scale metabolism rates calculated in DO units into carbon efflux. The dramatic response of anaerobic respiration to labile carbon has implications for changes in stream metabolism rates with anthropogenic impacts (inputs of labile carbon from wastewater pollution and eutrophication). This manuscript is in preparation.

In Chapter 4, I question the validity of attributing stream excess CO_2 (efflux – net ecosystem production) to lateral CO_2 loss from the terrestrial landscape (a la Hotchkiss and others 2015). I test this common practice by measuring CO_2 fluxes from the terrestrial uplands, riparian corridor, and stream channel along a river network that has contrasting catchment geologies. I find that most of excess CO_2 actually sources from ecosystem respiration within the river corridor, with major implications for the global carbon balance. I also had hoped to estimate reach-scale stream anaerobic respiration with a CO_2 mass balance, but ultimately concluded that the magnitude of the anaerobic respiration flux was so small compared to other CO_2 fluxes that CO_2 mass balance was not an appropriate method. This manuscript is in preparation.

CHAPTER 2
BENTHIC LIGHT REGIMES PREDICT PRIMARY PRODUCTION AND CONSTRAIN LIGHT USE EFFICIENCY

Introduction

A small fraction of light energy that enters ecosystems is converted to chemical energy via photosynthesis. This conversion efficiency is a key aspect of ecosystem metabolic regimes and exert direct and indirect influences on nearly all biological and biogeochemical processes. At the scale of forest stands and stream reaches, light use efficiency (LUE) describes conversion of incident photosynthetically active radiation (PAR) into gross primary production (GPP):

$$PAR \times LUE = GPP \quad (2\text{-}1)$$

Thus defined, LUE quantifies the intrinsic capacity of chloroplasts to fix solar energy (i.e., leaf-scale photosynthetic efficiency) with the ability of the autotroph communities to capture light (related to autotroph density and canopy structure). In terrestrial ecosystems, efficiency can be estimated using absorbed PAR or indexed to biomass accrual (i.e., net primary production, NPP), but we purposely define LUE using the broadest definitions for light inputs and metabolic response to facilitate direct comparisons with aquatic systems where these efficiency refinements are less developed. Although quantum yield is relatively constant across plant species from diverse light environments (Singsaas and others 2001), LUE is subject to other ecosystem limitations (e.g., biomass, nutrients, water, temperature) that affect light capture and physiology. For example, nitrogen may limit plant growth and photosynthetic physiology (Field 1991), lowering light capture efficiency. Likewise, systems with low biomass, either because of persistent low light or recent disturbance, can exhibit low LUE (e.g. Sawall and Hochberg 2018).

Understanding LUE patterns across systems has been foundational to studies of the energetic basis of ecosystem functions. Odum (1956a) suggested LUE is generally far below the theoretical maximum at the cellular (26.7%; Weyer and others 2010) or leaf level (13% and 17% for C3 and C4 plants, respectively; Zhu and others 2008), despite long evolutionary selection due to tradeoffs between efficiency (i.e., LUE) and useful power output (i.e., GPP), which select against higher efficiency in favor of higher power output (the Maximum Power Principle). Maximum observed values at the leaf level are closer to 10% (Björkman and Demmig 1987), but far lower still (~2-3%) at the ecosystem level for healthy plant communities under optimal conditions (Rabinowitch 1945; Monteith and Moss 1977). Further, the Functional Convergence Hypothesis (Field 1991) suggests that photosynthetic capacity is optimized similarly across species, implying LUE convergence at multiple scales and across ecosystem types when other productivity limitations are relaxed. Revealing maximum efficiency when other growth factors are non-limiting was shown elegantly for rainfall use efficiency across biomes (Huxman and others 2004). Together these theoretical predictions imply that departure from maximum power output (i.e., predicted GPP given incident PAR) is diagnostic of factors other than light limiting productivity, and when those factors are supplied sufficiently, observed efficiencies should converge.

In flowing waters, LUE estimates are central for meaningful progress toward characterizing stream metabolic regimes. The metabolic regimes concept (Bernhardt and others 2018) provides a framework for evaluating long-term dynamics and cross-scale controls on GPP. Annual patterns of stream GPP are principally set by the “river climate” consisting of temporal variation in solar energy and flow-induced disturbance: A

“maximum envelope” for GPP is set by incident light, given a measure of LUE, then bed-scouring disturbance (and resulting biomass limitation, e.g. Fisher and others 1982) and nutrient limitation reduce the realized productivity. A well-constrained LUE value in the absence of disturbance is essential for constructing a tenable GPP maximum envelope. Moreover, the light regime has been a major focus for lotic ecology for decades (Vannote and others 1980), but with the tacit assumption that temporal and spatial light variation is far larger than variation in LUE. Although the light regime clearly drives lotic GPP variation across biomes (Mulholland and others 2001) and over time (Roberts and others 2007), poorly constrained LUE values may help explain why we have had limited success developing robust universal relationships between measured light and GPP (Bernhardt and others 2018).

Published LUE values vary substantially both within (Hill and others 2001) and across (Flemer 1970) streams, and whereas LUE estimates from aquatic systems are fewer than those from terrestrial systems, they exhibit a greater range of values. Standardizing LUE to consider GPP per unit incident PAR (see Methods) reveals striking divergence among studies. The first study to derive LUE across lotic systems (spring-fed rivers) yielded a value of 4% (Odum 1957a). Studies on individual streams reported values both lower (0.3 - 2% in Hill and others 2001; 0.08% - 1.2% in Hornberger and others 1976) and higher (e.g., 0.1% - 7.2% in Bott and others 1985). Values from lentic systems appear far lower (0.04 - 0.16% in Lindeman 1942; 0.004 - 2% in Brylinsky 1980), whereas values from marine systems appear higher (4.9% in a coral reef; Barnes and Lazar 1993). In contrast, eddy-covariance methods across terrestrial biomes yielded LUE values between 0.3% and 3.2% (Garbulsky and others

2010), with a cross-site mean of 1.9% (2.3% ± 0.9% in Turner and others 2003; 1.5% in Schwalm and others 2006). Crops exhibit slightly higher values (1.3% to 2.8%; Monteith and Moss 1977; Turner and others 2003; Garbulsky and others 2010; Slattery and Ort 2015). Large differences in both the mean and variance of LUE values between aquatic and terrestrial systems appears contrary to the Functional Convergence Hypothesis (Field 1991), which suggests photosynthetic capacity is optimized similarly across species and implies LUE convergence at multiple scales and across ecosystem types when other productivity limitations are relaxed. Some aquatic studies, however, report LUE values similar to terrestrial ecosystems (Wassink 1959) – or at least no statistically significant difference (Sand-Jensen and others 2007) – underscoring the need to develop a systematic approach to calculating and comparing LUE across aquatic systems.

Differences in lotic LUE hve several plausible explanations. First, LUE may vary because GPP is limited by something other than light such as nutrients – though this is generally thought to be less prevalent in flowing waters than in other aquatic systems (King and others 2014; Covino and others 2018) – or autotroph biomass. Second, divergence between terrestrial and aquatic LUE may arise because light inputs used to estimate LUE may not reflect conditions experienced by aquatic autotrophs. Stream studies that consider light inputs generally acknowledge canopy attenuation, using measured stream surface PAR (Young and Huryn 1996; Hill and Dimick 2002; Beaulieu and others 2013) or proxies such as open sky irradiance (Dodds and others 2013) or cloud cover (Hall and others 2015) in low canopy settings, or measure canopy cover directly (Hoellein and others 2013). Where autotrophy is dominated by attached or

rooted taxa (Hilton and others 2006), however, PAR reaching the benthos, not the stream surface, is most relevant for predicting GPP. Water column light attenuation varies with discharge both directly via changes in water depth (i.e., light pathlength) and indirectly via mobilization of sediment and dissolved color (Davies-Colley and Smith 2001). Optical water quality is difficult to measure continuously *in situ* because of reflective scatter, biofouling of sensors, and strong currents, so time-series of direct measurements of benthic PAR are rare (but see Acuña and others 2004). Because LUE relates energy outputs to inputs, it is crucial that GPP and benthic PAR are measured simultaneously, and that inputs are realistically quantified to ensure informative cross-site and cross-ecosystem LUE comparisons.

Although few studies have measured metabolism and light simultaneously, wider availability of *in situ* sensors to measure dissolved oxygen and light at high frequency is poised to change this. Recent advances in GPP inference (Appling and others 2018a) across many locations (Appling and others 2018b) provides a growing database from which to establish stream metabolic responses across sites. Likewise, reach-scale models representing spatial and temporal patterns of benthic light have emerged (Julian and others 2008a) and are increasingly sophisticated in representing light attenuation caused by geomorphic and riparian shading (Savoy and others, *in review*) and water column attenuation (Davies-Colley and Nagels 2008). Coupling these new tools to enumerate atmospheric, canopy, and water column light attenuation (Figure 2-1A) with new GPP inference techniques was a natural next step and our primary goal in this work. Specifically, using improved characterizations of benthic light inputs (energy in) and GPP responses (energy out) across a gradient of lowland rivers in Florida, we

tested the following hypotheses: 1) GPP predictions across sites will be substantially improved with more rigorous characterization of the benthic light regime, and 2) LUE values for flowing waters converge when calculated using benthic light.

Methods

Study Sites

We selected eleven stream reaches in north Florida, USA spanning gradients in channel width and dissolved color (Table 2-1). The reaches comprise 2nd to 5th orders, and all have intact riparian forest buffers. The dramatic gradient in dissolved color that guided site selection arises from geologic and source-water variability. The low-order blackwater streams and rivers (DRAIN, SF700, and SF1500) are colored by aromatic dissolved organic matter (DOM) that leaches from swamps and pine flatwoods common in sandy low-relief watersheds of the coastal plain (Meyer 1990). In contrast, spring-fed rivers (e.g., MILL, ICHE, SILUP) are hydrologically sourced entirely from the karstic Upper Floridan Aquifer (Scott and others 2004), which provides a stable flow of remarkably clear (Duarte and others 2010), alkaline water. Three sites (SF2500, SF2800, and ALEX) represent a time-varying blend of these contrasting end-members, with low-discharge periods dominated by aquifer water, and high discharge dominated by blackwater runoff (Fork and Heffernan 2014; Hensley and others 2019). Flow variation is a critical control on stream color, creating gradients in time and in space (Table 2-1). Compared with DOM, suspended particles are a tiny component of water column optical density (Hensley and others 2019), justifying our exclusive focus on dissolved color for water column light attenuation in these streams.

The density and composition of autotrophs varies dramatically across sites, largely in response to dissolved color gradients. Spring-fed rivers are dominated by

dense rooted macrophyte beds (Odum 1957b; Heffernan and others 2010), whereas blackwaters have sparse benthic and epilithic algal communities. Biomass is intermediate where color varies with flow, except in ALEX which supports dense macrophyte beds because of shallow channel morphology and relatively high proportion of aquifer water even under high-flow conditions. Although floods are important aspects of the hydrologic regimes, particularly in the blackwater sites, bed-moving disturbances are rare and thus influence the metabolic regime minimally, simplifying the inference of LUE from light and GPP measurements.

Data Collection and Modeling

Time series

Open sky total irradiance (E_{sky}; W m^{-2}) and barometric pressure were obtained from nearby (mean distance = 26 km) Florida Automated Weather Network (FAWN; fawn.ifas.ufl.edu) stations, where irradiance is measured every 15 minutes with a Campbell LI200X Silicon Pyranometer calibrated between 400 and 1100 nm. Dissolved oxygen (DO), temperature, and fluorescent dissolved organic matter (fDOM) were measured *in situ* at a minimum of hourly intervals. At all 7 Santa Fe River and Ichetucknee River sites, we measured DO using an optical sensor (Onset HOBO U-26, Bourne, Massachusetts, USA) which also measured temperature. We measured fDOM using an in-situ fluorometer with excitation/emission wavelengths of 320/470 nm (Turner Designs Cyclops-7, San Jose, California, USA). Sensors were cleaned monthly and calibrated at least yearly. Biofouling especially affected fDOM sensors, so a linear correction was applied between calibrations following USGS guidelines (Wagner and others 2006). At Silver River and Alexander Springs Creek, DO, temperature, and fDOM were measured by the St Johns River Water Management District

(https://www.sjrwmd.com/data/water-quality/) using a multiparameter sonde (YSI EXO2, Yellow Springs, Ohio, USA).

Light model

High variability in measurements of light below the canopy and at the riverbed (Villamizar and others 2014) necessitated modeling of stream surface and benthic light. We followed the benthic light availability model (BLAM; Julian and others 2008), in which open sky irradiance is successively adjusted by canopy transmission (c), stream surface light penetration (f) and water column transmission (w) (Figure 2-1A).

Riparian Canopy Attenuation

We modeled canopy light transmission (c) as a function of date, location, river geometry, and vegetation structure using StreamLight (Savoy and others *in review*) an open-source software package (R Core Team 2017) that outputs hourly stream surface PAR. StreamLight combines models of stream shade (SHADE2; Li and others 2012) and radiative transfer (Campbell and Norman 1998) to estimate temporally dynamic stream surface PAR. Leaf area index (LAI) in the radiative transfer model is from the Moderate Resolution Imaging Spectroradiometer (MODIS) 4-day composite LAI product (MCD15A3H) (Myneni and others 2015). To improve model accuracy, we replaced remote-sensed open sky irradiance and canopy height with site-specific measurements. We used a single measured azimuth for straight river reaches (defined operationally as mean travel distance of O_2 or $0.7 \times u / k_{O2}$; where u is stream velocity, m d^{-1}, and k_{O2} is the gas exchange rate, d^{-1}; Lamberti and Hauer 2017). For rivers with significant azimuth variation, we estimated daily canopy transmittance as a length-weighted mean of multiple segments, each with a representative azimuth.

We deployed three HOBO light sensors in riparian forests adjacent to each reach to corroborate MODIS FPAR values, which are derived from LAI (slope = 1.08, R^2 = 0.29, n = 56). We also measured riparian LAI using a plant canopy analyzer (Licor LAI-2200C, Lincoln, Nebraska, USA). Field measurements (n = 4), were significantly correlated with MODIS estimates and although spatial variation for LAI was only modestly predicted (R^2 = 0.37), the magnitude of field and MODIS measurements aligned (slope = 1.2).

Stream Surface Reflectance

The proportion of light entering the water column (*f*) is thus defined by:

$$f = 1 - R_s \tag{2-2}$$

where R_S is stream surface reflectance (unitless). Hourly reflectance can be calculated from the solar zenith angle according to Fresnel's equation (Kirk 1994) which assumes flat water. Calculated reflectance had daily means between 2 and 12% over the course of year. Reflectance measurements taken manually (see below) were higher than values using Fresnel's equation (mean R_S = 0.28, sd = 0.12, n = 21). Because we sought a conservative light transmission model (i.e., lowest attenuation), we used reflectance computed with Fresnel's equation.

Water Column Attenuation

Lambert's law describes exponential attenuation of monochromatic light passing through pure water. Although PAR is a spectral integral of many wavelengths and river water is not pure, we approximated water column transmission of light to the benthos (*w*) following those idealized assumptions:

$$w = e^{-K_d z} \tag{2-3}$$

where z is water depth (m), and K_d is the downwelling light attenuation coefficient (m^{-1}).

Beer's law describes light absorbance as a function of concentration of attenuating species (particulates and dissolved substances). In our case, high concentrations of chromophoric DOM in blackwaters are the attenuating species, not particulates as all sites have low and minimally variable turbidity. We used continuous fDOM measurements as a proxy, which correlates strongly with the aromatic fraction of dissolved organic matter (McKnight and others 2001). From fDOM measurements, we predicted K_d based on synchronous field observations of light extinction with depth. These involved one HOBO pendant light sensor (180 – 1200 nm range) deployed above the water and pointed south to avoid shadows (measuring at 0.1 Hz), while another was lowered through the water column along with a pressure transducer (Onset HOBO U20, Bourne, Massachusetts, USA) to track sensor depth. Light profiles were collected between 10:00 and 14:00 to minimize surface reflectance. The resulting K_d vs. fDOM relationship was linear ($K_d = 0.0378 \times fDOM + 0.23$, $R^2 = 0.86$, n = 24) with the intercept fixed to mean K_d values in the spring sites. Water column light profiles conducted using an underwater PAR sensor (Licor LI-192, Lincoln, Nebraska, USA) yielded K_d values strongly correlated with pendant total light sensors (slope = 1.07, R^2 = 0.88).

Because of the exponential relationship in Equation 2-3, use of a mean reach depth in Equation 2-3 would likely overestimate average reach water column transmission of light. Instead, we applied Equation 2-3 to a spatial distribution of depths in the reach, then averaged the resulting transmission values. To model the depth distribution for the entire reach, we used depth distributions from channel cross-section

measurements (n = 2 to 10) on each reach. Measured depths were binned (0.2 m increments), and the density of observations in each bin was adjusted based on measured water level variation. For water levels deeper than on the survey date, we increased the wetted width based on bank slopes from the channel cross-sections. We used Equation 3 to calculate light transmission based on depth distributions yielding a weighted mean water column light transmission (w).

Overall Light Model

Benthic light (E_{bed}) was calculated hourly as:

$$E_{bed} = E_{sky} \times c \times f \times w \quad (2\text{-}4)$$

where E_{sky} is open sky light, c is proportional canopy transmittance, f is proportional light penetrating the stream surface, and w is proportional water column transmittance. Open sky, stream surface, and benthic light were averaged over 24 hours to determine corresponding daily light values.

Because weather stations were off-site, we also deployed a pendant light sensor (Onset HOBO UA-002-64, Bourne, Massachusetts, USA) in an open field adjacent to five reaches to verify FAWN measurements were representative of local site conditions (mean $R^2 = 0.61$).

We compared model predictions of benthic light against HOBO pendant light sensors deployed in the water column at known depth in four locations. Modeled light transmission (n = 49) was modestly correlated with measured light ($R^2 = 0.26$), with slope equal to 1. Our light model, however, consistently predicted higher transmission than we observed (by ~12%), likely because light sensors were placed near shaded river banks or had biofilms growing on them.

Metabolism

For all non-spring fed rivers, we calculated daily GPP (g-O_2 m^{-2} d^{-1}) using the single-station open water method (Odum 1956) implemented using inverse modeling in streamMetabolizer (github.com/USGS-R/streamMetabolizer). Essentially, streamMetabolizer chooses combinations of daily GPP, daily ecosystem respiration (ER), and reaeration coefficient (k_{600}) that best fit observed DO. streamMetabolizer requires a high temporal resolution light input solely to partition its daily GPP estimates throughout the day. We used open sky light (E_{sky}) as this light input because it would reflect the mid-day and afternoon cloud shading common to Florida, but would not incorporate our mechanistic light model, hence ensuring the independence of light and GPP data for our study.

We used streamMetabolizer's Bayesian parameter estimation with pooling of k_{600} based on discharge to ensure k_{600} was similar on days with similar discharge (Appling and others 2018a). Modeled k_{600} values were constrained with means of priors based on unanchored floating dome measurements (see below), literature floating dome measurements (Munch and others 2006; Khadka and others 2014), as well as model estimates using channel hydraulics (Raymond and others 2012). Standard deviations of k_{600} priors was set between 1.0 and 1.5, depending on our confidence of k_{600} estimates.

We measured k_{600} directly using the floating dome method (Copeland and Duffer 1964) with modifications. A clear, rectangular storage container (area = 0.084 m^2) was overturned on the water surface, supported by flotation collars to penetrated 5 cm into the water, yielding a constant headspace volume of 15.5 L. CO_2 was injected into the headspace, and concentration was measured continuously using a submersible infrared gas analyzer (IRGA) (Eosense eosGP 0 – 20,000 ppm, Dartmouth, Nova Scotia,

Canada) as the dome floated downstream. We also monitored river water CO_2 concentrations below the dome with a second sensor. Measurements were recorded every minute, with the slope between concentration and time defining the molar CO_2 flux from chamber to water, from which we estimated k_{600} following Khadka and others (2014).

Groundwater at the vents of our spring-fed rivers is routinely undersaturated in DO, violating the single-station metabolism model assumption that nighttime DO values reflect only the balance between ER and gas exchange. To estimate metabolism for spring-fed systems, we used a two-station method (Odum 1956) following Hensley and others (2015). In one river reach (SILLOW) both metabolism methods are applicable. In that reach, GPP and ER determined using streamMetabolizer compared favorably with estimates from the two-station method (slope = 0.92, R^2 = 0.69).

Light use efficiency (LUE)

LUE relates GPP to available light. There are, however, myriad ways to report both numerator and denominator (Monteith 1972), potentially confounding comparisons among studies. We define LUE as:

$$LUE = \frac{GPP}{incident\ PAR} \times 100 \quad (2\text{-}5)$$

Whereas daily photosynthesis-irradiance curves are hyperbolic indicating light saturation, time- and space-integrated curves are linear (Hornberger and others 1976; Sawall and Hochberg 2018) justifying estimation of LUE using a linear fitted slope of light versus GPP. We focused exclusively on LUE for the entire range of natural irradiances, so efficiencies reported here are generally lower than photosynthetic efficiency at low irradiance (α) common in the literature. Standardizing GPP to energy

units (kJ m^{-2} d^{-1}) required assuming a photosynthetic quotient of 1 and that each gram of organic matter contains 0.37 g-C (McBride and Cohen 2019). Standardizing PAR to the same energy units required assuming 1 $\frac{W}{m^2}$ is equivalent to 4.6 $\frac{\mu mol}{m^2 s}$. Because open sky total irradiance was measured (i.e., including wavelengths outside the PAR waveband; 400 – 700 nm), we corrected open sky light by 0.5 (Monteith 1972).

To standardize LUE values to GPP/incident PAR across studies for meaningful comparison, we made several assumptions:

1. GPP is two times NPP (Whittaker and Likens 1973) and NPP equals biomass accrual,
2. PAR was half of total solar irradiance (Monteith 1972),
3. Intercepted PAR (IPAR) equals absorbed PAR (APAR) (Gallo and Daughtry 1984) and that APAR varies by ecosystem type (0.3×PAR for row crops and grasslands, 0.5×PAR for taiga and temperate forests, 0.6×PAR for tropical forests; Peng and others 2012), and
4. Carbon is 47.5% of organic matter in terrestrial systems (Raich and others 1991).

To standardize reported variance, we assumed normal distribution of data and approximated sd as $\frac{IQR}{1.35}$ or $\frac{range}{4}$.

Data analysis

Our first hypothesis led to the prediction that benthic light is more strongly correlated with GPP than either open sky or stream surface light. To test the hypothesis, we evaluated correlations (r) between GPP and open sky, stream surface, and benthic light, at each site individually and for all sites combined. We further evaluated benthic light predictions using a general linear model (GLM) implemented in R (R Core Team 2019). Our model specifically considers the role of site in imputed LUE, both as a factor influencing the model intercept (i.e., site main effects) and fitted slopes (i.e., site × light interactions). This yielded three models: a) GPP predicted only by daily light (i.e., no site

effects), b) GPP predicted by main effects of daily light and site (main effects model), and c) GPP predicted by interactions between daily light and site (interaction model). Because including site effects precludes generality, however, we further evaluated model configurations using proxies for measured site effects; mean benthic light during the period of record emerged as the best proxy. We evaluated model fit using the adjusted coefficient of determination (R^2) and the Akaike Information Criterion (AIC).

To test our second hypothesis that LUE converges across streams after accounting for benthic light availability, we compared fitted slopes for the main effects model (i.e., universal LUE) with fitted slopes from an interaction model (i.e., varying LUE by site). We expected the main effects model performance to be comparable with the interaction model if LUE converged (i.e., can be treated as a constant across sites). Moreover, we expected a full consideration of benthic light (i.e., daily and mean light) to produce LUE values with less variation than LUE calculated for each individual site.

Results

Benthic Light Availability

The relative importance of canopy and water column light attenuation varied among sites with stream width and color (Table 2-1; Figure 2-1B). Water column attenuation was equal to or greater than canopy attenuation for all sites except shaded, shallow, and exceptionally clear MILL (Table 2-1). Even clear waters with depths ~ 2 m (SILUP, SILLOW) exhibited 40% attenuation of stream surface light at the bed; colored waters of similar depth (SF1500, SF2500) lost ~ 90% of stream surface light at the bed. Notably, water column attenuation exceeded canopy percent reduction even in shaded, shallow creeks (DRAIN). In all combinations of stream size and color, benthic light was markedly lower than open sky light, illustrating the importance of considering cumulative

attenuation for obtaining realistic LUE values. Using open sky or stream surface light underestimates LUE by 67% and 50%, respectively, compared with benthic light.

Light and GPP

The prediction of daily GPP by daily light improved substantially after each successive light attenuating step. The correlation using open sky light ($r = 0.32$) was poor across sites, but improved markedly after accounting for canopy attenuation ($r = 0.53$), and improved even more after accounting for stream reflection and water column attenuation ($r = 0.80$, Figure 2-2).

The irradiance vs. GPP relationship clearly exhibits site-level effects (Figure 2-2), suggesting a global correlation model neglects crucial information. Indeed, the global GLM using only benthic light (i.e., neglecting site effects) explains 64% of GPP variation (AIC 34705, 2 df). This increases to 92% of GPP variation after including site as a main effect in the GLM (AIC 27843, 12 df). This main-effects model does not permit variation in LUE (i.e., the slope of the daily light effect is constant across sites), but adjusts the intercept by site. Further complexity to allow slope to vary by site (i.e., a site-by-light interaction model), improved the model slightly ($R^2 = 0.94$) and significantly based on AIC comparisons (AIC 26840, 22 df).

Adding site effects generated marked improvement in model fit, but precludes model application to new settings. To remedy this, we explored covariance between fitted site effects and ancillary site data. Fitted site effects (i.e., intercepts in the main effects model) were strongly correlated with mean benthic light ($r = 0.82$, $p = 0.002$), mean temperature ($r = 0.62$, $p = 0.043$), and mean nitrate ($r = 0.91$, $p < 0.001$, although the strong correlation may be driven by dramatically different chemistry between spring and blackwater sites). Because mean light is available at all sites for which daily light

variation is known, we constructed models to predict GPP using daily and mean benthic light (Table 2-2). These models improved significantly versus the base model (GPP vs. daily benthic light), explaining 78% of GPP variation (AIC 32445, 3 df) using main effects (i.e., a global LUE) and 80% of variation with an interaction (i.e., site variation in LUE) (AIC 32141, 4 df). This same model formulation using open sky or stream surface light data resulted in far poorer model performance (R^2 = 0.76 using benthic light versus R^2 = 0.37 using open sky or R^2 = 0.32 using stream surface light in the main effects model). Whereas mean light was calculated from daily light, the Variance Inflation Factor (VIF) for including both variables was 2.14, well below published thresholds for multicollinearity concerns (Thompson and others 2017).

Light Use Efficiency

Site specific LUE can be estimated individually, with a mean (± SD) LUE across sites of 0.5% (±0.6%) using open sky irradiance, 0.8% (± 0.6%) using stream surface light, and 1.5% (± 1.3%) using benthic light (Figure 2-3). Coefficients of variation (CV) for LUE were 1.04, 0.80, and 0.84 using open sky, stream surface, and benthic light, respectively, indicating that although LUE increased markedly, LUE variation across sites did not decrease when using stream surface or benthic light.

Cross-site LUE estimates depend strongly on light inputs and model selection. The most naïve LUE estimate considers the association between daily light and GPP without site effects. LUE from this fitted slope ranged from 0.9% using open sky irradiance, to 1.6% using stream surface light, and 3.7% using benthic light. This four-fold increase in LUE between open sky and benthic irradiance highlights the perils of neglecting canopy or water column light attenuation. A regression between site mean GPP and site mean benthic light (i.e., distilling each site time series into a single mean

value) resulted in LUE of 5.4% (Figure 2-2C), with an R^2 of 0.81. This is the approach used by Odum (1957b) from which a 4% LUE was obtained. Both regressions of either daily or mean benthic light yield high LUE, but are likely confounded by evidence for site effects. A more representative approach to LUE estimation considers site main effects in the global GLM. In that model, the estimated LUE (fitted slope) applies to all sites with values of 0.5% for open sky irradiance, 1.0% for stream surface irradiance, and 1.9% for benthic irradiance. With interactions between daily light and site, LUE values are identical to estimates for each site individually.

Models predicting GPP based on both daily and mean benthic light yielded similar LUE values. Our main effects model yields a single LUE across sites of 1.9% (Table 2-2). Including an interaction yielded LUE values similar to those obtained for each site individually except for two sites (slope = 0.81 intercept = 0.0055, R^2 = 0.85 without sites SF2500 and SF2800). Even with these two anomalous sites, however, the range of LUE reduced by 2 times when modeled as an interaction between daily and mean light (CV = 0.70) compared to individual site LUE values (CV = 0.84) (Figure 2-3). Variance in LUE may not have converged when only considering daily light, but did converge when we considered the full light regime of daily and mean benthic light. Mean LUE from the interaction model was 1.3% ± 0.9% (1.5% ±0.9% excluding SF2500 and SF2800). LUE generally increased with higher mean benthic light (r = 0.92 excluding SF2500 and SF2800).

Discussion

Water Column Attenuation is Critical to Stream Light Regimes

Ignoring stream water column light attenuation dramatically overestimates light available for autotrophs, particularly for deep, colored, and/or turbid systems. Indeed,

we observed the proportional reduction in light through the water column was often larger than through the canopy, even for narrow, shaded, shallow creeks (e.g., DRAIN; Table 2-1). Since light transmission declines exponentially with depth, even our clearest systems (SILUP and ICHE) attenuate >30% of light between the stream surface and bed because they are also deep (> 1 m). Moreover, temporal variation in water column light attenuation (largely discharge driven), is asynchronous with temporal variation (largely seasonal) in canopy attenuation. Consequently, open sky and stream surface light both misrepresent the magnitude of available light and fail to adequately capture its variation. Although we focused on DOM as the primary water column attenuating species, turbidity is likely another common light-attenuating factor in flowing waters (Julian and others 2008b; Hall and others 2015), with effects that would also be overlooked by stream surface light alone.

Benthic Light Regimes Best Predict GPP

Rigorously representing variation in benthic light inputs dramatically improved GPP predictions across sites. Light versus GPP correlations increased markedly with each incremental improvement in light characterization from open sky to stream surface to benthic light (Figure 2-2), supporting Hypothesis 1. Moreover, representing the benthic light regime also significantly improved GPP predictions, with mean benthic light serving as the most effective proxy for significant site-effects in our general linear models. Main effects and interaction models yielded similar adjusted R^2, both of which improved considerably over a model with daily light only (Table 2-2). Notably, similar model formulations using stream surface and open sky light yielded no meaningful improvement over the already weaker explanatory power of daily variation, illustrating

how critical enumerating the appropriate light regime is for predicting metabolic responses.

Improvements in GPP predictions with fitted site effects, and strong covariance of those effects with mean benthic light, may capture the capacity of autotrophs to utilize more light via higher biomass. In our main effects models, site impacts the fitted intercept, suggesting a fixed increase in GPP with higher mean light, regardless of daily bed irradiance. It is well documented that low autotroph biomass generally reduces primary production (Rosemond and others 2000), and site observations strongly support massive biomass variation. Whereas this supports interpreting site effects (and, by extension, mean light effects) as a measure of biomass stocks, we recognize that benthic communities comprise autotrophs that vary greatly in mass (e.g., unicellular algae/bacteria vs. macrophytes), so “biomass” may insufficiently capture site effects across systems. Further work is needed to link these effects explicitly to chloroplast density, but we note that aquatic communities respond strongly to long-term light conditions (Phlips and others 2000; Mulholland and others 2001) supporting the general inference that mean benthic light serves as a surrogate for biomass, and thus the system’s ability to capture incoming light. We observed a marked decline in model performance between using fitted site effects and using only mean benthic light (R^2 = 0.92 vs 0.78, respectively), which we attribute to the complex mechanisms that control biomass accumulation, which are only partially captured by mean light. Indeed, we considered alternative antecedent periods for estimating the mean light effect, reasoning that biomass accumulation has a particular time scale, but using mean benthic light over the prior week, month, or 3 months did not improve GPP predictions

compared with the mean light for the entire period of record. We note that our model R^2 of 0.78 is nevertheless far better than has been reported elsewhere for flowing waters (Acuña and others 2004; Roberts and others 2007; Beaulieu and others 2013; Dodds and others 2013). It seems likely this success derives from explicitly considering daily benthic light and also enumerating antecedent light effects on autotroph biomass (via mean benthic light), a consideration generally missing from metabolism studies. A crucial caveat to our results is that lotic systems with frequent scouring floods, where the biomass effect is poorly captured using mean light, requires a more sophisticated representation of biomass removal and recovery.

Light Use Efficiency Converges with Benthic Light

Full consideration of benthic light regimes supports Hypothesis 2 by indicating LUE convergence in two ways: First, we observe a reduction of LUE variation across sites with the full light model, and second, resulting LUE values align far more closely with values from other ecosystems. For the first convergence, we note at the outset that LUE values from individual site regressions are highly variable (-0.01 to 3.9%). This spatial variation appears to arise because of differences in mean benthic light, as discussed above. Recall that LUE encompasses both intrinsic chloroplast efficiency and autotroph light capture, which is determined by system biomass. Differences in canopy density dramatically affect LUE in terrestrial ecosystems (e.g., sparse tundra LUE ~ 0.4% vs densely canopied tropical forests LUE ~ 3.3%; Garbulsky and others 2010), leading to the use of absorbed (APAR) or intercepted PAR (IPAR) to calculate LUE values that are comparable across varying light capture (Gitelson and Gamon 2015). Measuring absorbed PAR in streams is challenging, but we demonstrate we can account for biomass and thus light capture differences among sites in our linear models

when we include mean benthic light. Indeed, our main effects model predicts GPP exceedingly well with a fixed LUE across sites (1.9%) because it adjusts the intercepts using mean light; this model suggests that a universal LUE is not untenable. A more statistically defensible but only slightly improved model, which considers daily light and mean light interactions, cuts LUE variation in half among sites (Figure 2-3). This supports a convergent LUE in flowing waters when considering the full benthic light regime, which accounts for both daily variation in energy inputs and site variation in light capture.

Model performance using only light is comparable for model configurations that consider only main effects (R^2= 0.78) and interactions (R^2 = 0.8), although AIC differs substantially. We propose that both models be considered for implications regarding LUE. The main effects model establishes a universal LUE value that easily allows extrapolating predictions to new sites. The interaction model, however, demonstrates the crucial role of biomass in adjusting LUE. LUE values from individual site regressions confirm that reaches with higher mean benthic light exhibited higher efficiencies (Figure 2-3; excluding SF2500 and SF2800 where metabolism is likely overestimated because of downstream transport of DO signals derived from high GPP spring sites in the effective reach). Resource use efficiency in forests can be higher with greater resource use (Binkley and others 2004), such that terrestrial LUE increases with increased light capture. Rather than “diminishing returns” with increased light at leaf and daily scales, an increase in LUE could be a consequence of higher “return on investment” because autotrophs invest in biomass growth under high input conditions, thereby enhancing

light capture, and thus increasing LUE. Whether this pattern applies for aquatic biofilm and macrophyte communities is unknown.

We also observed lotic LUE convergence with terrestrial values after accounting for benthic light regimes. Literature LUE values for freshwaters are low compared to terrestrial values, but generally neglect water column light attenuation. Our regional LUE values exhibited a range similar to other aquatic studies, but with a mean and standard deviation (1.5% ± 1.3%) in the middle of the range for crop and terrestrial systems (Figure 2-4). Explanations for lower LUE in aquatic ecosystems (Sand-Jensen 1997; Sand-Jensen and others 2007) include the inability for non-rigid aquatic canopies to optimize their structure for low and high light conditions, slower diffusion of O_2 and CO_2 in water, and background attenuation of incident light. Whereas the first two reasons may still be relevant, our work may obviate the need for them since accounting for benthic light availability places stream LUE values in the same range as terrestrial systems. Indeed, our main effects model converges on a LUE value (1.9%) identical to recent terrestrial values (mean of two cross-biome studies was 1.9%; Turner and others 2003; Schwalm and others 2006).

LUE convergence given differences in light capture aligns with evidence for universal quantum yields in plants and convergent LUE in terrestrial communities. At smaller scales, quantum yield convergence suggests a universal photosynthetic efficiency applicable across taxa. This efficiency depends on chloroplast thylakoid membranes dynamic enough to adjust the stoichiometry of these photosystems to maintain high quantum yield under diverse light conditions (Chow and others 1990). Assuming this mechanism for optimizing photosynthetic capacity is shared among

species as proposed in the Functional Convergence Hypothesis (Field 1991), we expect quantum yields to be relatively uniform, a prediction supported across many terrestrial species from diverse light habitats (Singsaas and others 2001). At larger scales, terrestrial plant communities that span a gradient of stress exhibit consistent LUE based on field experiments and remote-sensing (Field 1991). Since these LUE values are calculated based on APAR, accounting for biomass light capture, this suggests convergent LUE across terrestrial systems. Notably, some aquatic LUE estimates align with terrestrial values (Wassink 1959; Sand-Jensen and others 2007) supporting comparisons between aquatic and terrestrial communities. We note that primary production efficiency based on NPP is near 1% (Odum 1975). Assuming autotrophic respiration consumes 50% of GPP (Hall and Beaulieu 2013), that NPP efficiency yields a LUE based on GPP of 2%, nearly identical to what we observe.

Inference of LUE from synoptic across-site comparisons yields dramatic overestimates unless site variation in autotroph biomass is considered. When we estimated across-site LUE using mean GPP and mean light, we obtained a value three-fold higher than our final estimate (5.4% in Figure 2-2C vs. 1.9% in our final GLM). This approach was used in Odum (1957) to yield a LUE of 4% and can be extracted from inter-biome comparisons in Mulholland and others (2001) as 6.3%. This inflation arises because of positive covariance between long-term light and autotroph biomass stocks, which in turn allows greater light capture and thus a steeper slope between daily light and GPP. Although LUE values obtained in this way have some informative properties, it is both divergent from LUE values in other ecosystems and unlikely to be useful for predicting metabolic regimes of streams and rivers from models of light inputs. We

contend that our model, which considers both daily variation in benthic light and mean benthic light as a proxy for autotroph light capture, is more accurate for determining and predicting LUE across sites.

LUE convergence across sites (i.e., where mean benthic light is part of the light regime) enables predictions of expected GPP from light data alone. Like terrestrial ecologists characterize and monitor primary production over large areas (Hilker and others 2008), using a global value of LUE means aquatic ecologists can potentially map expected GPP from remote-sensed data: Remote-sensed open sky light can be used to model benthic light, which can be multiplied by LUE to determine the upper GPP envelope of rivers globally. Deviation from this “metabolic envelope” of expected GPP is, in turn, a powerful way to detect growth limitations other than light. This may include biomass limitation from disturbance or herbivory (Dodds and others 1996; Acuña and others 2004) and other factors that limit photosynthesis (Kolber and others 1990; Rosemond and others 2000).

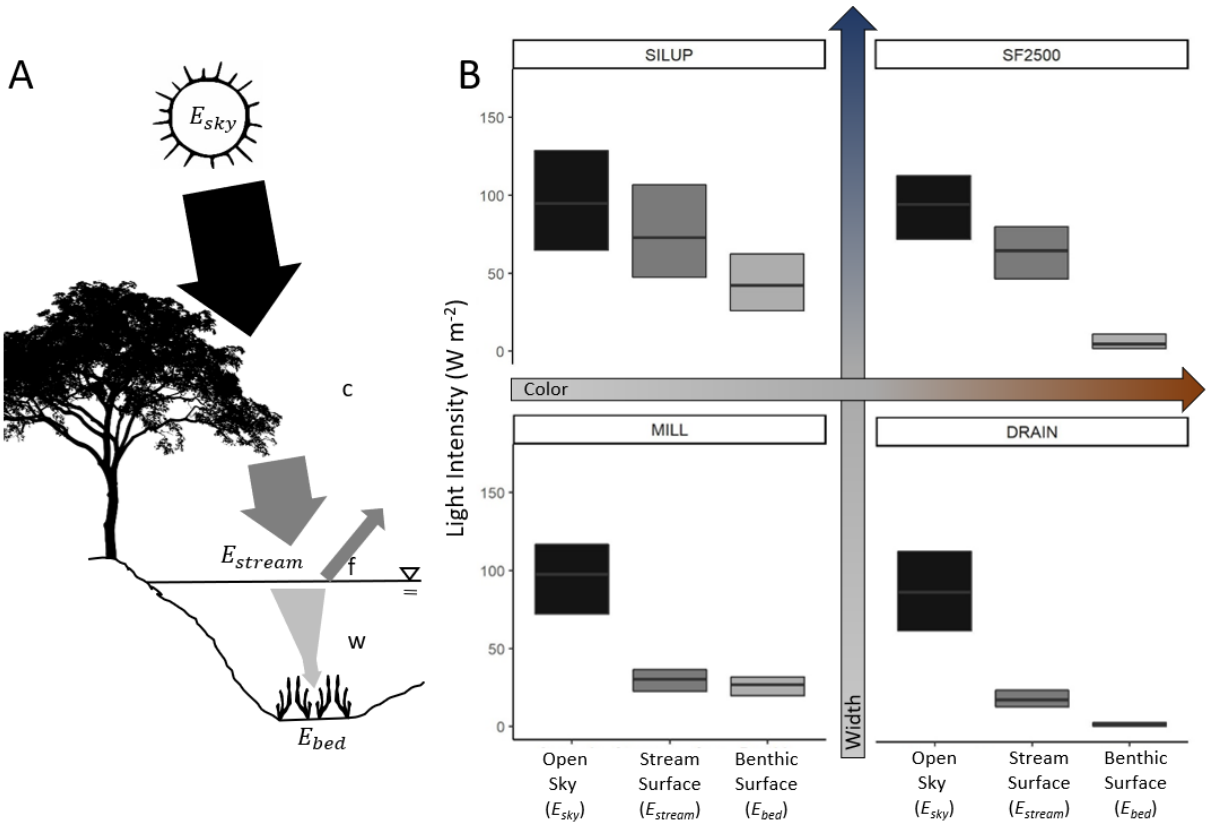

Figure 2-1. Light model and results. A) Conceptual framework of the Benthic Light Availability Model (adapted from Julian and others 2008). Open sky light (E_{sky}) is successively attenuated by canopy (*c*), reflectance (*f*), and water column (*w*) to obtain benthic light (E_{bed}). B) Measured E_{sky} along with modeled E_{stream} and E_{bed} for four sites spanning gradients of width (vertical axis) and color (horizontal axis).

Table 2-1. Site location (decimal degrees) and characteristics, including flow inter-quartile range (IQR), mean baseflow width and depth, and color (fluorescent dissolved organic matter, fDOM, measured as quinine sulfate equivalents, QSE). Also shown are the incremental percent reduction of light (mean and standard deviation) in the Benthic Light Availability Model between open sky (E_{sky}) and the stream surface (E_{stream}) and then between E_{stream} and the benthic surface (E_{bed}). Sites are grouped into blackwater (grey) and spring-fed rivers (white).

Site	Full name	Downstream station Latitude	Downstream station Longitude	Discharge IQR (m^3 s^{-1})	Baseflow stream width (m)
DRAIN	Drain Creek	29.8624	-82.2839	0.02 – 0.14	3
SF700	Santa Fe River 700	29.8461	-82.2197	0.2 – 1.8	5
SF2500	Santa Fe River 2500	29.8486	-82.7153	25 – 49	53
SF1500	Santa Fe River 1500	29.9217	-82.4264	0.6 – 6.4	27
SF2800	Santa Fe River 2800	29.9114	-82.8606	45 – 69	60
MILL	Mill Pond Creek	29.9644	-82.7621	0.88	11
ICHE	Ichetucknee River	29.9525	-82.7861	8 – 10	43
ALEX	Alexander Springs Creek	29.0461	-81.5083	3.1 – 3.6	59
SILMID	Silver River middle	29.2033	-82.0158	12 – 14	48
SILUP	Silver River upper	29.2162	-82.0457	12 – 14	74
SILLOW	Silver River lower	29.2100	-81.9930	13 – 17	33

Table 2-1. Continued

Site	Baseflow mean depth (m)	fDOM IQR (ppb QSE)	Light attenuation (%) E_{sky} to E_{stream}	Light attenuation (%) E_{stream} to E_{bed}
DRAIN	0.3	90 – 138	76 ± 10	84 ± 9
SF700	0.4	44 – 93	70 ± 11	73 ± 13
SF2500	2.0	21 – 102	31 ± 5	88 ± 10
SF1500	2.1	84 – 196	38 ± 4	96 ± 3
SF2800	2.9	19 – 58	22 ± 3	87 ± 10
MILL	0.4	2 – 5	68 ± 8	12 ± 2
ICHE	0.9	3 – 6	36 ± 4	27 ± 7
ALEX	1.4	12 – 69	26 ± 4	74 ± 20
SILMID	1.6	1 – 4	37 ± 6	37 ± 3
SILUP	2.1	0 – 1	22 ± 5	43 ± 2
SILLOW	2.2	4 – 6	49 ± 14	41 ± 9

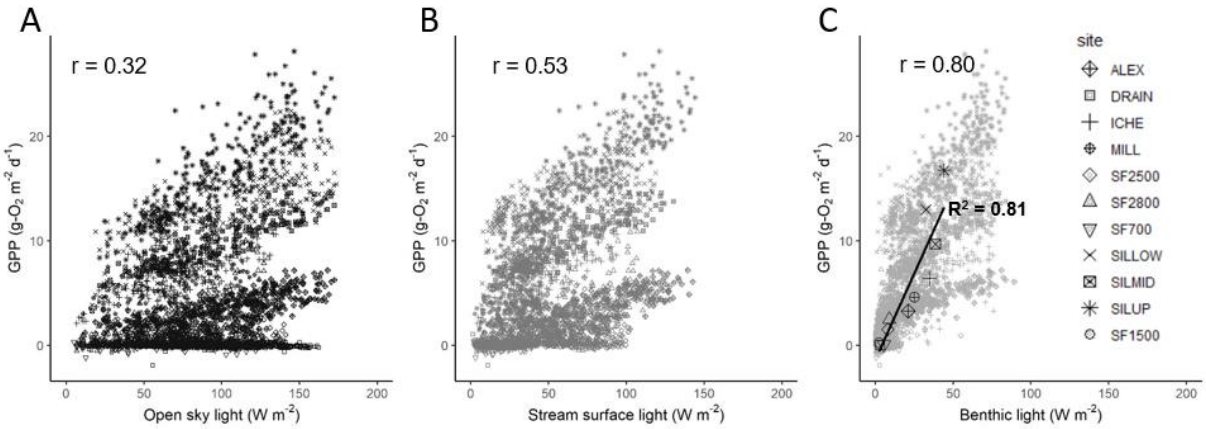

Figure 2-2. Global relationships between GPP and light for A) open sky, B) stream surface, and C) benthic light with correlation coefficients. For the benthic light model, we also show the regression between site mean GPP and site mean benthic light, which yields an overestimate of light use efficiency (LUE) of 5.4%.

Table 2-2. General linear model parameters for global models using daily and mean benthic light

Model: No site effects	GPP ~ Daily Light			
Coefficients	*Slope*	*SE*	*z-score*	*p-value*
Intercept	5.87	0.95	6.17	<2e-16
Daily Light	0.037	0.0004	89.43	<2e-16
Model Adjusted R^2	0.64			
F-statistic	7998 on 1, 4490 df; p < 2e-16			

Model: Main effects	GPP ~ Daily Light + Mean Light			
Coefficients	*Slope*	*SE*	*z-score*	*p-value*
Intercept	-19.14	0.087	-21.95	< 2e-16
Daily Light	0.019	0.0005	39.05	< 2e-16
Mean Light	0.035	0.0006	54.21	< 2e-16
Model Adjusted R^2	0.78			
F-statistic	8085 on 2, 4489 df; p < 2e-16			

Model: Interaction	GPP ~ Daily Light × Mean Light			
Coefficients	*Slope*	*SE*	*z-score*	*p-value*
Intercept	-7.90	1.05	-7.50	< 2e-16
Daily Light	0.0012	0.0011	1.08	0.279
Mean Light	0.028	0.00074	37.76	< 2e-16
Daily Light: Mean Light	0.000007	0.0000004	17.77	< 2e-16
Model Adjusted R^2	0.80			
F-statistic	5873 on 3, 4488 df; p < 2e-16			

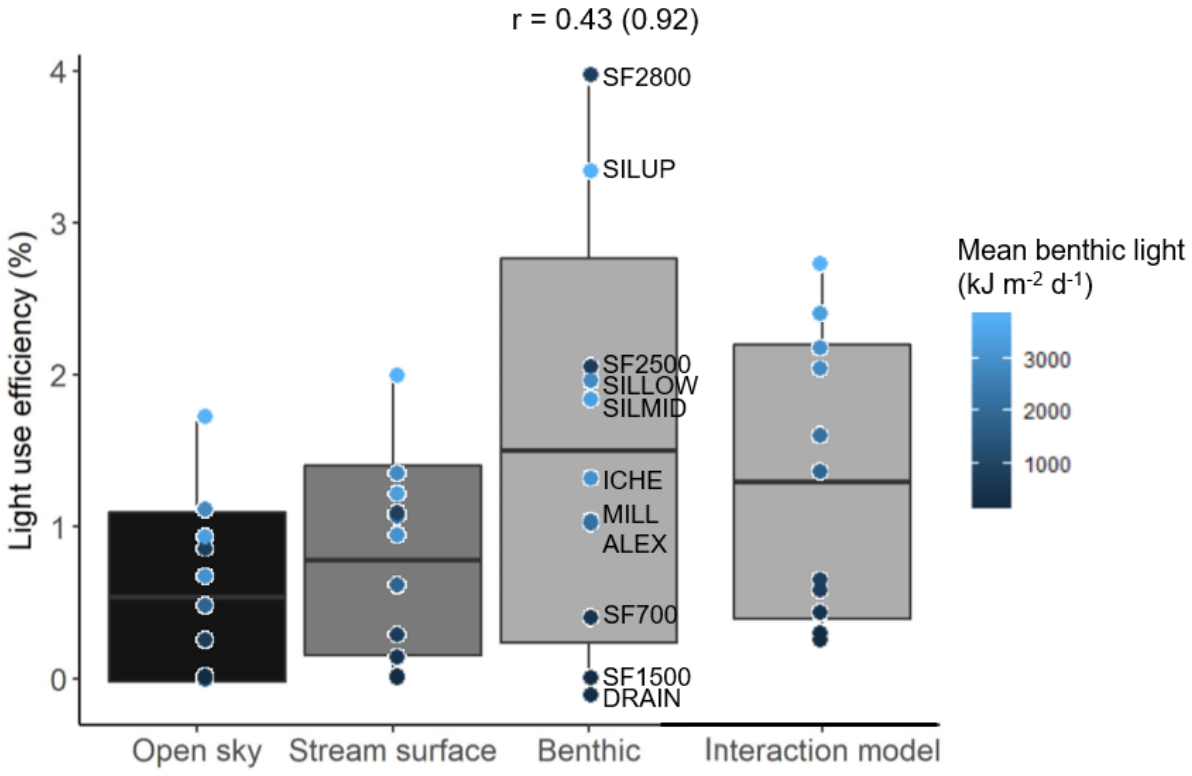

Figure 2-3. Distribution of individual site light use efficiency (LUE) calculated with open sky, stream surface, and benthic daily light, and predicted LUE using the interaction model, which considers daily and mean benthic light. Boxes are means and one standard deviation; whiskers show range. Correlation between light and LUE reported for benthic light (correlation excluding anomalous sites SF2500 and SF2800 in parentheses, see Discussion).

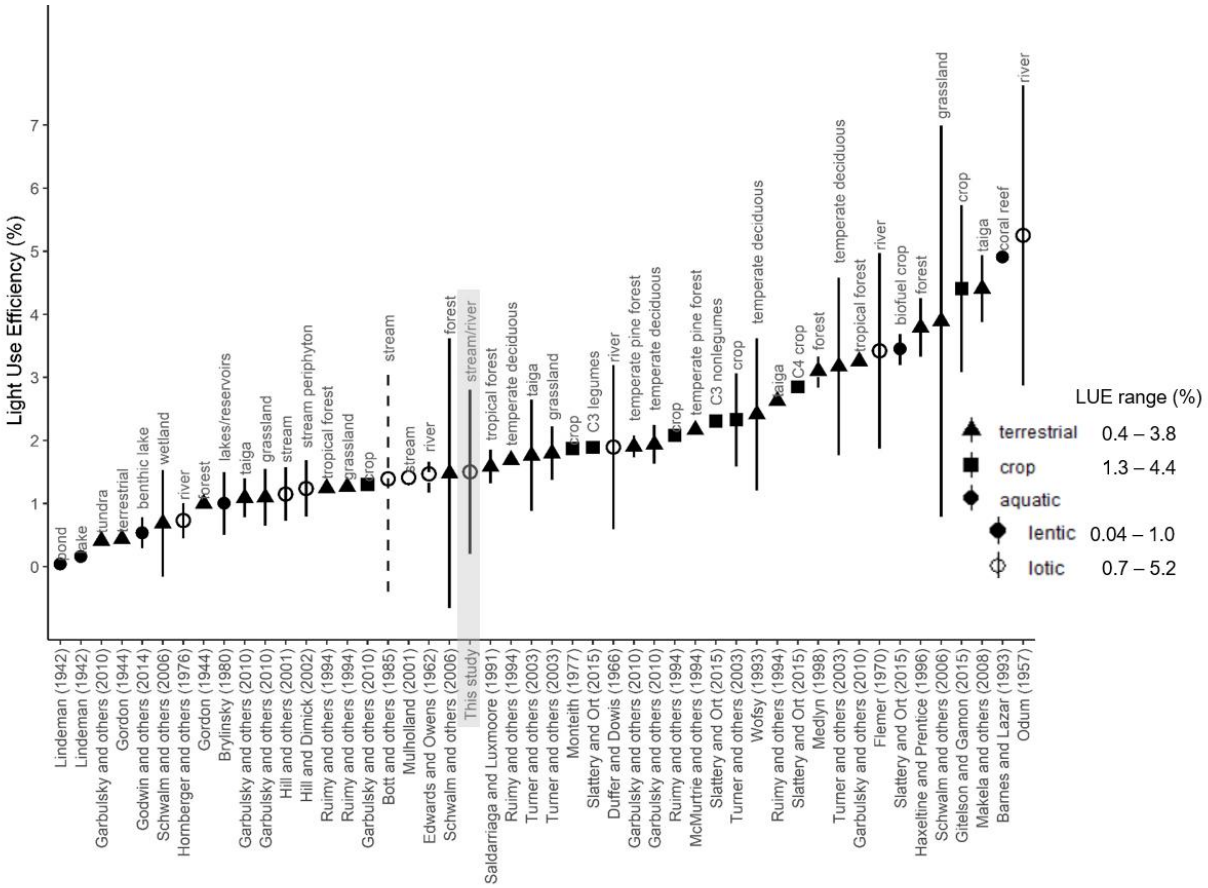

Figure 2-4. Literature light use efficiency (LUE) values (means with standard deviations) across ecosystem types. Literature values were standardized as described in supplemental materials. Dashed lines were used if only ranges of means were reported. To facilitate comparison with the literature, we report individual site LUEs from our study here, although our models show that LUE converges on 1.9% after accounting for the full benthic light regime (i.e. daily and mean light).

CHAPTER 3
RESPIRATORY QUOTIENT AND ANAEROBIC RESPIRATION AT POINT SCALES IN A HIGHLY PRODUCTIVE RIVER

Introduction

CO_2 evasion from streams and rivers is a globally important carbon flux (3.9 Pg-C y^{-1}; Drake and others 2018), and fluvial net ecosystem production (NEP, gross primary production minus community respiration) drives 28% of those emissions (Hotchkiss and others 2015). Because metabolic fluxes in streams are almost always calculated from the diurnal changes in oxygen concentrations, implicit in our metabolic carbon flux estimates is an assumption about the molar ratio of carbon dioxide biologically produced to oxygen consumed, i.e. the respiratory quotient (RQ). The most common assumption is that this ratio is 1.0, based on the complete oxidation of glucose ($CH_2O + O_2 \rightarrow CO_2 + H_2O$). RQs that departs from unity results in over/underestimates in the ecosystem respiration flux and alter the attribution of internal vs. external sources of stream CO_2 fluxes.

RQ refers to aerobic respiration by organisms or cells and is biochemically constrained by organic matter substrate (Berggren, Lapierre and del Giorgio, 2012). Natural variation in RQ arises from the type of organic matter respired (Masiello and others 2008). Aerobic respiration of proteins and lipids, as opposed to pure carbohydrates, lowers the RQ from 1 to 0.7 (del Giorgio and Williams, 2005). Some studies assume community RQ is 0.85 based on aerobic decomposition of living tissues (Boucher, Clavier and Garrigue, 1994), although prokaryotic metabolism can yield RQs > 1 (Murray and Rich, 1995). RQ based on marine planktonic stoichiometry is 0.89 (Hedges and others 2002), but higher if the respiration product is nitrate instead of ammonia (Richardson and others 2013). RQ in streams and rivers is rarely measured,

but was calculated as 1.3 or 1.0, based on mineralization of particulate organic material (POM) or dissolved organic matter (DOM), respectively (Richardson and others 2013).

"Apparent" (Sobek and others 2017) or "community" RQ (Boucher, Clavier and Garrigue, 1994; Berggren and others 2012) is obtained from coupled O_2 and CO_2 fluxes at the ecosystem-level. It is biochemically constrained by organic substrate (Del Giorgio and Williams, 2007; Berggren and others 2012), and also controlled by all biotic processes that use or release O_2 or CO_2 in the dark, including aerobic and anaerobic metabolism and biological oxidation of reduced compounds (e.g. chemoautotrophic processes such as nitrification). Freshwater measurements of community RQ have yielded a broad range of results. Lentic water column RQ values converged at 1.2 (Berggren and others 2012) with photooxidation driving RQ even higher (Allesson, Ström and Berggren, 2016), but sediment core RQs are generally < 1 (Sobek and others 2017). Measured community RQ in river microcosms averaged 0.7 (Beyers, 1963). This range presents a challenge in selecting a representative value for estimating carbon fluxes from oxygen metabolism.

Empirical community RQ values are valuable because they enable estimation of total anaerobic respiration rates (minus methanogenesis). Stream ecologists usually sum across individual terminal electron acceptors (i.e. nitrate, iron, manganese, sulfate) to estimate anaerobic respiration (Baker and others 1999). In flowing waters that are assumed to be well-oxygenated, anaerobic respiration is thought to be balanced by oxidation. That is, whereas anaerobic respiration, which produces CO_2 without consuming oxygen, occurs deeper in the sediments, the reduced products (e.g. Fe^{++}, ammonia, HS^-) diffuse into the aerobic zone where they are oxidized, consuming

oxygen without producing CO_2. The sediment accumulation of reduced compounds results in an “oxygen debt” with the result that higher observed community RQ values are common in marine (Boucher and others 1994; Glud, 2008) and lentic sediments (Wetzel and others 1972; Rich, 1975; Sobek and others 2017). Measurement of aerobic community RQ and community RQ during induced anoxic conditions provides an opportunity to estimate anaerobic respiration by removing oxidation. Boucher and others (1994) applied this logic to estimated that anaerobic respiration accounted for 40% of total respiration in a tropical lagoon. To our knowledge, this has not been explored in lotic settings.

Few empirical studies have quantified community RQ values in lotic ecosystems. They are difficult to measure (e.g. Hargrave and Connolly, 1978; Naiman and Sedell, 1980), in part because of challenges in integrating the water column and sediment in a representative way, and partly because advection, reaeration, and diurnal oxygen variation caused by photosynthesis make it difficult to attribute gas fluxes uniquely to respiration. Benthic chamber mesocosms offer one tool to quantify riverine RQ. Aquatic ecologists have a long history of using mesocosms to bridge the gap between simple, but artificial laboratory environments and complex natural settings where there is limited capacity to isolate or control processes (Odum, 1984). To isolate river respiration processes from photosynthesis, we designed shaded benthic chamber mesocosms that enable whole-ecosystem representation. Since hyporheic respiration is estimated to account for >40% of ecosystem respiration (Battin and others 2003), it is critical for respiration studies in chambers to capture both water column processes and sediment processes. In natural systems, where spatial variability in physical and chemical drivers

is substantial, benthic chambers further enable the interrogation of the biotic and abiotic factors that control metabolic rates and processes (Reijo and others 2018). Like bottle incubation studies, benthic chambers allow resource manipulations over wider concentration gradients (e.g., oxygen or nitrate; Hensley and Cohen 2020) than can be observed naturally or experimentally, particularly given the challenges of manipulating solute composition over entire reaches. Unlike most bottle incubations, however, metabolism measured in benthic chambers scales reasonably well to whole-reach metabolism (i.e., without chamber artifacts) (Reijo and others 2018) and nutrient retention processes (Hensley and Cohen 2020), likely because benthic chambers perturb key constituents in ecosystems minimally. Our chambers were instrumented to measure dissolved oxygen (DO) and CO_2 at high temporal resolution, allowing measurement of respiration rates and community RQ both with and without labile carbon enrichment. With that experimental design, we sought to test the hypotheses that 1) RQ values are 1 because of the respiration of relatively labile carbon in our highly productive river system, and 2) anaerobic respiration accounts for a considerable proportion of total respiration.

Methods

Benthic Chamber Design

Our benthic chambers were designed to isolate a realistic vertical section of the river, including sediments and water column, as well as interactions with the atmosphere (Figure 3-1). Although we intentionally precluded longitudinal flow to isolate the chemical signals of ecosystem processes in a single “packet” of water, we preserved well-mixed vertical circulation using submersed pumps (model: DC30A-1230; 4 L min-1). Benthic chamber construction is described in detail in Reijo and others

(2018) and was updated to include two removable deck plates (15-cm diameter) installed on the upstream and downstream faces of the chamber to allow chamber flushing with river water between deployments. To isolate ecosystem respiration (i.e. prevent photosynthesis), we blocked incoming sunlight by wrapping the plexiglass sides with opaque fabric and covered the chamber top with a 90 cm × 90 cm reflective shade material to limit internal warming. This horizontal covering was elevated 13 cm above the chamber using rebar anchor rods to ensure continued gas exchange. A pendant light meter (Onset HOBO UA-002-64, Massachusetts, USA) confirmed that negligible light entered the shaded chamber.

Benthic chambers were instrumented with an optical DO sensor (Onset HOBO U-26, Massachusetts, USA) that also measured temperature, paired with a submersible infrared CO_2 gas analyzer (0 – 5000 ppm, 0 – 20,000 ppm range, Eosense eosGP, Nova Scotia, Canada) connected to a datalogger (Campbell Scientific CR800, Utah, USA). Sensors were calibrated before the start of each experiment to water-saturated air for DO and CO_2 gas of known concentrations and to each other. pH (digital ISFET probe, Campbell Scientific, CS526, Utah, USA) was measured in one of the control chambers (location 7). Sensors and pumps were submerged at a depth of ~20 cm.

Study Site

The Ichetucknee River is an 8-km-long, low-gradient (0.7 m/km; Khadka, Martin and Kurz, 2017) spring-fed river, which flows into the blackwater Santa Fe River in north-central Florida, USA. River water emerges entirely from six large springs and many smaller springs. Like other rivers fed by springs from the Upper Floridan Aquifer, the discharge, temperature, and chemistry are remarkably stable (Odum, 1957). The major springs and the first 5 km of river lie within Ichetucknee Springs State Park. Our

experiments were conducted in a reach known as the grassy flats, approximately 1200 m downstream of the headspring, where the channel morphology is wider (50 – 100 m; de Montety and others 2011) and shallower (0.2 – 0.5 m; Khadka and others 2017) than other reaches.

The remarkably clear, thermally-stable, and nutrient-rich water of the Ichetucknee River results in a highly productive lotic ecosystem, with rates of gross primary production (GPP) that slightly exceed aerobic ecosystem respiration (ER) (10.1 and 8.5 g-O_2 m^{-2} d^{-1}, respectively; Heffernan and Cohen 2010). The entire river supports dense beds of submerged eelgrass (*Sagittaria kurziana* and *Vallesnaria americana*) covering 78% of the benthic area, and in the grassy flats, emergent macrophytes (*Zizania aquatica*) are interspersed within these eelgrass beds (de Montety and others 2011). Care was taken to enclose only submerged eelgrass within our benthic chambers. Other primary producers include benthic and epiphytic filamentous algae, which can account for more than 50% of primary production in these spring-fed rivers, despite their small biomass (McBride and Cohen, 2019). Although aquifer water discharging from spring vents have some of the lowest dissolved organic carbon (DOC) concentrations in the world, macrophytes exude 17% of GPP as DOC, contributing to large accretion of DOC longitudinally (Duarte and others 2010). Sediment thickness is spatially heterogenous, ranging from bare rock to >2 m of fine-grained silt, organic matter, and shell material (Hensley and Cohen, 2012).

From October 2018 to April 2019, Ichetucknee River had higher than normal flow (10.4 m^3 s^{-1}) with a mean temperature and specific conductance of 21.4 °C and 302 µS cm^{-1}, respectively. Mean DO in the fall (no spring data available because of sensor

failures) was 4.9 mg L^{-1}, mean pCO_2 was 2766 ppm, and mean pH was 7.13. Bicarbonate alkalinity was 2.91 mM (de Montety and others 2011).

Deployments

Up to four chambers were deployed simultaneously for 3-4 days at a time in Oct – Nov 2018 and Mar 2019. Chambers were moved after several deployments for a total of eight locations and 39 deployments. Chambers were flushed for >20 minutes between deployments, which, given a mean water velocity of 0.052 m s^{-1} where the chambers were deployed, was more than sufficient (flushing >4.5 m^3) to turn over the water volume of the chamber. Two of the four chambers each week were control chambers, and two were dosed with 3.69 g-C of sugar (sucrose, 42% carbon) to approximate 3 times the amount of carbon respired by aerobes under normal river conditions.

For each deployment, chambers were flushed, resealed, then dosed with sugar and a conservative tracer (KCl). Water depth was also measured. Water samples were collected from within each chamber in 20 mL scintillation vials before additions, after additions were thoroughly mixed with chamber water, and again at the end of the 3-4 day deployment. Water samples were immediately hand-filtered (0.45 µm pore size), stored on ice, and frozen for later analysis of DOC, Ca++, and Cl-. DOC, calcium, and chloride were measured using a Shimadzu TOC-5000A total organic carbon analyzer, Dionex model 500DX ion chromatograph (IC), and Accumet XL250 (Fisher Scientific, USA), respectively. To assess potential chamber leakage, we dosed chambers with 100 mL of 32000 ppm KCl solution to enrich chambers ~15 mg L^{-1} above ambient chloride concentration of ~10 mg L^{-1} (Kurz and others 2015) when they were moved to a new location. The loss of Cl- throughout the deployment was compared to the complete

turnover of water in the chambers. We considered <10% leakage from diffusive exchange with hyporheic pore waters (Kurz and others 2015) acceptable. In total, we discarded data from five deployments due to leakage.

Reaeration

To account for oxygen gained and CO_2 lost through gas exchange, we measured gas transfer velocities (k_{CO2} and k_{O2}; m d^{-1}) for shaded benthic chambers. We measured k_{CO2} empirically using two methods: The first was a floating dome method (Copeland and Duffer, 1964) with modifications. A clear, plastic storage container (area = 0.084 m^2) was overturned on the water surface, supported by flotation collars to penetrate 5 cm into the water, yielding a constant headspace volume of 15.5 L. CO_2 was injected into the headspace, and partial pressures ($pCO_{2,air}$, ppm) were measured every minute for >20 minutes. We also monitored river water pCO_2 ($pCO_{2,water}$, ppm) below the dome with a second sensor to determine the equilibrium value.

The second method for assessing gas exchange was CO_2 injection following the logic of McDowell and Johnson (2018). CO_2 gas (~650 kPa in the tank) was bubbled at 10 PSIG through a ceramic diffuser at the bottom of the chamber for 1 minute, driving water concentrations to well above ambient levels (~15000 – 20000 ppm). The air in the chamber was fanned for 5 minutes to ensure CO_2 gas (which is heavier than air) did not sit at the air-water interface and slow natural atmospheric diffusion. Water pCO_2 was logged every 15 minutes for at least 24 hours.

The slope of CO_2 concentrations vs. time defines the molar CO_2 flux (FCO_2, mol m^{-2} d^{-1}), from which we estimated k_{CO2} following Khadka, Martin and Jin (2014) and McDowell and Johnson (2018) for the floating dome and gas injection methods,

respectively. For the floating dome, we used the ideal gas law to convert pCO_2 change (P, ppm d^{-1}, converted to atm by dividing by 10^6) to molar change (n, d^{-1}):

$$n = \frac{PV}{RT} \tag{3-1}$$

where V is the floating dome volume (L), T is air temperature (K), and R is the ideal gas constant (0.0825 atm L mol^{-1} K^{-1}). F_{CO2} is n divided by the floating dome footprint (m^2). For the gas injection, the linear pCO_2 change is converted to molar change with Henry's law and divided by the benthic chamber footprint. For both methods, we solved for k_{CO2} (d^{-1}) using:

$$k_{CO_2} = \frac{F_{CO_2}}{(K_H \times 1000 \times z)\left(pCO_{2,water} - pCO_{2,air}\right)} \tag{3-2}$$

where K_H is the temperature dependent Henry's constant (0.034 M atm^{-1} at 25 °C) and z is mean water depth (m).

In total, we conducted five floating dome and five gas injections. Wind speeds were recorded at the nearest Florida Automated Weather Network (fawn.ifas.ufl.edu) station (Alachua) and used to determine the exponent for Schmidt number conversions. k_{CO2} was converted to k_{600}, from which we estimated k_{O2} using Schmidt number scaling (Raymond and others 2012).

Data Analysis

To compare gas fluxes on a molar basis, we converted pCO_2 measured with CO_2 sensors in ppm to dissolved CO_2 concentration ($CO_{2,stream}$, M) using Henry's Law:

$$CO_{2,stream} = K_H \times \frac{pCO_2}{10^6} \tag{3-3}$$

DO concentrations in mg L^{-1} were converted to M using the atomic mass of oxygen.

Metabolic fluxes of DO (*metDO*; M d^{-1}) and CO_2 (*metCO2*; M d^{-1}) were calculated as the difference between observed changes in stream concentrations ($\Delta DO/\Delta t$ and $\Delta CO2/\Delta t$) and reaeration fluxes:

$$metDO = \frac{\Delta DO}{\Delta t} - k_{O2}(DO_{sat} - DO_{stream}) \quad (3\text{-}4)$$

$$metCO2 = \frac{\Delta CO_2}{\Delta t} + k_{CO2}\left(CO_{2,stream} - CO_{2,sat}\right) \quad (3\text{-}5)$$

where DO_{sat} is the saturation DO at a specific water temperature and $CO_{2,sat}$ is the dissolved CO_2 equilibrated with air (400 ppm). Metabolic fluxes were smoothed using moving averages (1.5 hour windows), then converted to benthic fluxes by multiplying by chamber water depth. We compared *metCO2* between control and sugar treatments with a two-sample t-test.

To calculate apparent aerobic RQ for each deployment, we calculated the ratio of cumulative metabolic fluxes for CO_2 and DO when the chambers were not hypoxic (>2 mg L^{-1}):

$$RQ = \frac{\sum metCO2}{\sum metDO} \quad (3\text{-}6)$$

To test the hypothesis that RQ was the commonly assumed 1 in both control and sugar treatments, we used a one-sample, two-tailed t-test. We also calculated the community RQ for the ~3 days when chambers were anoxic (RQ_{anoxia}, chambers were open to gas exchange with the atmosphere, so there was oxygen consumed even when DO < 0.5 mg L^{-1}).

We calculated the proportion of total respiration that was anaerobic respiration (*ANR*):

$$ANR = \frac{RQ_{anoxia} - RQ}{RQ_{anoxia}} \times 100 \quad (3\text{-}7)$$

Results

Since community RQ represent only biological fluxes, observed changes in gas concentrations in benthic chambers were corrected for reaeration fluxes. Mean k_{600} from 10 empirical measurements was 0.46 ± 0.16 d^{-1}. This is lower than k_{600} for the Ichetucknee River calculated from equations (3.03 d^{-1}; Raymond and others 2012), but we expected the walls and top of the benthic chamber to impede wind flow and hence, reaeration. Mean water depth in chambers was 0.58 ± 0.09 m, resulting in a mean water volume of 214 L.

CO_2 metabolic fluxes in benthic chambers were nearly identical to DO metabolic fluxes during control deployments, but twice as high in sugar treatments (Figure 3-2). Initial metabolic CO_2 fluxes, which we equated with benthic chamber ER, averaged 113.0 mmol m^{-2} d^{-1} (equivalent to 1.36 g-C m^{-2} d^{-1}). Control deployments typically reached anoxia (with the reaeration correction) within 24 hours, with sugar treatments sometimes reaching anoxia within a few hours. After anoxia was reached, DO metabolic fluxes averaged 82.7 ± 16.2 mmol m^{-2} d^{-1}, which is essentially reaeration's contribution of oxygen to the chamber water. Meanwhile, CO_2 metabolic fluxes averaged 87.7 ± 24.5 mmol m^{-2} d^{-1} in control chambers and 182.7 ± 62.8 mmol m^{-2} d^{-1} in sugar treatments. Metabolic CO_2 fluxes in the control and sugar treatments were significantly different from one another ($p = 0.01$). Metabolic CO_2 fluxes were also much more variable in sugar treatments than control: The standard deviation for CO_2 fluxes in sugar

treatments averaged 102.7 mmol m^{-2} d^{-1}, compared to 23.1 mmol m^{-2} d^{-1} for control treatments.

Control and sugar treatments exhibited different patterns regarding the quantity of DOC over the 3 – 4 day benthic chamber deployments. Ichetucknee River DOC was 2.86 mg L^{-1} at grassy flats. DOC increased by 1.67 ± 2.10 mg L^{-1} during control deployments, but for sugar treatments, average DOC change was -11.59 ± 7.11 mg L^{-1} following sugar additions. This is equivalent to 186.9 mmol m^{-2} d^{-1} of carbon consumed in sugar treatments and agrees very well with calculated metabolic CO_2 fluxes (182.7 mmol m^{-2} d^{-1}). Of the 9.94 g-C m^{-2} DOC added to sugar treatments, 68% was consumed over three-day deployments.

Ca^{++} concentrations (n = 3) were measured to determine if carbonate dynamics consumed or produced CO_2 in addition to metabolism. Measured calcium ion concentrations were inconclusive: Mean change in calcium concentration was 0.35 mM, but indicating calcite precipitation in some deployments and calcite dissolution in others (unrelated to controls or sugar treatments).

Mean aerobic community RQ for the control treatments was 0.8 ± 0.09. Mean aerobic RQ for the sugar treatments was 0.68 ± 0.23. Aerobic RQs for both treatments were significantly different from 1 ($p < 0.000$), but not significantly different from one another ($p = 0.240$; Figure 3-3). RQ_{anoxia} was 1.15 ± 0.22 and 2.10 ± 0.54 in control and sugar treatments, respectively, and were significantly different from aerobic RQ ($p < 0.019$). Anaerobic respiration was 28 ± 19% of total respiration and 39% of aerobic respiration in control chambers. In sugar treatments, anaerobic respiration was 65% of total respiration and 186% of aerobic respiration.

Discussion

The community respiratory quotient departed significantly from the assumed value of 1. Because we not only measured riverine RQ, but also to compared it to values measured during respiration of a known substrate (sucrose), we were able to draw two novel inferences. First, the organic matter respired aerobically was similar in composition and lability to carbohydrates since control and sugar treatments did not have significantly different RQ. We expected that in the highly productive and biomass-dense Ichetucknee River system, ER would have a large autotrophic respiration component. RQ in many plant species converges on 1 (Rabinowitch, 1945), suggesting plant respiration utilizes primarily carbohydrates. Submerged macrophytes in this system also exude approximately 17% of GPP as labile DOC (Duarte and others 2010), which fuels heterotrophic respiration. More refractory DOC from upstream and diffuse groundwater inputs fuel heterotrophic respiration in many streams and rivers, but GPP > ER at Ichetucknee, implying that there is always a source of labile, autochthonously-derived DOC that is preferentially respired, and diffuse groundwater inputs are miniscule (<3% of discharge; Kurz and others 2015), so refractory DOC is probably not an important organic matter substrate for ER. Results from various studies show dissolved organic matter provides 11 – 70% of organic substrate for stream ER (Kaplan and Cory, 2016), so the decomposition of particulate organic carbon could also be a major respiration pathway. Beyers (1963) calculated the RQ of respiring *Vallisneria* based on its composition to be 0.9 – slightly less than respiring solely carbohydrates. However, control chamber RQ was notably – but not significantly – higher than sugar treatment RQ, affirming that *Vallisneria* was probably not the principal substrate.

Our results further show that low RQ values were not determined by organic matter substrate, but rather by other processes that affect dissolved gases. If community RQ was principally dependent on organic matter stoichiometry, RQ in sugar treatments should have been 1 if DOC was the major substrate for ER or 0.9 (and above) if particulate organic carbon (i.e. degraded *Vallisneria*) was predominantly respired (Beyers, 1963). Recent studies have questioned the approach of estimating RQ strictly based on organic matter stoichiometry (Sobek and others 2017), which, along with our results (RQ = 0.8), suggest the relevance, or even primacy, of system-level controls. To explain that measured RQ in sugar treatments was <1, we propose either incomplete oxidation of DOC to CO_2 during respiration or consumption of CO_2 by carbonate buffering. Both scenarios would decrease the pCO_2 measured by our sensors, resulting in lower RQ values.

In a hard-water system such as Ichetucknee River, carbonate buffering needs to be considered when calculating community RQ. Carbonate buffering could have lowered our community RQ values in two ways: First, in high alkalinity waters, some of the CO_2 produced during respiration may be dissolving $CaCO_3$ and thus converted to bicarbonate. As a result, the concentration gradient of CO_2 between the atmosphere and water is not as great, leading to slightly lower reaeration rates (Stets and others 2017) and thus underestimating metabolic CO_2 flux based on Equation 3-5. Second, it is also possible that although Ichetucknee River never gets undersaturated with respect to calcite over the diel cycle (de Montety and others 2011), calcite dissolution is a chamber artifact that lowers measured RQ values. We do not have Ca^{++} ion concentrations before and after every deployment to detect consistent patterns in calcite dynamics and

correct for the corresponding alkalinity shift (see Boucher, Clavier and Garrigue, 1994). Our limited Ca^{++} data nevertheless indicate both net calcite dissolution during some deployments and net precipitation during others.

Anaerobic respiration accounted for a low, but significant portion of total ecosystem respiration in control chambers. In anoxic control chambers, DO and CO_2 metabolic fluxes were almost equal, which suggests that there is little anaerobic respiration (which produces CO_2 without consuming DO) and the metabolic DO and CO_2 fluxes represent aerobic respiration using the reaeration of O_2. Such a conclusion, however, is predicated on a community RQ of 1: Considering measured community RQ values are <1, anaerobic respiration is definitely occurring. Our estimate of anaerobic respiration (39% of aerobic respiration) based on the difference between RQ and RQ_{anoxia} is realistic given denitrification rates in this system: Heffernan and Cohen (2010) found denitrification rates averaging 428 mg NO_3-N m^{-2} d^{-1}, which assuming complete conversion of nitrate to N_2 gas, amounts to 38.2 mmol-C m^{-2} d^{-1}, which is 41% of aerobic respiration observed in open waters at Ichetucknee River. Denitrification is only one of the possible anaerobic respiration pathways, although the most likely in riverine systems.

We raised community RQ considerably with sugar additions in anoxic chambers, presumably by stimulating anaerobic respiration with a labile carbon source. From this response, we infer that the organic matter usually available for anaerobic respiration is more refractory than sucrose. It has been estimated that up to 90% of a microbial community can be dormant at any given time (Nemergut and others 2013), awaiting the departure of environmental stressors such as substrate limitation, so the surge in

anaerobic respiration with labile carbon addition is not surprising. Metabolic CO_2 fluxes from anaerobic respiration were variable, perhaps because of uneven delivery of sugar to sediments where the majority of respiration occurs.

Community RQ values from our control chambers, which mimic natural river conditions as faithfully as possible, were within the ranges, but less variable and lower than literature values from other aquatic systems (Figure 3-4). In freshwaters, many more community RQ values have been measured for lentic systems than for lotic systems. Our *in situ* mesocosm RQ values were similar to Beyers's (1963) nighttime RQ values from laboratory microcosms. In that study, the microcosms were established with water, carbonate sediments, and *Vallisneria* (with attendant epiphytic algae) from a spring-fed river, underscoring the compositional similarity with our chambers.

Our community RQ values are on the low side of literature values, with major implications for estimated carbon fluxes. Using a community RQ of 0.80, the ER carbon flux of Ichetucknee River is substantially lower compared to assuming a value of 1.0 (i.e., ER = 2.54 vs 3.17 g-C m^{-2} d^{-1}). This change, in turn, doubles ecosystem NEP (1.23 vs 0.60 g-C m^{-2} d^{-1}). Because many lotic systems are more heterotrophic than the Ichetucknee River, and support respiration with more refractory dissolved and particulate organic carbon, our RQ values may not be generalizable, leading to smaller impacts on carbon flux estimates. Nevertheless, if our findings regarding the RQ are widely applicable, the impacts to the global estimates of NEP would be substantial, implying 9% less stream CO_2 evasion that is attributed to internal metabolic processes. This shift in the attribution of stream carbon fluxes, coupled with a recent synthesis

across lakes suggesting RQ is substantially greater than 1 (Berggren and others 2012), cautions freshwater ecologists to consider RQ assumptions carefully.

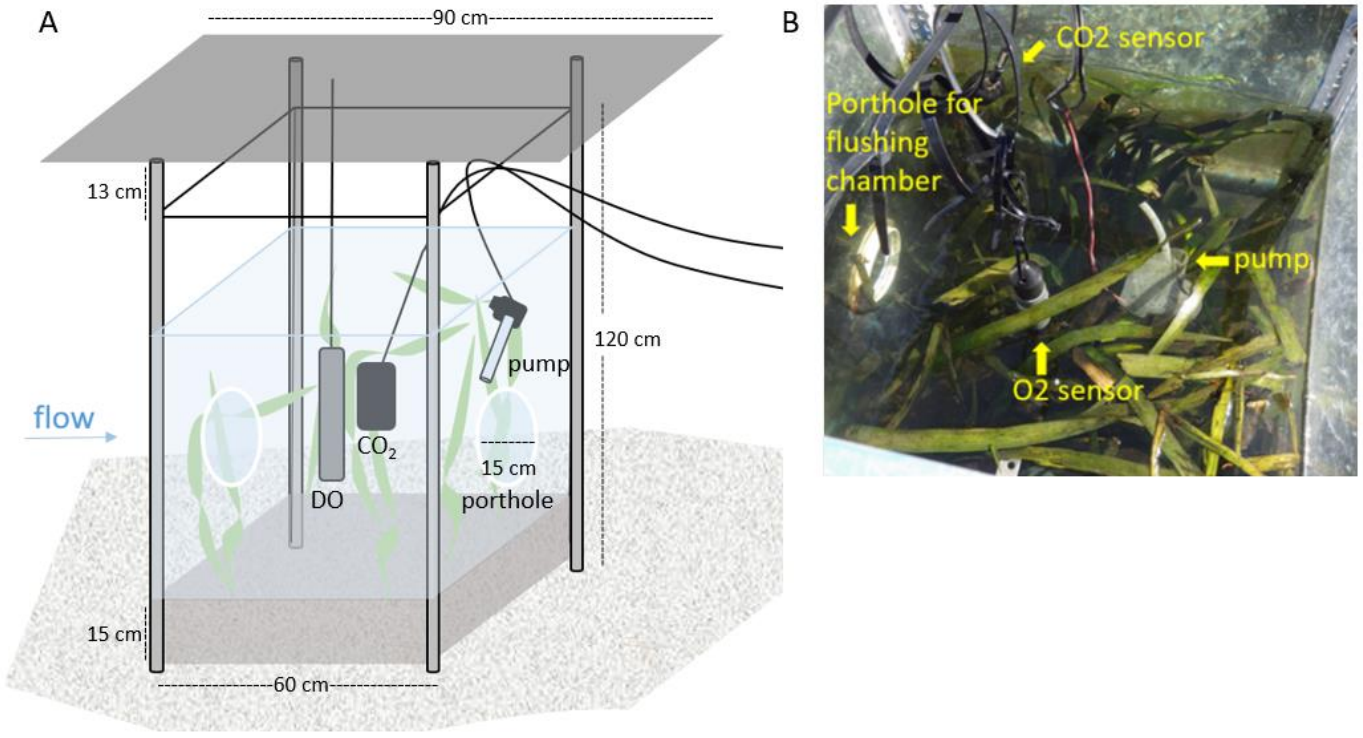

Figure 3-1. Schematic (A) of benthic chamber with photo of interior (B).

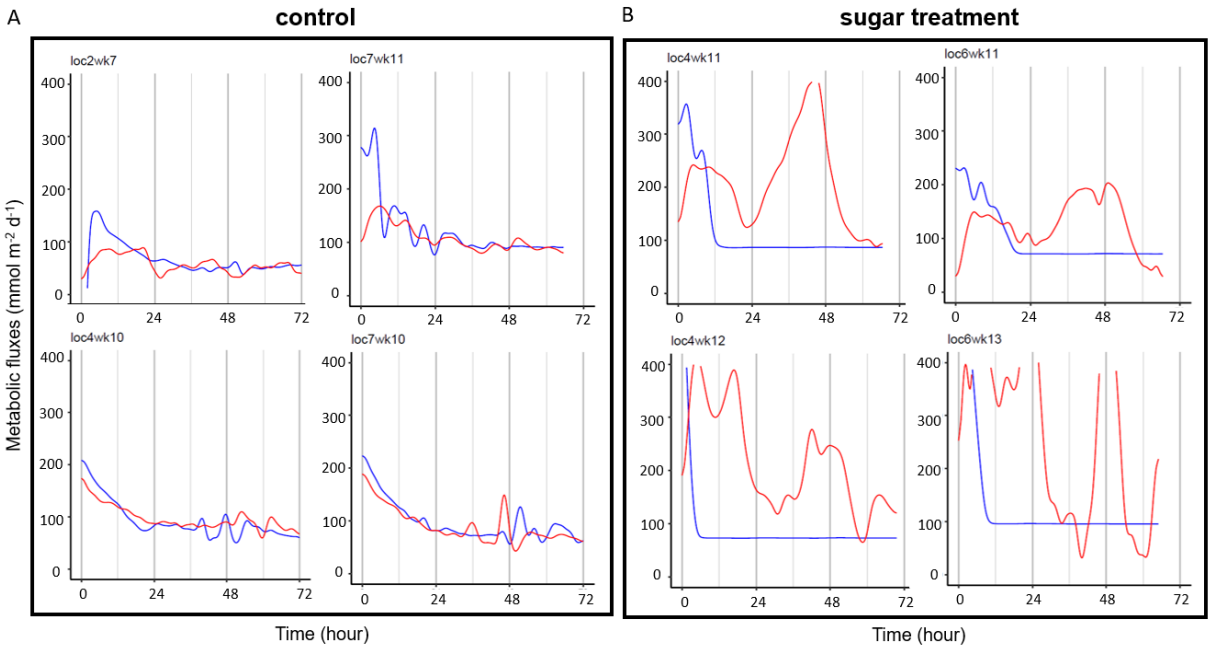

Figure 3-2. Dissolved oxygen (blue) and CO_2 (red) metabolic fluxes in control (A) and sugar treatments (B).

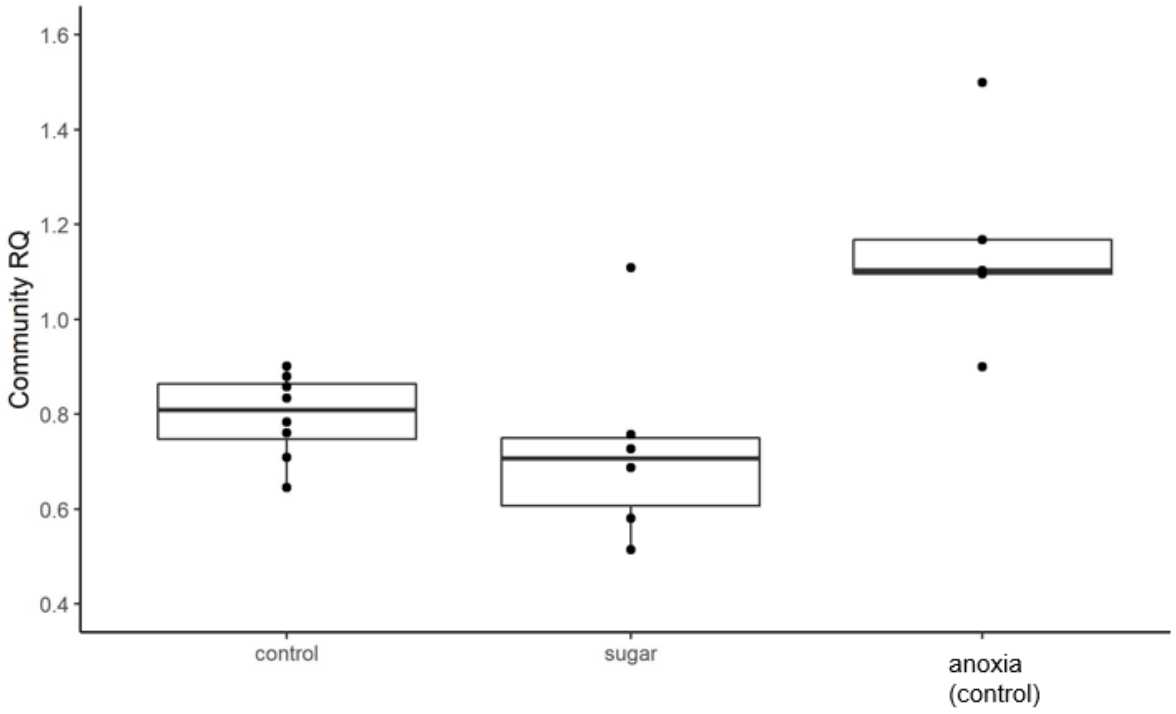

Figure 3-3. Community respiratory quotient (RQ) values measured in benthic chambers.

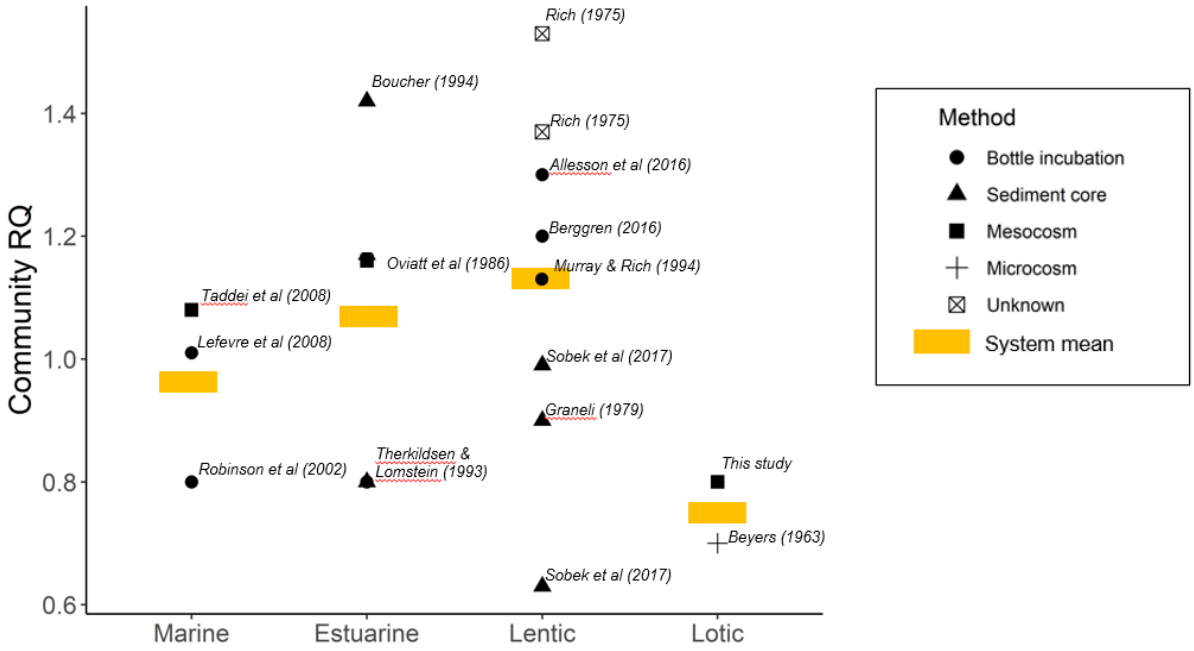

Figure 3-4. Empirical mean community respiratory quotient (RQ) values from the aquatic literature.

CHAPTER 4
CO_2 EVADING FROM A LOWLAND STREAM NETWORK ORIGINATES MOSTLY WITHIN THE RIVER CORRIDOR

Introduction

Inland waters are control points for continental carbon budgets (Cole and others 2007; Ciais and others 2008) with riverine carbon evasion similar in magnitude to "missing" lateral drainage fluxes from terrestrial soils (Siemens 2003). Globally, terrestrial net ecosystem production (NEP; gross primary production minus community respiration) is estimated to be 4.5 Pg-C y^{-1} (Drake and others 2018) that is either stored or exported. Land accumulation is estimated to be 2.6 Pg-C y^{-1} (Drake and others 2018) implying 1.9 Pg-C y^{-1} lateral carbon transfer from land to the inland water networks that drain it. The terrestrial carbon subsidy to inland waters can also be estimated using "active pipe" mass balance in the receiving waters that considers CO_2 evasion, downstream transport, and sediment burial (Cole and others 2007). Estimates of CO_2 outgassing (fCO_2) from inland waters – 86% from streams and rivers – have recently been revised upward to 3.9 Pg-C y^{-1} globally, necessitating lateral carbon transfer of 5.1 Pg-C y^{-1} from the terrestrial landscape to freshwaters (Drake and others 2018). This lateral carbon transfer is nearly twice that estimated using terrestrial mass balance. Clearly, advances in mass accounting of CO_2 evasion imply a dramatic and unexplained deviation (3.2 Pg-C y^{-1}) between estimates of terrestrial carbon lateral export and the resulting river network losses. Explaining this discrepancy is integral to resolving the role of inland water networks in the global C cycle.

There are two main pathways – the "reactor" and "chimney" – for terrestrial carbon to subsidize riverine fCO_2, both of which are routinely measured. The "reactor" pathway arises from lateral transport of terrestrially-derived organic matter, which fuels

in-stream aerobic ecosystem respiration (AR), producing CO_2 in the stream that then evades (Cole and others 2001; Mayorga and others 2005). The “chimney” pathway, in contrast, arises from in-stream evasion of inorganic carbon derived from soil respiration and/or mineral weathering; subsurface flowpaths deliver water supersaturated with CO_2 to streams, which rapidly degasses as stream waters equilibrate with the atmosphere (Johnson and others 2008; Duvert and others 2019). The amount of CO_2 that moves through the reactor pathway is estimated with stream net ecosystem production (NEP), defined as the balance between gross primary production (GPP) which consumes CO_2 and aerobic respiration (AR) which produces it. The amount of CO_2 that moves through the chimney pathway is estimated as the difference between fCO_2 and NEP. In a study of 187 US streams and rivers, Hotchkiss and others (2015) found 72% of fCO_2 is from external (i.e. terrestrial) inorganic C inputs (median flux per stream benthic area = 2.22 g-C m^{-2} d^{-1}), with smaller streams primarily acting as chimneys and the reactor pathway becoming increasingly important in larger rivers. Applying this fraction to the global stream and river CO_2 efflux yields 2.8 Pg-C y^{-1} of CO_2 mass transfer from terrestrial ecosystems to flowing waters. This number is greater than terrestrial mass balance estimates of total lateral carbon transfer and 55% of freshwater estimates. Unlike the reactor pathway, ecologists have rarely measured the chimney pathway directly (only by difference as described above), so these numbers have not been verified.

Existing conceptual models of CO_2 mass transfer separate the landscape into terrestrial or aquatic components, largely ignoring riparian wetlands that exist at their interface. Wetlands are structurally and functionally distinct from both freshwater and terrestrial environments. They comprise 7% of total land area in all latitudes (i.e. boreal,

temperate, subtropical, and tropical) (Abril and Borges 2019) , and although not all wetlands border flowing waters, stream riparian zones are ubiquitous and connectivity between wetlands and flowing waters are important even when they are sporadic. Wetlands in river valleys are extensive in low-lying areas (Meyer 1990; Abril and others 2014) with riparian width strongly correlated to drainage area (McGlynn and Seibert 2003). Riparian zones also buffer headwaters (Leith and others 2015), especially in low-gradient catchments where seasonally-inundated conditions typical of wetland environments can extend far from the stream channel. High-water-table conditions typical in these settings (Burt and others 2002) create distinctive plant communities compared to those in surrounding uplands (Naiman and Décamps 1997), high organic matter accumulation (Mitra and others 2005), and strong redox gradients that enable important biogeochemical reactions (Vidon and others 2010). Moreover, frequently saturated conditions inhibit soil ventilation which limits CO_2 loss from respiration that occurs underwater. The combination of high primary production and reduced ventilation enables groundwater CO_2 concentrations to become greatly elevated along riparian flowpaths towards streams and rivers resulting in a “wetland CO_2 pump” (Abril and Borges 2019). Strong and persistent bi-directional coupling between streams and adjacent riparian wetlands has prompted recent syntheses to focus on the river corridor – that is, the wetted channel plus the hyporheic and riparian zones – as a single operational unit (Harvey and Gooseff 2015). Abril and Borges (2019) further argue that inclusion of riparian wetlands as a carbon source distinct from true “upland” terrestrial subsidies to inland waters is crucial to enumerating the “active pipe” process. To

understand the spatial origins of the mass contributing to the chimney efflux pathway likely requires considering the parsed contributions of riparian wetlands.

Because groundwater often flows through riparian zones before reaching the river channel, these shallow-water-table environments can exert a disproportionate influence on stream chemistry (Seibert and others 2009). Specifically, groundwater carbon loads that discharge to the river channel may arise from the terrestrial system or from the river corridor itself. Groundwater transport through riparian zones substantially increases concentrations of dissolved organic carbon (DOC) (Chestnut and McDowell 2000) and associated major and trace elements (Lidman and others 2017). Isotopic evidence suggests stream DOC is derived primarily from the riparian zone not uplands (Mayorga and others 2005; Ledesma and others 2018). Where riparian groundwater CO_2 concentrations are higher than in uplands, it follows that lateral inputs of CO_2 are also preferentially sourced from within the river corridor (Leith and others 2015; Eriksson 2016). The overarching hypothesis of this work is that the river corridor plays an outsized role in the source of inorganic carbon to inland waters. Our conceptual framework includes riparian zones in the CO_2 mass balance of landscapes (Figure 4-1), and from this framework we sought to partition the CO_2 fluxes to streams into the fraction originating from the terrestrial landscape (TER) vs. the fraction entrained in the riparian zone (RIP). We hypothesized that the mass of lateral CO_2 inputs is dominated by river corridor sources, and that, by extension, the carbon subsidy to streams attributed to terrestrial environments is smaller than previously estimated, and better aligned with terrestrial mass balance estimates.

Methods

Study Sites

The Santa Fe River, a major tributary of the Suwannee River, is 121 km long and drains 3585 km^2 of the southeastern coastal plain in Florida, USA. The climate is warm (mean annual temperature = 21°C) and relatively humid (mean annual precipitation = 1248 mm yr^{-1}; 2008-2018, Florida Automated Weather Network). The Santa Fe River and its tributaries are bordered by riparian forests along their entire length that can be quite extensive given the low gradient of the riverbed (mean bed slope = 0.74 m/km Hensley and others 2019). These riparian forests vary in width (52 – 1422 m) and constitute 6% of the watershed area and are dominated by buttressed cypress and hardwoods (Florida Natural Areas Inventory 1990). Considering that subtropical latitudes efflux disproportionately high amounts of CO_2 to the atmosphere compared to higher latitudes (Lauerwald and others 2015), and lowlands have high riparian wetland area, partitioning the sources of CO_2 in this particular river network is especially relevant to understanding global carbon cycling.

We selected seven stream reaches that encompass second (DRAIN), third (SF700, NR1000), fourth (SF1500), and fifth order (SF2500, SF2800) streams/rivers. ICHE is technically a second-order river, but because it is fed by several first-magnitude springs, it has high discharge (8.5 m^3 s^{-1}). Our sites also reflect differences in landscape geology within the watershed (Figure 4-2). The Santa Fe River drainage basin is entirely underlain by the Upper Floridan Aquifer (UFA), but in the upper watershed (DRAIN, SF700, NR1000, SF1500), a relatively impermeable clay layer, the Miocene Hawthorne Group, confines the UFA and supports numerous streams, lakes, and wetlands perched on the landscape surface. In the lower watershed (ICHE, SF2500, SF2800), the

Hawthorne Group confining layer has been eroded away so that the carbonate UFA is no longer confined and the Santa Fe River receives discrete lateral inputs from artesian UFA springs, which dominate at low flow. At higher flow, overland and subsurface – not deep aquifer – flow constitute a larger proportion of river water (Hensley and others 2019). Surface waters in the lower watershed are limited to the river and its associated riparian ecosystems. While most of the Santa Fe River is gaining, the reach near the transition between confined and unconfined watershed where the entire Santa Fe River goes underground for approximately 5 km before re-emerging again, and several other settings around sinkholes, it becomes a losing river. The large volume of the UFA stabilizes discharge in the lower Santa Fe River, whereas the upper Santa Fe River responds rapidly to rain events and often dries out during droughts. The lithological transition between the upper and lower basins watershed regions results in important differences in water chemistry. The upper Santa Fe River has acidic, high-DOC water characteristics of “blackwaters”, and the lower reaches have alkaline waters with high buffering capacity and low temperature variation which imply high connectivity with the UFA (Khadka and others 2014; Jin and others 2015). Although land use and vegetation cover differ between the upper (primarily pine flatwoods/plantations) and lower catchments (primarily pasture), the entire watershed remains less altered than other river basins.

Differences in water clarity and stream size result in substantial differences in stream metabolic rates (Kirk and others, *in review*): The dark-colored and shaded upper river reaches have gross primary production (GPP) just above zero, whereas the clear, wide, spring-fed rivers have high GPP driven by dense aquatic macrophyte beds and

their attached algal communities (Odum 1957). The lower Santa Fe River exhibits large variation in GPP due to the time-varying blend of colored and clear water. Aerobic ecosystem respiration (AR) rates are always high but trend with GPP, with highest AR rates in spring-fed rivers where GPP:AR is closest to 1 (Odum 1957).

Data Collection and Calculations

Although direct measurements of lateral inputs of water and solutes are less common than reach-scale mass balance approaches to estimate terrestrial-to-aquatic carbon transfer, they are necessary to constrain lateral CO_2 inputs to streams and rivers. To test our hypothesis required measurements of stream CO_2 evasion (fCO_2), in-stream aerobic metabolism, lateral water fluxes (q_L), and groundwater CO_2 concentrations near the stream edge and uphill from the river corridor edge. Because of sensor failures, we were able to measure all fluxes for most sites for 3 – 7 months, but only for late January – February at SF700 and a few days in early September at SF2800 (Table 4-1).

Stream CO_2 evasion

CO_2 evasion (fCO_2, g-C m^2 d^{-1}) from stream to atmosphere was based on Fick's law of diffusion:

$$fCO_2 = k_{CO_2}\left(pCO_{2,stream} - pCO_{2,atm}\right) \times \frac{K_H}{10^6} \times 12gC \times 1000 \times z \qquad (4\text{-}1)$$

where k_{CO2} is the reaeration coefficient (d^{-1}), $pCO_{2,stream}$ is the partial pressure of CO_2 in air equilibrated with the stream water (ppm), $pCO_{2,atm}$ is the partial pressure of CO_2 in air (assumed 400 ppm), K_H is the temperature dependent Henry's constant (mol L^{-1} atm^{-1}), and z is mean stream depth (m). Stream pCO_2 was measured with a submersible infrared gas analyzer (0 – 20000 or 0 – 30000 ppm range, Eosense eosGP, Nova

Scotia, Canada) connected to a datalogger (Campbell Scientific CR1000, Utah, USA) that recorded every 15 minutes. CO_2 sensors came factory calibrated and were checked against air before every use and against known CO_2 gas concentrations yearly. We measured the pressure experienced by the underwater sensor using a pressure transducer (Onset HOBO U20, Bourne, Massachusetts, USA), from which we post-corrected pCO_2 measurements.

k_{CO2} was obtained from k_{600} using stream temperature and Schmidt number scaling (Raymond and others 2012). k_{600} was estimated from channel hydraulics (Raymond and others 2012), and both literature (Munch and others 2006; Khadka and others 2014, 2017) and new floating dome measurements. Our floating dome measurements of k_{600} followed Copeland and Duffer (1964) with modifications. A clear, rectangular storage container (area = 0.084 m^2) was overturned on the water surface, supported by flotation collars to penetrate 5 cm into the water, yielding a constant headspace volume of 15.5 L. CO_2 was injected into the headspace, and pCO_2 was measured every minute using an Eosense sensor (0 – 20000 ppm range) as the dome floated downstream. We also monitored river pCO_2 below the dome with a second identical sensor. The fitted slope between concentration and time defines the molar CO_2 flux, from which we estimated k_{600}, using the approach of Khadka and others (2014).

Stream metabolism

To measure stream metabolism required continuous time series of dissolved oxygen (DO) and temperature which were obtained from an *in situ* optical sensor (Onset HOBO U-26, Bourne, Massachusetts, USA), which logged every 15 minutes. DO sensors were calibrated every 7 months.

Net ecosystem production (*NEP*, g-C m^{-2} d^{-1}) is

$$NEP = (GPP + AR) \times \frac{12g\ C}{32g\ O_2} \quad (4\text{-}2)$$

where *GPP* is daily gross primary production (g-O2 m^{-2} d^{-1}) and *AR* is daily ecosystem respiration (g-O2 m^{-2} d^{-1}, a negative value). For all sites except the spring fed ICHE, we determined GPP and AR using the single-station open channel method (Odum 1956) implemented using inverse modeling in streamMetabolizer (Appling and others 2018; github.com/USGS-R/streamMetabolizer). StreamMetabolizer's Bayesian parameter estimation option ensures the reaeration coefficient (k_{600}) is similar on days with similar discharge (Appling and others 2018a). Modeled k_{600} mean values, but not variance, were constrained with empirical equations and floating dome measurements as described above. Groundwater at the vents of our spring-fed rivers is undersaturated with DO, violating the one-station metabolism model assumption that nighttime DO values reflect only the balance between ER and gas exchange. To estimate metabolism at ICHE, we used a two-station method (Odum 1956) following Hensley and others (2015).

Lateral CO_2 fluxes

Water Fluxes

All river sites except DRAIN were co-located with US Geological Survey (USGS) continuous discharge gages. At DRAIN, a discharge-stage rating curve was developed over five years from monthly field estimates and continuous stream stage (Hensley and others 2020). We measured mean width and depth at 4 – 11 transects within each study reach and used these empirical measurements to adjust hydraulic geometry equations (Leopold and Maddock 1953) using USGS data at the most downstream transect. In

2019, discharge in the Santa Fe River network was higher than the ten-year average (50.6 m^3 s^{-1} at SF2800) by 18% (2010-2019, Florida Automated Weather Network).

We estimated lateral inflow of water to the channel (q_L) using mass balance approaches appropriate for larger spatial measurement scales (Kalbus and others 2006). Lateral CO_2 fluxes (see below) calculated from lateral inflow using discharge will be overestimates following precipitation events. Streamflow is composed of both rapid overland flow and slower, groundwater-sourced baseflow (Ward and Robinson 1990). Because surface runoff is not likely to accumulate as much soil CO_2, we calculated q_L using baseflow instead of total stream discharge. We used hydrograph separation based on a recursive digital filter (Nathan and McMahon 1990) in the EcoHydRology open-source software package in R (Fuka and others 2018). This method separates high-frequency surface runoff variation from low-frequency baseflow variation. The α filter parameter was determined empirically at each site as the regressed slope of discharge at day *i*+1 plotted against discharge at day *i* during the baseflow portion of the recession limb of the hydrograph (Eckhardt 2008; Bosch and others 2017). The filter was passed twice over the streamflow record. Quickflow is often shallow groundwater that has been pushed out by storm event water, especially in low-lying areas. Nevertheless, analytical hydrograph separation can be used successfully in lowland basins, although it tends to overestimate surface runoff (23% vs 10% stream discharge using tracer-based flow separation techniques; Gonzales and others 2009), and hence underestimates baseflow and lateral inflow from groundwater.

We calculated q_L in two ways: First, we calculated upslope contributing area (UCA) in the manner of Leach and others (2017) with the Hydrology toolset in ArcMAP

10.6 (ESRI, Redlands, CA) from a publicly available digital elevation model (DEM) (USGS National Elevation Dataset, 30 m cell resolution, 1.5 m contours). The DEM was filled to remove closed depressions, from which flow direction and then flow accumulation were calculated. For each study reach (defined as *0.7u/k* upstream of the gage where *u* is stream velocity in m d^{-1} and k_{600} is reaeration coefficient in d^{-1}; Lamberti and Hauer 2017), we regressed flow accumulated vs. distance upstream of the gage, with the slope indicating the proportional flow accumulation per unit stream length (*ΔUCA*, m^{-1}). Only river segments without major tributaries were considered for our regressions. Multiplying by stream baseflow (Q_{base}) gives lateral inflow per unit length (q_L; $m^3\ s^{-1}\ m^{-1}$):

$$q_L = \Delta UCA \times Q_{base} \tag{4-3}$$

Assuming that flow accumulation is proportional to drainage area is likely valid in the upper Santa Fe River sites, but less applicable in the karstic lower watershed where aquifer inflow dominates.

Our second incremental streamflow method was based on changes in stream discharge between USGS gages (ΔQ_{base}):

$$q_L = \frac{\Delta Q_{base}}{\Delta x} \tag{4-4}$$

where Δx is the downstream distance between gages. We used the gages corresponding to study sites as well as other gages monitored intermittently by the USGS, but where the local water management district had modeled discharge from continuously-monitored stations (e.g. 02320849 and 02320815, Suwanee River Water Management District 2007). The thalweg distance between gages from aerial imagery was used to estimate Δx. To control for overestimation of q_L from discrete tributary

inputs, we estimated and removed flow accumulation from all mapped tributaries (discharge > 0.5 $m^3 s^{-1}$).

In the lower Santa Fe River network, lateral inflow from the landscape (TER) either flows through the riparian corridor on the way to the river channel (i.e. our conceptual model in the upper Santa Fe network) or flows into the aquifer where it eventually enters the river channel at discrete spring vents. To estimate streamflow accumulation from the aquifer ($q_{L,aquifer}$; 0.0019 $m^3 s^{-1} m^{-1}$), we used longitudinal changes in discharge collected by the local water management district (Suwanee River Water Management District 2019) for 10 km of SF2500 that includes 28 named springs distributed along the entire reach. Assuming spring inputs to the river are relatively constant, the difference between river "pickup" between gages and $q_{L,aquifer}$ is lateral inflow from the landscape (q_L):

$$q_L = \frac{\Delta Q_{base}}{\Delta x} - q_{L,aquifer} \quad (4\text{-}5)$$

Since the SF2800 reach has far fewer springs, we determined q_L using Equation 4-4, recognizing that they will be slight overestimates.

At spring-fed ICHE, neither UCA or delta Q methods were used to determine q_L since flow accumulation came almost entirely from the aquifer at discrete input locations. Previous studies using ion, dye, and radon mass balance approaches estimate 12 to 16% of flow did not originate from the larger, named springs (Kurz and others 2015; Khadka and others 2017) and 23% of this unaccounted flow originated from diffuse groundwater inflows (the remainder originating from smaller, unnamed springs; Kurz and others 2015). Therefore, at ICHE, we estimated time-varying q_L as

$$q_L = \frac{Q_{base} \times 0.16 \times 0.23}{x} \quad (4\text{-}6)$$

where *x* is reach length. The rest of Q_{base} was attributed to aquifer inputs.

To further validate UCA and mass balance estimates, diffuse groundwater flow was measured at high resolution at DRAIN and ICHE from April – October and June – October, respectively. At DRAIN, two sets of wells were installed in the riparian zone perpendicular to the stream and 50 m from one another: In each set, one well was located adjacent (13 m) to the stream and the other was located near the outer edge of the riparian corridor (36 m from stream). At ICHE, only wells adjacent to the river were installed because of installation difficulties in the exposed carbonate rocks at the edge of the river valley. Each well was instrumented with a pressure transducer that logged every 15 minutes. An additional sensor was deployed at a fixed height in the stream to calculate the head difference between wells and the stream. Wells were surveyed to determine relative elevations and distances between the sensors, which in turn, enabled calculation of head difference (*ΔH*, m) between the wells and stream. Groundwater inflow per unit stream length (q_L) was calculated based on Darcy's law (Dahm and Valett 1996):

$$q_L = -K \frac{\Delta H}{L} \times b \quad (4\text{-}7)$$

where *K* is hydraulic conductivity (m s^{-1}), *L* is the horizontal distance (m) between the well and stream, and *b* is the vertical distance (m) to an impermeable layer. We used the vertical distance to the clay horizon (1 m adjacent to river, 1.5 m at riparian edge) to approximate b at DRAIN and the depth of bedrock in the stream channel (3 m; Kurz and others 2015) to approximate b at ICHE. Hydraulic conductivity was measured empirically with a falling-head slug test (Hvorslev 1951).

We used a mean q_L averaged from all methods, except at SF2500 and SF2800 where we used only the ΔQ method. We also calculated proportional groundwater input rates (k_{gw}) as q_L divided by stream discharge.

Groundwater CO_2 Concentrations

pCO_2 in well water at DRAIN and ICHE (representing the water source end members) were measured monthly using Eosense sensors (0 – 120000 ppm range). Wells were screened between 0.5 – 1.5 m below ground to integrate groundwater pCO_2 and were capped between measurements. Wells were purged prior to measurements. Sensors were deployed long enough to reach equilibrium, although we likely underestimated the highest groundwater pCO_2 concentrations because of time constraints.

We also took synoptic groundwater pCO_2 measurements in augered holes at each of the remaining sites. Concentrations were obtained from both the riparian corridor and upland groundwater. Since groundwater pCO_2 varied far less than lateral water flux calculated with either stream baseflow (Figure 4-3) or discharge, we felt comfortable using a synoptic groundwater pCO_2 value to calculate lateral CO_2 mass flux, recognizing that our estimated fluxes would not fully capture temporal variation in lateral CO_2. For the lower Santa Fe River sites with high aquifer connectivity, we assumed spring vent CO_2 concentrations reflected upland soil concentrations (ICHE t-test, $p = 0.15$).

Lateral CO_2 Fluxes

Lateral CO_2 mass flux (*LI*, g-C m^2 d^{-1} on a stream benthic area basis) was calculated by

$$LI = q_L \times C_{gw} \times \frac{K_H}{10^6} \times 12gC \times 1000 \times 86400 \times \frac{1}{w} \quad (4\text{-}8)$$

where $pCO_{2,gw}$ is the groundwater CO_2 concentration in ppm and w is stream width (m). We used upland $pCO_{2,gw}$ to determine upland CO_2 mass flux (TER) and riparian $pCO_{2,gw}$ to determine LI entering the river channel ($LI_{channel}$). The riparian corridor CO_2 contribution to the river (RIP) was

$$RIP = LI_{channel} - TER \quad (4\text{-}9)$$

The aquifer contribution to the river (AQU, g-C m^{-2} d^{-1}) was based on Equation 4-8, but with $q_{L,aquifer}$ and upland $pCO_{2,gw}$.

CO_2 mass balance

The CO_2 mass balance on a benthic area basis is

$$fCO_2 + NEP = RIP + TER + other \quad (4\text{-}10)$$

We assumed the stream CO_2 mass did not change from one day to another, corroborated by stable stream CO_2 observations. We originally sought to solve the CO_2 mass balance for "other" believing it represented stream anaerobic respiration, but realized the anaerobic respiration flux was miniscule in comparison to other fluxes; hence, CO_2 mass balance would not be the appropriate method to estimate anaerobic respiration.

In most cases, we could assume CO_2 mass did not change longitudinally, so the difference between downstream export and upstream input (including AQU) would be zero. In the lower river network, however, this export-input difference (NEX) was not zero because of large spring inputs. Since the CO_2 dissolved in aquifer water ultimately sources from the terrestrial springshed, we subsumed NEX as part of TER. NEX is irrelevant to the upper river network where the aquifer is confined.

All daily fluxes were reported on a benthic area basis. We also scaled the lateral transfer of CO_2 in RIP and TER to the areal footprint of the riparian corridor (RIP_{yield}) and terrestrial uplands (TER_{yield}), respectively, to calculate carbon yields:

$$RIP_{yield} = LI \times \frac{w}{W_{rip}} \times 365 \quad (4\text{-}12)$$

$$TER_{yield} = LI \times \frac{w}{W_{up} - W_{rip}} \times 365 \quad (4\text{-}13)$$

where W_{up} and W_{rip} are the average widths of the upland and riparian watersheds, respectively. W_{up} was calculated as ΔUCA divided by stream reach length. Ten riparian widths evenly spaced along the study reach were measured in ArcMap based on the National Wetlands Inventory wetlands layer and averaged to estimate W_{rip}.

Monte Carlo Simulation

We acknowledge significant uncertainties in the multiple CO_2 fluxes, and sought to fully represent these using Monte Carlo simulations of fluxes at each site. We specified mean values of dissolved gas concentrations, temperature, and channel geometry for the entire period of record in 2019, and also distributions that reflect our uncertainty in each mean. Groundwater pCO_2 were normal distributions with means based on the synoptic measurements with standard deviations set at 40% of the mean (based on our $pCO_{2,gw}$ data at DRAIN where we had the most samples, n = 27). We used uniform distributions of q_L to encompass the range of values from our different methods; The lower range was the mean of the 20th percentile of q_L calculated with different methods, and the upper range was the mean of the 80th percentile. k_{600} were normal distributions based on the mean and sd of mean daily k_{600} outputs from

streamMetabolizer (or because k_{600} was fixed at ICHE for two-station calculations, we used the sd from SF2800). Likewise, GPP and AR were also normal distributions based on mean and sd of mean daily values. We used a uniform distribution between 0.8 and 1.2 for the respiratory quotient (RQ). Estimates of total flux uncertainty were derived from the distribution across 10000 simulations, each with randomly selected values drawn from the resulting distributions of the component variables.

Results

Variation in hydrology, channel morphology and water chemistry across the sites was substantial, reinforcing the important controls of network position and geologic context (Table 4-1). All river reaches were supersaturated with CO_2 (mean pCO_2: 2465 – 7455 ppm). Riparian groundwater pCO_2 were significantly higher in the upper Santa Fe catchment than in the lower catchment (56935 vs 18521 ppm, $p = 0.007$), but there was no significant difference between upland groundwater concentrations ($p = 0.52$). Notably, riparian groundwater pCO_2 were 1.5 to 5.6 times higher than upland concentrations.

Streamflow was flashier in the upper Santa Fe River network than in the lower: consequently, baseflow was lower than discharge by 45% in the upper network, but not in the lower (4% lower; Table 4-1). At all sites, baseflow separation reduced variation in flow by 46% (reduction in standard deviations, excluding ICHE, a spring-fed river with very constant discharge).

There was strong agreement among methods used to estimate q_L (Figure 4-4). SF700, NEW, and SF1500 showed no significant difference between q_L determined using UCA and delta Q methods. At DRAIN, point measurements of q_L in riparian wells agreed with the larger-scale delta Q method, but not with the UCA method. At ICHE, q_L

calculated from well hydraulic gradients was an order of magnitude smaller than q_L calculated by dye, ion, or radon mass balance in previous studies. Measured hydraulic conductivity was 9×10^{-6} and 1×10^{-6} m s^{-1} in the riparian wells at ICHE and 4.9×10^{-6} at DRAIN. Distance to limestone bedrock at ICHE was estimated as 3m from sediment profiles (Kurz and others 2015). Distance to the impermeable clay layer at DRAIN was between 1 and 1.5 m.

CO_2 fluxes into and out of the river channel varied over time and space (Figure 4-5), but broad patterns emerged from our data. Mean fCO_2 across the river network was 5.69 g-C m^{-2} d^{-1} (Figure 4-6B). The removal of CO_2 from the stream water column was dominated by fCO_2 since GPP hovered near zero (Figure 4-6C), except at ICHE where GPP (3.57 g-C m^{-2} d^{-1}) was almost as large as evasion (4.68 g-C m^{-2} d^{-1}). AR was a major CO_2 flux into the river channel at all sites (mean 3.44 g-C m^{-2} d^{-1}, Figure 4-6D). With high AR and little GPP, NEP almost always added CO_2 to the system (2.79 g-C m^{-2} d^{-1}, except in ICHE where AR and GPP balanced), accounting for 49% of fCO_2 on average (0 – 94% range).

The difference between fCO_2 and NEP, which we term “excess CO_2”, is on average 3.41 g-C m^{-2} $d^{-1}$and partitioned differently between the upper and lower river network. Three times more CO_2 came from the river corridor (RIP, 2.45 g-C m^{-2} d^{-1}) than from the terrestrial uplands (TER, 0.77 g-C m^{-2} d^{-1}) in the upper Santa Fe River (Figure 4-6E and F). In contrast, the reverse is true in the lower river network: Almost five times more CO_2 sourced from TER (3.43 g-C m^{-2} d^{-1}) than RIP (0.77 g-C m^{-2} d^{-1}). This was mostly driven by high TER at ICHE and SF2500 (mean 4.79 g-C m^{-2} d^{-1}) caused by large aquifer lateral flux. Without the aquifer lateral flux, TER at SF2800 was similar to

the upper river network (0.73 g-C m^{-2} d^{-1}). Every square meter of riparian area contributes on average 58 times more CO_2 than terrestrial uplands (Figure 4-7C). Annual terrestrial carbon yields averaged 0.07 g-C m^{-2} catchment area whereas annual riparian yields averaged 4.51 g-C m^{-2}.

By summing the NEP and RIP contributions to the river, we can account for, on average, 80% of fCO_2 in our study sites. The one exception is the entirely spring-fed ICHE with large aquifer contributions of CO_2 (i.e. high TER) and low metabolic contributions of CO_2 (i.e. near zero NEP). Excluding ICHE, the river corridor accounts for 64 to 100% of fCO_2 at individual sites.

At all sites, fluxes into and out of the system did not balance (labeled “other” in Figure 4-6A): Most sites were missing a process that consumed CO_2 (mean 2.02 g-C m^{-2} d^{-1}), whereas at SF1500 and SF2800, the missing process contributed CO_2 to the system (mean 1.45 g-C m^{-2} d^{-1}). We put error bars on measured CO_2 fluxes with Monte Carlo simulations using site means (Table 4-1) and prior distributions that captured our uncertainties in parameters, especially groundwater CO_2 concentrations, k_{600} (Table 4-1), and q_L (Figure 4-4). 25 – 75% high density credible intervals from posterior distributions mostly aligned with the interquartile ranges of our measured fluxes (Figure 4-6), suggesting that measured fluxes reliably captured our uncertainties regarding component terms used to estimate those fluxes.

Discussion

The metabolic fluxes of GPP and AR in our study network differed from streams and rivers globally. For comparison, we used the Appling and others (2018b) dataset which included streams and rivers across the USA with a spread of discharges similar to our sites. Our GPP fluxes were more extreme: All upper river sites (blackwaters) had

GPP below the 15% quantile (0.14 g-C m^{-2} d^{-1}) for the broader USA, and ICHE had GPP in the 95% quantile. All sites had positive AR greater than the median across the USA (1.35 g-C m^{-2} d^{-1}), with the median for our river network falling at the 90% quantile. We note that these comparisons assume a community respiratory quotient (RQ, moles of CO_2 produced: moles of O_2 consumed) of 1, which may not be valid and would have a large impact on converted AR carbon fluxes. In fact, mean RQ measured at ICHE was 0.8 (see Chapter 3), which would reduce the AR carbon flux by 20%.

Because of low GPP and high AR, NEP at our study reaches were larger sources of CO_2 to the atmosphere than to other streams and rivers of comparable size globally (Hotchkiss and others 2015; Figure 4-7A). With high NEP contributing CO_2 to fCO_2, we observed equal importance of both reactor and chimney pathways. Whereas Hotchkiss and others (2015) found a median 28% of CO_2 efflux from streams and rivers was attributable to internal production – and by difference, 72% came from other sources primarily lateral inputs of CO_2 – our study sites showed a more even split between the internal and external sources of CO_2. At our sites, NEP contributed a mean 49% of the CO_2 mass to total stream evasion and was much higher than predicted by Hotchkiss and others (2015). All stream reaches acted as strong reactors respiring organic carbon subsidies to the river channel, with the exception of the highly productive and wide ICHE where spring inputs are very low in dissolved organic carbon (Duarte and others 2010).

Patterns in the equally important chimney pathway were driven by both stream size and catchment geology. Stream size was the dominant control on the efflux rate of external CO_2 inputs (Figure 4-7B). The declining pattern of excess CO_2 (fCO_2 – NEP)

was driven partly by declining proportional groundwater input rates (Figure 4-7C): Groundwater inflow becomes a smaller fraction of discharge in larger streams and rivers, and as a consequence the lateral CO_2 flux also becomes smaller relative to other CO2 fluxes. Excess CO_2, however, from our study differed from Hotchkiss and others (2015) expectations (Figure 4-7B) at a number of sites. At lower order streams, Hotchkiss and others (2015) predicted higher variability in excess CO_2, which we also observed. At ICHE and SF2500, observed excess CO_2 was higher than predictions because of enormous aquifer inputs of CO_2. For comparison, lateral CO_2 fluxes for the lowland Howard River ($Q = 0.16\ m^3\ s^{-1}$) and partly spring-fed Daly River ($Q = 36\ m^3\ s^{-1}$) in Australia were 1.7 g-C $m^{-2}\ d^{-1}$and 6.7 g-C $m^{-2}\ d^{-1}$, respectively (Duvert and others 2019), which were of the same order of magnitude as our total lateral CO_2 fluxes.

Geology was an important control on the relative importance of riparian vs. terrestrial sources. RIP exceeded TER in the upper basin, but the reverse was true in the lower basin (Figure 4-5B and 4-6D,E). This pattern is driven by differences in drainage pathways. Drainage water carrying soil respiration CO_2 flows downward into the aquifer in the karst plain of the lower basin and mostly bypasses riverine riparian zones. Meanwhile, in the upper basin underlain by an impermeable clay, water carrying soil respiration CO_2 from the uplands has nowhere to go except laterally, thus entraining riparian CO_2 along the way to the stream. Thus, CO_2 yields from riparian areas in the upper basin are two – even three – orders of magnitude higher than terrestrial yields, in contrast to the lower basin (Figure 4-7D).

Across all sites, TER is not large enough to sustain the excess CO_2 that is usually attributed to lateral inorganic carbon transfer from terrestrial systems. Even

considering possible methodological biases in our estimations of groundwater inflow, q_L is too small to account for the excess CO_2 observed (Figure 4-7C). Consequently, our measured TER was only on average 58% of excess CO_2. Measured RIP was more than enough to account for the difference between measured TER and excess CO_2. Our findings are similar to those from low-order boreal streams (Leith and others 2015; Lupon and others 2019) that emphasizes the contribution of river corridor CO_2 to stream CO_2 evasion. Like our study, Leith and others (2015) specifically measured RIP and TER in a boreal catchment as 3008 and 1144 mg-C m-2 of catchment area per year, respectively, similar to our averages. The authors contend that Hotchkiss and others (2015) erroneously used groundwater CO_2 concentrations of 20000+ ppm that better reflect riparian groundwater (Greenway and others 2006) to estimate the lateral water flux needed to sustain enough terrestrial CO_2 inputs to explain excess CO_2. Mass balance calculations are only as good as their conceptual framework as the Cole and others (2007) “active pipe” demonstrated, and these results highlight the potential error in landscape mass balance estimates of terrestrial-to-aquatic CO_2 transfer if the functionally-unique, CO_2-rich riparian zone is omitted.

Carbonate buffering in high alkalinity waters, like our spring-fed study sites, likely leads to marked underestimation of fCO_2. In most study reaches, the CO_2 mass balance cannot close without invoking an “other” process that consumes CO_2 (Figure 4-5 and 4-6F). Given that carbonate rocks underlie our watershed and high alkalinities prevail at some of our sites (>1000 meq L^{-1}), this CO_2 sink is likely to be carbonate buffering (Stets and others 2017). Because some fraction of dissolved CO_2 is tied up in keeping $CaCO_3$ in solution, stream pCO_2 is lowered, leading to a smaller air-water CO_2 gradient

and smaller fCO_2. Without the carbonate buffering, fCO_2 and thus excess CO_2 would be even larger, and TER would be an even smaller contributor to stream CO_2 evasion. Carbonate buffering further underscores why TER cannot sufficiently explain excess CO_2.

By summing NEP and RIP, we confirmed our hypothesis that most CO_2 evading from a lowland river network originates within the river corridor. Furthermore, the organic carbon that is respired in the stream creating net heterotrophy also disproportionately sources from the river corridor. A number of studies have pointed to the riparian corridor as the major source of DOC to streams in many biomes (Buffam and others 2011; Strohmeier and others 2013; Ledesma and others 2015). In another blackwater stream of the southeastern coastal plain, DOC leached from wetland soils accounted for 63% of organic carbon entering the stream (Dosskey and Bertsch 1994). Soil particulate organic carbon (POC) is transported from the hillslope to streams during high discharge events, but the flux is miniscule compared to dissolved counterparts (Tank and others 2018). Most of the POC that ends up in streams is likely leaf litter and channel debris (Dosskey and Bertsch 1994), which comes from the adjacent riparian corridor. Although the relative proportion of carbon forms (i.e. CO_2/bicarbonate/DOC/POC) in terrestrial-to-aquatic fluxes differs by region (Tank and others 2018), these riparian fluxes suggest that the river corridor, in contrast to uplands, may be the source of most of the carbon – not only CO_2 – that enters streams.

Although ours were regional results, we can apply the same proportion of riparian vs terrestrial carbon subsidies to global streams and rivers to illustrate how inclusion of the riparian corridor can help close the continental carbon budget. If we assumed our

network average 58% of excess CO_2 (2.8 Pg-C y^{-1}; see Introduction) came from TER, 1.62 Pg-C y^{-1} would be attributed to lateral CO_2 transfer from terrestrial uplands. The terrestrial-to-aquatic organic carbon transfer is estimated as 0.75 Pg-C y^{-1} (Jenerette and Lal 2005), so together CO_2 and organic carbon would account for 2.37 Pg-C y^{-1}. Without an accounting of other lateral inorganic carbon (e.g. bicarbonate) transfer, this number is much closer to the 1.9 Pg-C y^{-1} total lateral carbon transfer estimated from terrestrial mass balance. By replumbing the inland water pipe to account for riparian areas in our lateral carbon transfer framework (Abril and Borges 2019), we come closer to resolving the discrepancy between terrestrial and aquatic carbon mass balance.

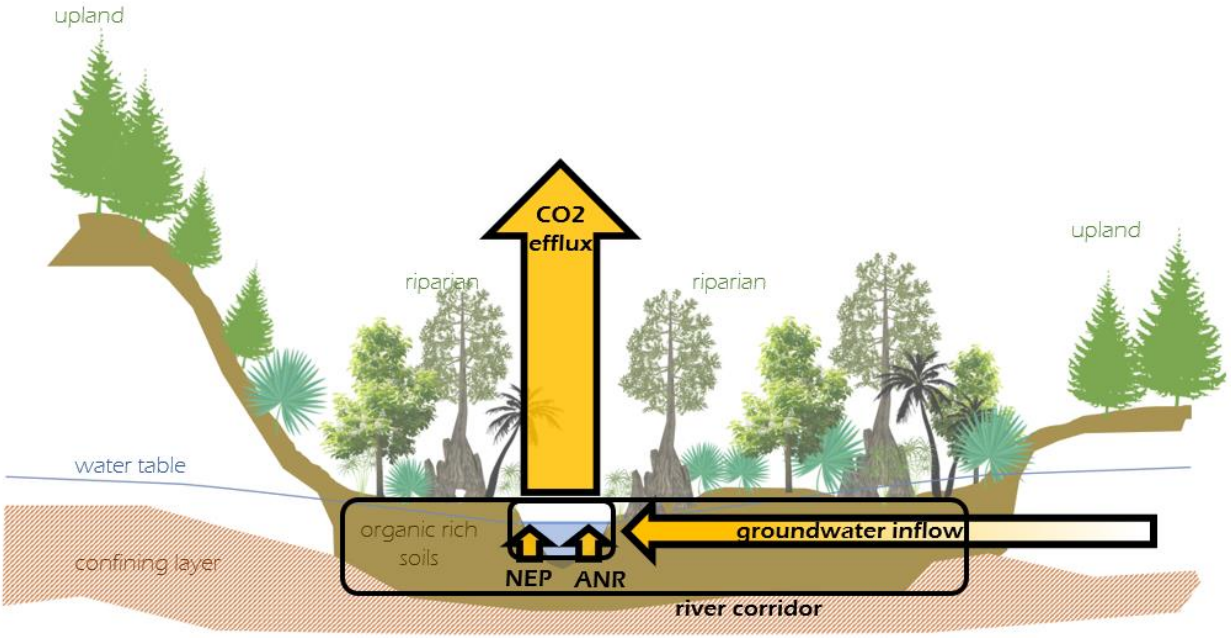

Figure 4-1. Conceptual diagram showing that CO_2 arriving in the stream channel from lateral inputs does not reflect the CO_2 drained from terrestrial uplands (TER). Instead lateral CO_2 fluxes include CO_2 from riparian soil respiration that is carried by groundwater inflow to the river channel (RIP). In-stream CO_2 contributions include net ecosystem production (NEP) and anaerobic (ANR) processes.

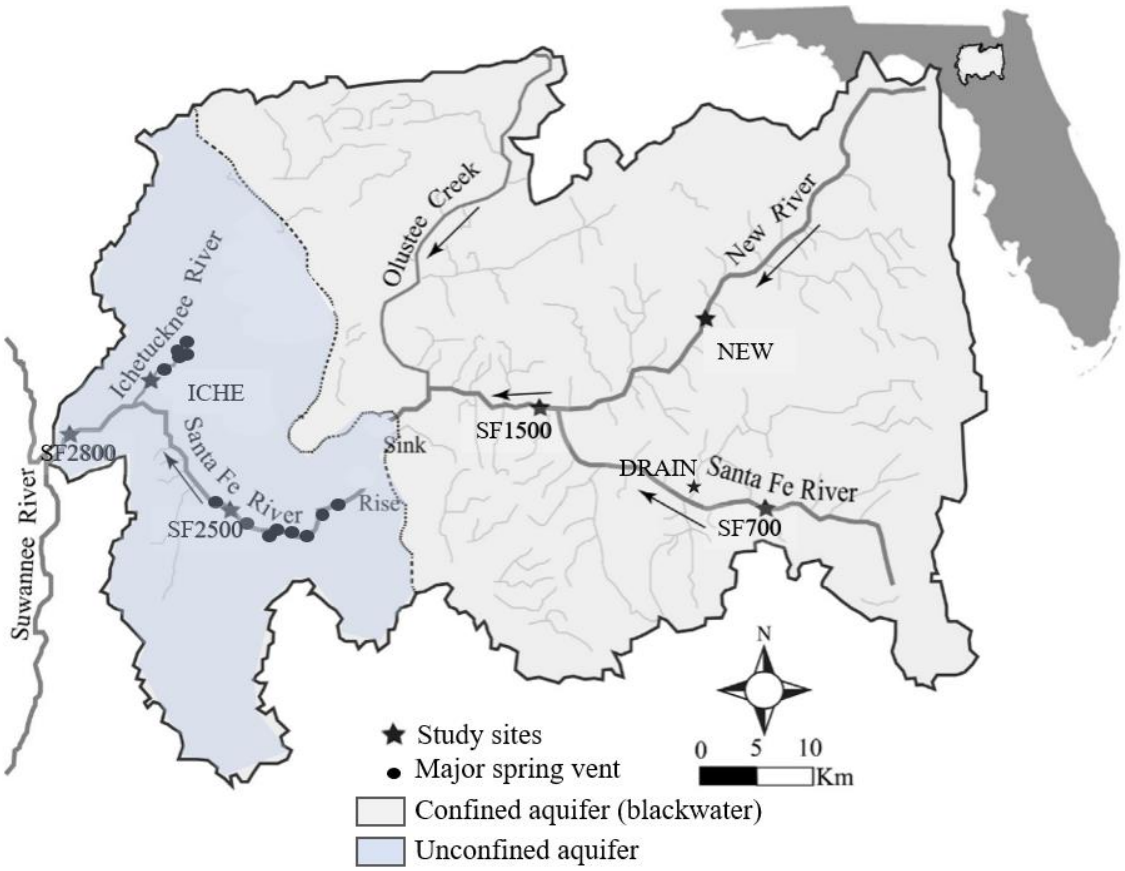

Figure 4-2. Santa Fe River watershed and study sites. Modified from Khadka et al (2014).

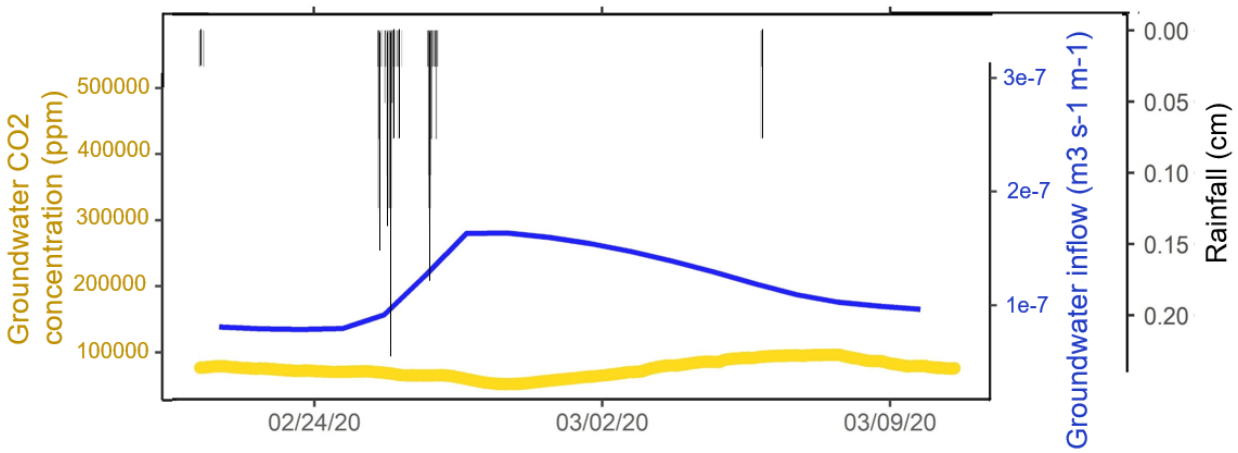

Figure 4-3. Comparing the temporal variability in groundwater CO_2 concentrations (gold) with groundwater inflow (blue) at DRAIN. Y-axes for both are scaled to one order of magnitude. CO_2 concentrations were measured continuously in the riparian groundwater during three weeks that included a major rain event. Groundwater inflow was calculated based on stream baseflow (which already damps discharge variability) and upslope contributing area.

Table 4-1. Site characteristics used in Monte Carlo simulation. Alkalinity data were taken from Khadka et al (2014). The number of days in 2019 when we could estimate terrestrial and riparian corridor CO_2 fluxes is given in the last column.

Site	Full name	Downstream station Latitude	Downstream station Longitude	Median discharge (m^3 s^{-1})	Median baseflow (m^3 s^{-1})
DRAIN	Drain Creek	29.8624	-82.2839	0.016 ± 0.155	0.009 ± 0.049
SF700	Santa Fe River near Graham	29.8461	-82.2197	0.45 ± 1.27	0.24 ± 0.57
NEW	New River	29.9981	-82.2742	0.39 ± 3.62	0.27 ± 1.65
SF1500	Santa Fe River near Worthington Springs	29.9217	-82.4264	1.81 ±11.65	0.77 ± 4.37
ICHE	Ichetucknee River	29.9525	-82.7861	9.57 ± 0.85	9.38 ± 0.78
SF2500	Santa Fe River near Ft. White	29.8486	-82.7153	38.3 ± 13.7	36.1 ± 8.5
SF2800	Santa Fe River near Hildreth	29.9114	-82.8606	50.9 ± 16.1	49.0 ± 8.9

Table 4-1. Continued

Site	Mean width (m)	Mean depth (m)	Velocity at median discharge (m s^{-1})	Mean water temperature (°C)	Mean DO (% saturation)	Mean stream CO_2 (ppm)	Up groun CO_2
DRAIN	1	0.4	0.06	20.1	68	7455	11000
SF700	6	0.5	0.15	17.4	78	3443	10292
NEW	6	1.0	0.16	21.3	57	2883	11000
SF1500	24	1.6	0.31	21.0	70	4302	10887
ICHE	42	1.0	0.45	21.8	59	2465	5902
SF2500	49	1.8	0.42	22.1	57	6039	8579
SF2800	46	3.6	0.32	20.6	65	4909	13054

Table 4-1. Continued

Site	Riparian groundwater CO_2 (ppm)	k_{600} (d^{-1})	GPP ($g\text{-}O_2\ m^{-2}\ d^{-1}$)	AR ($g\text{-}O_2\ m^{-2}\ d^{-1}$)	Alkalinity ($meq\ L^{-1}$)	Mean pH	# days
DRAIN	50109 ± 16971	6.41 ± 2.74	0.03 ± 0.43	-6.59 ± 4.25		4.33	146
SF700	42333 ± 16933	4.09 ± 1.57	0.04 ± 0.12	-4.24 ± 3.18	0.7 ± 0.6	5.09	52
NEW	73943 ± 16971	2.82 ± 0.85	-0.23 ± 0.51	-10.22 ± 2.64	0.9 ± 0.4	5.91	96
SF1500	61358 ± 24543	2.28 ± 0.56	0.47 ± 0.80	-11.24 ± 2.96	0.6 ± 0.3	6.14	205
ICHE	21624 ± 9024	2.6 ± 0.37	7.77 ± 3.48	-6.97 ± 3.37	2.9 ± 0.3	7.15	85
SF2500	12653 ± 5061	1.53 ± 0.37	2.74 ± 3.27	-15.16 ± 3.71	2.9 ± 0.4	7.06	108
SF2800	21286 ± 8514	0.67 ± 0.01	1.38 ± 2.21	-9.04 ± 2.53	2.8 ± 0.1	7.67	3

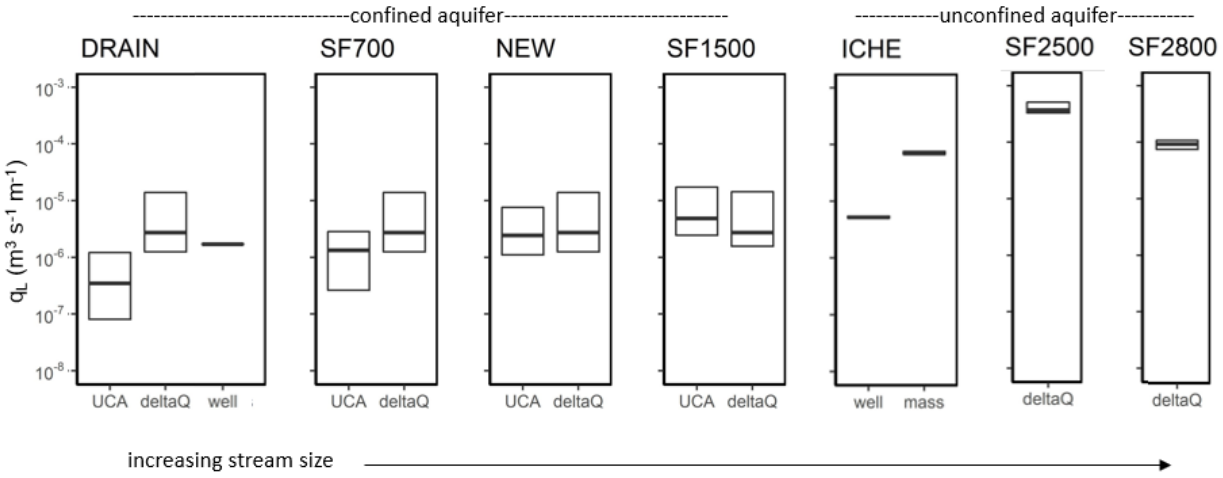

Figure 4-4. Comparison of groundwater inflows (q_L) estimated with various methods, including upslope contributing area (UCA), longitudinal change in discharge (deltaQ), Darcy's law (well), and ion/dye/radon mass balance (mass). Boxes represent the 25-75th percentiles.

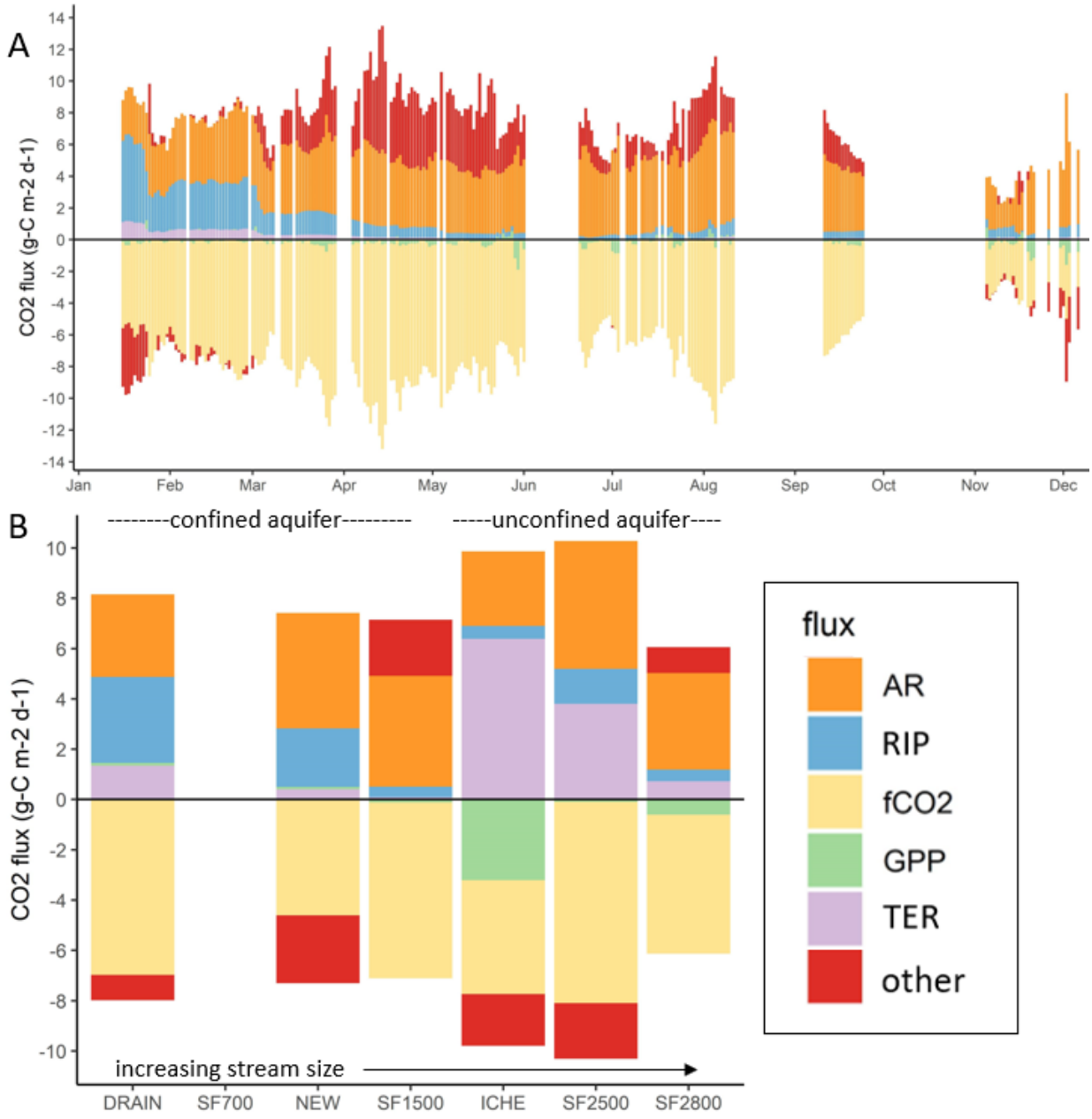

Figure 4-5. Variation of CO_2 fluxes over time at SF1500 (A) and across the river network from late August to early September 2019 (B). fCO_2 (CO_2 evasion to atmosphere) and GPP are considered negative fluxes because CO_2 leaves the river channel. AR (aerobic respiration), RIP (lateral CO_2 from the riparian corridor), and TER (lateral CO_2 from the terrestrial uplands) are considered positive fluxes that bring CO_2 into the river channel.

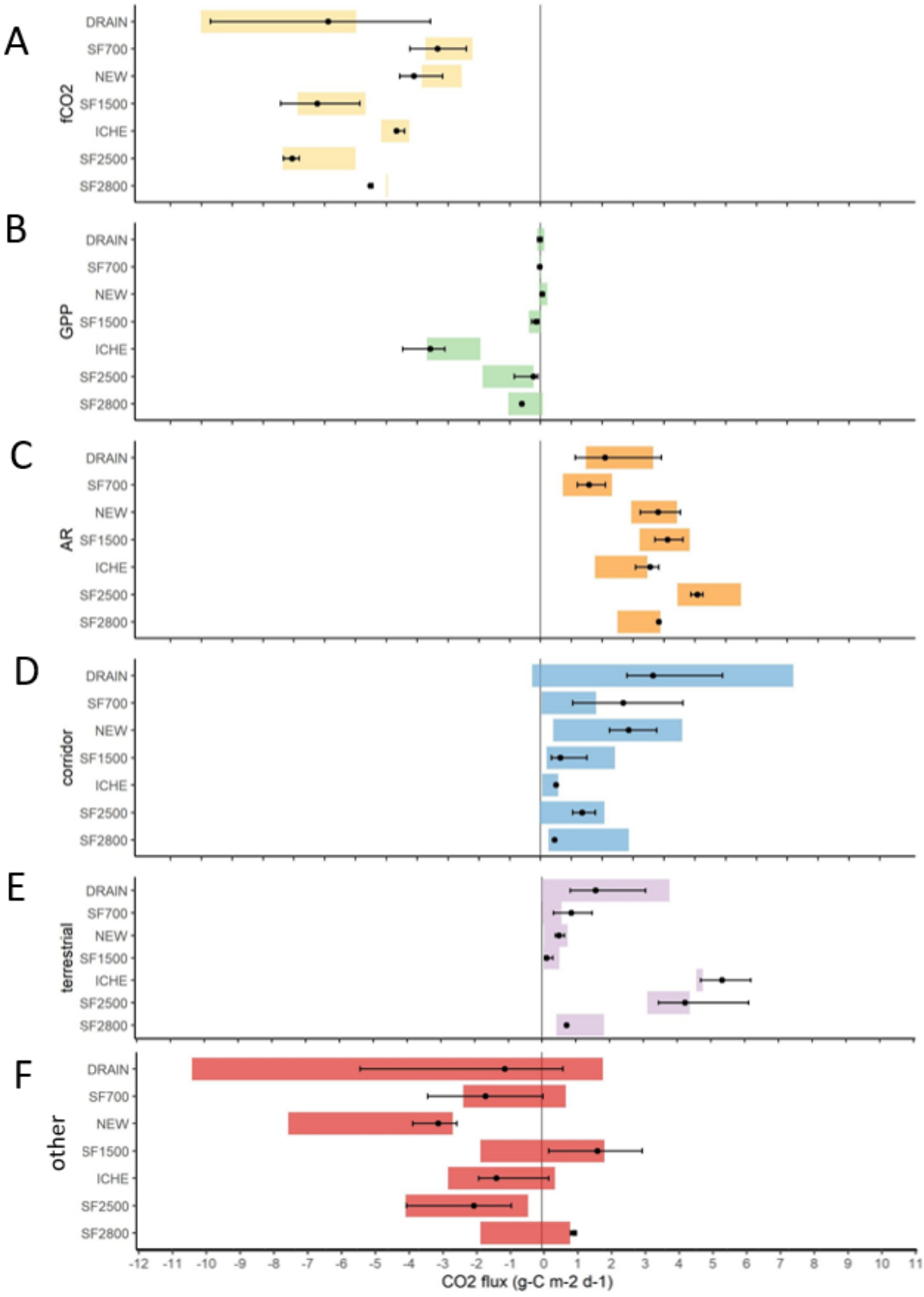
A
fCO2
DRAIN
SF700
NEW
SF1500
ICHE
SF2500
SF2800
B
GPP
C
AR
D
corridor
E
terrestrial
F
other
-12 -11 -10 -9 -8 -7 -6 -5 -4 -3 -2 -1 0 1 2 3 4 5 6 7 8 9 10 11
CO2 flux (g-C m-2 d-1)

Figure 4-6. Variation and uncertainty in CO_2 fluxes. Points and error bars represent median and interquartile range of measured fluxes, respectively. Colored rectangles represent 25-75% of high density credible intervals from Monte Carlo simulation of mean site conditions.

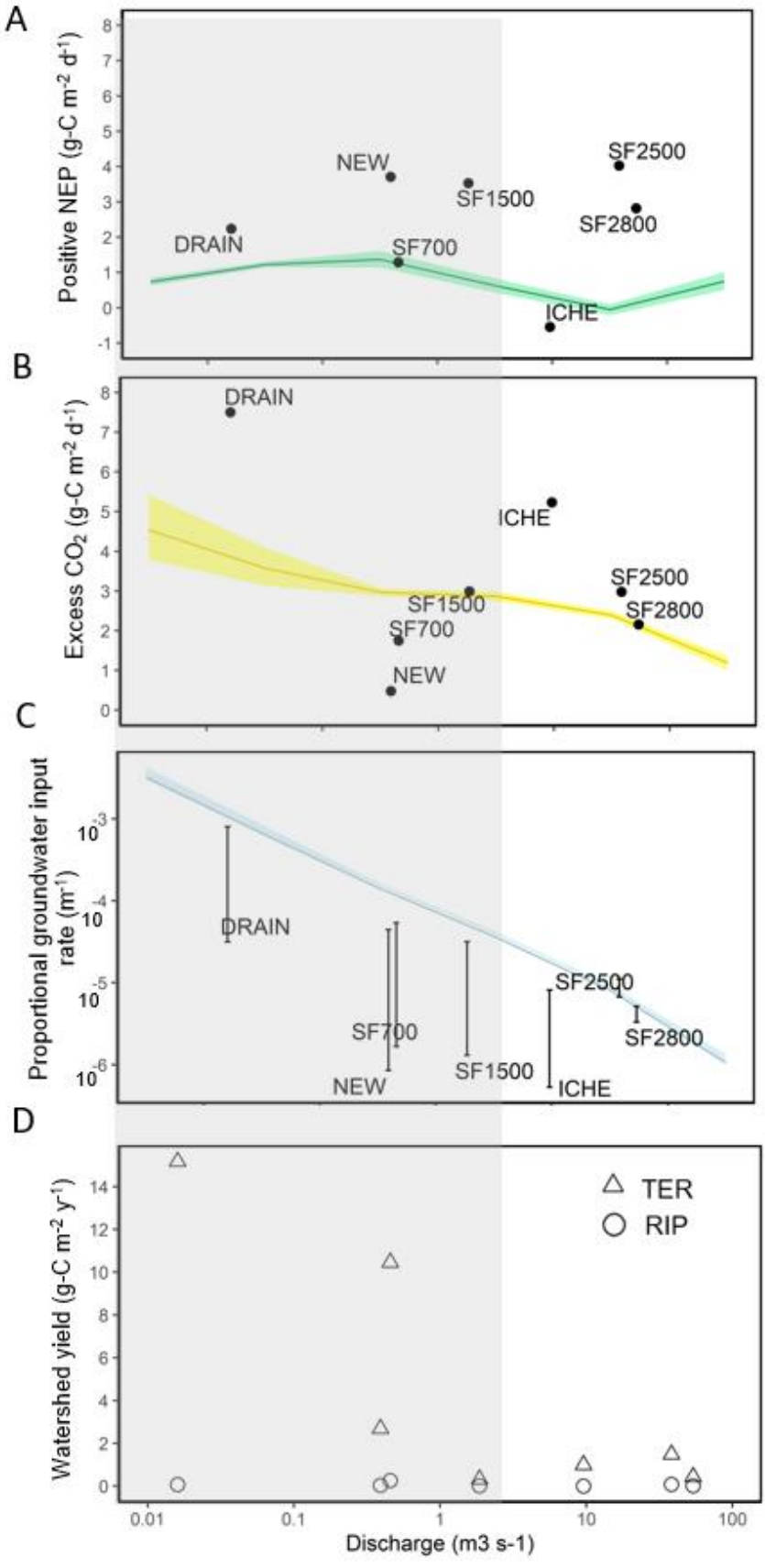

Figure 4-7. Lateral CO_2

relationships with stream size. Shaded side represents upper river network, whereas white side represents lower river network with unconfined aquifer. A) NEP and (B) excess CO_2 (CO_2 evasion not attributed to NEP) from our Monte Carlo simulations. Green and yellow shaded regions include 25-75% high density credible interval from Hotchkiss et al (2015) simulations. C) Groundwater inflow (range) at our study reaches. Blue line represents proportional groundwater input rates (k_{gw}) if all excess CO_2 came from groundwater inputs (Hotchkiss et al 2015). The line assumes a groundwater pCO_2 of 13000 ppm, which represents the high end of upland groundwater pCO_2 measured in our watershed. D) Annual lateral CO_2 export from terrestrial uplands (circles) and riparian corridor (triangles).

CHAPTER 5
CONCLUSIONS

This dissertation aimed to enhance our understanding of lotic metabolism at various scales through dissolved gas measurement. It explored three common – but not necessarily valid – assumptions about stream ecology in its major findings:

Benthic Light is Critical to Calculating LUE and Predicting Maximum GPP

Light is a primary control on gross primary production (GPP), yet measurement of light is not universal among stream metabolism studies. Furthermore, if light is measured, it is primarily stream surface or open sky light for shaded streams and large rivers, respectively. Chapter 2, however, definitively showed how poorly open sky and stream surface light predict GPP and that they underestimate light use efficiency (LUE), even for clear or shallow systems. The water column can attenuate as much as 96% of stream surface light. Furthermore, when LUE based on benthic light is corrected for the autotrophic community's light capture ability, I was able to explain >78% of variation in GPP across sites, and values for LUE converged across our regional sites, and the mean was identical to mean LUE values from terrestrial systems (1.9%). A convergent riverine LUE allows easy prediction of maximum GPP from benthic light data, against which disturbance and nutrient limitation can be inferred.

Aerobic RQ is Less than Unity in a Productive River

In Chapter 3, I empirically measured the community respiratory quotient (RQ; moles CO_2 produced/moles O_2 consumed) in mesocosms during aerobic respiration of natural organic matter and sugar. RQ is assumed in many metabolism studies to convert metabolic rates measured in oxygen units to carbon fluxes. Most studies

assume the RQ is 1 based on theoretical aerobic respiration of carbohydrates, but RQ is almost never empirically measured. I found that aerobic community RQ was 0.80, lower than expectations from a highly productive river. This has major implications for NEP carbon fluxes.

Anaerobic respiration in streams and rivers is generally perceived as minimal because of the relatively well-mixed water column of flowing waters. Using RQ measured in oxic and anoxic conditions, I estimated ANR to be a large fraction (28%) of total respiration. The similarity with previously measured denitrification rates suggests riverine ANR is predominately from denitrification.

Most CO_2 Efflux Sources from the River Corridor

To date, the difference between stream CO_2 evasion and net ecosystem production (NEP), which we term excess CO_2, is often attributed to terrestrial-to-aquatic inorganic carbon transfer. In the global carbon budget, however, stream ecologists' estimates of excess CO_2 are far greater than the terrestrial ecologists' estimates of lateral carbon loss. Chapter 4 showed that this discrepancy may be the consequence of hydrologically connected riparian wetlands that border most stream channels, particularly in lowland catchments, which can contribute most (72%) of the excess CO_2, and twice as much as terrestrial uplands. Terrestrial-to-aquatic CO_2 transfer is overestimated if the contribution from riparian wetlands is not considered.

LIST OF REFERENCES

Abril G, Borges A V. 2019. Ideas and perspectives: Carbon leaks from flooded land: Do we need to replumb the inland water active pipe? Biogeosciences 16:769–84.

Abril G, Bouillon S, Darchambeau F, Teodoru CR, Marwick TR, Tamooh F, Ochieng Omengo F, Geeraert N, Deirmendjian L, Polsenaere P, Borges A V. 2015. Technical note: Large overestimation of pCO2 calculated from pH and alkalinity in acidic, organic-rich freshwaters. Biogeosciences 12:67–78.

Abril G, Martinez JM, Artigas LF, Moreira-Turcq P, Benedetti MF, Vidal L, Meziane T, Kim JH, Bernardes MC, Savoye N, Deborde J, Souza EL, Albéric P, Landim De Souza MF, Roland F. 2014. Amazon River carbon dioxide outgassing fuelled by wetlands. Nature 505:395–8.

Acuña V, Giorgi A, Muñoz I, Uehlinger U, Sabater S. 2004. Flow extremes and benthic organic matter shape the metabolism of a headwater Mediterranean stream. Freshw Biol 49:960–71.

Allesson L, Ström L, Berggren M. 2016. Impact of photochemical processing of DOC on the bacterioplankton respiratory quotient in aquatic ecosystems. Geophys Res Lett 43:7538–45.

Appling AP, Hall RO, Yackulic CB, Arroita M. 2018a. Overcoming Equifinality: Leveraging Long Time Series for Stream Metabolism Estimation. J Geophys Res Biogeosciences 123:624–45.

Appling AP, Read JS, Winslow LA, Arroita M, Bernhardt ES, Griffiths NA, Hall RO, Harvey JW, Heffernan JB, Stanley EH, Stets EG, Yackulic CB. 2018b. Data descriptor: The metabolic regimes of 356 rivers in the United States. Sci Data 5:1–14.

Baker MA, Dahm CN, Valett HM. 1999. Acetate retention and metabolism in the hyporheic zone of a mountain stream. Limnol Oceanogr 44:1530–9.

Barnesa DJ, Lazarb B. 1993. Metabolic performance of a shallow reef patch near Eilat on the Red Sea. J Exp Mar Bio Ecol 174:1–13.

Battin TJ, Kaplan LA, Newbold JD, Hendricks SP. 2003. A mixing model analysis of stream solute dynamics and the contribution of a hyporheic zone to ecosystem function. Freshw Biol 48:995–1014.

Beaulieu JJ, Arango CP, Balz DA, Shuster WD. 2013. Continuous monitoring reveals multiple controls on ecosystem metabolism in a suburban stream. Freshw Biol 58:918–37.

Berggren M, Lapierre J-F, del Giorgio PA. 2012. Magnitude and regulation of bacterioplankton respiratory quotient across freshwater environmental gradients. ISME J 6:984–93.

Bernhardt ES, Heffernan JB, Grimm NB, Stanley EH, Harvey JW, Arroita M, Appling AP, Cohen MJ, McDowell WH, Hall RO, Read JS, Roberts BJ, Stets EG, Yackulic CB. 2018. The metabolic regimes of flowing waters. Limnol Oceanogr 63:S99–118.

Beyers RJ. 1963. The Metabolism of Twelve Aquatic Laboratory Microecosystems. Ecol Monogr 33:281–306.

Binkley D, Stape JL, Ryan MG. 2004. Thinking about efficiency of resource use in forests. For Ecol Manage 193:5–16.

Björkman O, Demmig B. 1987. Photon yield of O 2 evolution and chlorophyll fluorescence characteristics at 77 K among vascular plants of diverse origins. Planta 170:489–504.

Bosch DD, Arnold JG, Allen PG, Lim KJ, Park YS. 2017. Temporal variations in baseflow for the Little River experimental watershed in South Georgia, USA. J Hydrol Reg Stud 10:110–21. http://dx.doi.org/10.1016/j.ejrh.2017.02.002

Bott TL, Brock JT, Dunn CS, Naiman RJ, Ovink RW, Petersen RC. 1985. Benthic community metabolism in four temperate stream systems: An inter-biome comparison and evaluation of the river continuum concept. Hydrobiologia 123:3–45.

Boucher G, Clavier J, Garrigue C. 1994. Oxygen and carbon dioxide fluxes at the water-sediment interface of a tropical lagoon. Mar Ecol Prog Ser 107:185–94.

Brylinsky M. 1980. Estimating the productivity of lakes and reservoirs. In: Le Cren ED, Lowe-McConnell RH, editors. The functioning of freshwater ecosystems. New York: Cambridge University Press. p 588.

Buffam I, Turner MG, Desai AR, Hanson PC, Rusak JA, Lottig NR, Stanley EH, Carpenter SR. 2011. Integrating aquatic and terrestrial components to construct a complete carbon budget for a north temperate lake district. Glob Chang Biol 17:1193–211.

Burt TP, Pinay G, Matheson FE, Haycock NE, Butturini A, Clement JC, Danielescu S, Dowrick DJ, Hefting MM, Hillbricht-Ilkowska A, Maitre V. 2002. Water table fluctuations in the riparian zone: Comparative results from a pan-European experiment. J Hydrol 265:129–48.

Campbell GS, Norman JM. 1998. An introduction to environmental biophysics. 2nd editio. New York: Springer

Chestnut TJ, McDowell WH. 2000. C and N dynamics in the riparian and hyporheic zones of a tropical stream, Luquillo Mountains, Puerto Rico. J North Am Benthol Soc 19:199–214.

Chow WS, Melis A, Anderson JM. 1990. Adjustments of photosystem stoichiometry in chloroplasts improve the quantum efficiency of photosynthesis. Proc Natl Acad Sci 87:7502–6.

Ciais P, Borges A V., Abril G, Meybeck M, Folberth G, Hauglustaine D, Janssens IA. 2008. The impact of lateral carbon fluxes on the European carbon balance. Biogeosciences 5:1259–71.

Cole JJ, Caraco NF. 2001. Carbon in catchments: connecting terrestrial carbon losses with aquatic metabolism. Mar Freshw Res 52:101–10.

Cole JJ, Cole JJ, Caraco NF, Caraco NF. 2001. Carbon in catchments: connecting terrestrial carbon losses with aquatic metabolism. Mar Freshw Res 52:101. http://www.publish.csiro.au/?paper=MF00084

Cole JJ, Prairie YT, Caraco NF, Mcdowell WH, Tranvik LJ, Striegl RG, Duarte CM, Kortelainen P, Downing JA, Middelburg JJ, Melack J. 2007. Plumbing the Global Carbon Cycle: Integrating Inland Waters into the Terrestrial Carbon Budget. Ecosystems 10:171–84.

Copeland BJ, Duffer WR. 1964. Use of a Clear Plastic Dome To Measure Gaseous Diffusion Rates in Natural Waters. Limnol Oceanogr 9:494–9.

Covino TP, Bernhardt ES, Heffernan JB. 2018. Measuring and interpreting relationships between nutrient supply, demand, and limitation. Freshw Sci 37:448–55.

Dahm CN, Valett HM. 1996. Hyporheic zones. In: Hauer R, Lamberti GA, editors. Methods in stream ecology. New York, USA: Academic Press. p 673.

Davies-Colley RJ, Nagels JW. 2008. Predicting light penetration into river waters. J Geophys Res 113:G03028.

Davies-Colley RJ, Smith DG. 2001. Turbidity, suspended sediment, and water clarity: A review. J Am Water Resour Assoc 37:1085–101.

Dodds WK, Hutson RE, Eichem AC, Evans MA, Gudder DA, Fritz KM, Gray L. 1996. The relationship of floods, drying, flow and light to primary production and producer biomass in a prairie stream. Hydrobiologia 333:151–9.

Dodds WK, Veach AM, Ruffing CM, Larson DM, Fischer JL, Costigan KH. 2013. Abiotic controls and temporal variability of river metabolism: multiyear analyses of Mississippi and Chattahoochee River data. Freshw Sci 32:1073–87.

Dosskey MG, Bertsch PM. 1994. Forest sources and pathways of organic matter transport to a blackwater stream: a hydrologic approach. Biogeochemistry 24:1–19.

Drake TW, Raymond PA, Spencer RGM. 2018. Terrestrial carbon inputs to inland waters: A current synthesis of estimates and uncertainty. Limnol Oceanogr Lett 3:132–42.

Drever JI. 1988. The geochemistry of natural waters. 2nd ed. Englewood Cliffs, New Jersey: Prentice Hall

Duarte CM, Prairie YT, Frazer TK, Hoyer M V., Notestein SK, Martínez R, Dorsett A, Canfield DE. 2010. Rapid accretion of dissolved organic carbon in the springs of Florida: the most organic-poor natural waters. Biogeosciences 7:4051–7.

Duffer WR, Dowis TC. 1966. Primary productivity in a southern Great Plains stream. Limnol Oceanogr 11:143–51.

Duvert C, Bossa M, Tyler KJ, Wynn JG, Munksgaard NC, Bird MI, Setterfield SA, Hutley LB. 2019. Groundwater-Derived DIC and Carbonate Buffering Enhance Fluvial CO2 Evasion in Two Australian Tropical Rivers. J Geophys Res Biogeosciences 124:312–27.

Eckhardt K. 2008. A comparison of baseflow indices, which were calculated with seven different baseflow separation methods. J Hydrol 352:168–73.

Edwards RW, Owens M. 1962. The Effects of Plants on River Conditions IV. The Oxygen Balance of a Chalk Stream. J Ecol 50:207–20.

Eriksson EH. 2016. Quantification of Terrestrial CO 2 Sources to a Headwater Stream in a Boreal Forest Catchment.

Field CB. 1991. Ecological scaling of carbon gain to stress and resource availability. In: Mooney HA, Winner WE, Pell EJ, editors. Response of plants to multiple stresses. Academic Press. p 422.

Fisher SG, Gray LJ, Grimm NB, Busch DE. 1982. Temporal Succession in a Desert Stream Ecosystem Following Flash Flooding. Ecol Monogr 52:93–110.

Flemer DA. 1970. Primary productivity of the North Branch of the Raritan River, New Jersey. Hydrobiologia 35:273–96.

Fork ML, Heffernan JB. 2014. Direct and Indirect Effects of Dissolved Organic Matter Source and Concentration on Denitrification in Northern Florida Rivers. Ecosystems 17:14–28.

Fuka D, Walter M, Archibald J, Steenhuis T, Easton Z. 2018. A community modeling foundation for Eco-Hydrology.

Gallo KP, Daughtry CST. 1984. Techniques for measuring intercepted and absorbed PAR in corn canopies. Purdue Univ - LARS Tech Rep 111284:752–6.

Garbulsky MF, Peñuelas J, Papale D, Ardö J, Goulden ML, Kiely G, Richardson AD, Rotenberg E, Veenendaal EM, Filella I. 2010. Patterns and controls of the variability of radiation use efficiency and primary productivity across terrestrial ecosystems. Glob Ecol Biogeogr 19:253–67.

Del Giorgio P, Williams P. 2007. Respiration in Aquatic Ecosystems. Respir Aquat Ecosyst:1–328.

Del Giorgio PA, Pace ML. 2008. Relative independence of dissolved organic carbon transport and processing in a large temperate river: The Hudson River as both pipe and reactor. Limnol Oceanogr 53:185–97.

del Giorgio PA, Williams PJ. 2005. Respiration in aquatic ecosystems. Oxford University Press

Gitelson AA, Gamon JA. 2015. The need for a common basis for defining light-use efficiency: Implications for productivity estimation. Remote Sens Environ 156:196–201.

Glud RN. 2008. Oxygen dynamics of marine sediments. Mar Biol Res 4:243–89.

Godwin SC, Jones SE, Weidel BC, Solomon CT. 2014. Dissolved organic carbon concentration controls benthic primary production: Results from in situ chambers in north-temperate lakes. Limnol Oceanogr 59:2112–20.

Gonzales AL, Nonner J, Heijkers J, Uhlenbrook S. 2009. Comparison of different base flow separation methods in a lowland catchment. Hydrol Earth Syst Sci 13:2055–68.

Greenway H, Armstrong W, Colmer TD. 2006. Conditions leading to high CO2 (>5 kPa) in waterlogged-flooded soils and possible effects on root growth and metabolism. Ann Bot 98:9–32.

Hall RO, Beaulieu JJ. 2013. Estimating autotrophic respiration in streams using daily metabolism data. Freshw Sci 32:507–16.

Hall RO, Yackulic CB, Kennedy TA, Yard MD, Rosi-Marshall EJ, Voichick N, Behn KE. 2015. Turbidity, light, temperature, and hydropeaking control primary productivity in the Colorado River, Grand Canyon. Limnol Oceanogr 60:512–26.

Hargrave BT, Connolly GF. 1978. A device to collect supernatant water for measurement of the flux of dissolved compounds across sediment surfaces. Limnol Oceanogr 23:1005–10.

Harvey JW, Gooseff M. 2015. River corridor science: Hydrologic exchange and ecological consequences from bedforms to basins. Water Resour Res 51:6893–922.

Haxeltine A, Prentice IC. 1996. A General Model for the Light-Use Efficiency of Primary Production. Funct Ecol 10:551–61.

Hedges JI, Baldock JA, Gélinas Y, Lee C, Peterson ML, Wakeham SG. 2002. The biochemical and elemental compositions of marine plankton: A NMR perspective. Mar Chem 78:47–63.

Heffernan JB, Cohen MJ. 2010. Direct and indirect coupling of primary production and diel nitrate dynamics in a subtropical spring-fed river. Limnol Oceanogr 55:677–88.

Heffernan JB, Cohen MJ, Frazer TK, Thomas RG, Rayfield TJ, Gulley J, Martin JB, Delfmo JJ, Graham WD. 2010. Hydrologie and biotic influences on nitrate removal in a subtropical spring-fed river. Limnol Oceanogr 55:249–63.

Hensley RT, Cohen MJ. 2012. Controls on solute transport in large spring-fed karst rivers. Limnol Oceanogr 57:912–24.

Hensley RT, Cohen MJ, Korhnak L V. 2015. Hydraulic effects of nitrogen removal in a tidal spring-fed river. Water Resour Res 51:1443–56.

Hensley RT, Decker PH, Flinders C, McLaughlin D, Schilling E, Cohen MJ. 2020. Fertilization has negligible effects on nutrient export and stream biota in two North Florida forested watersheds. For Ecol Manage 465:118096.

Hensley RT, Kirk L, Spangler M, Gooseff MN, Cohen MJ. 2019. Flow Extremes as Spatiotemporal Control Points on River Solute Fluxes and Metabolism. J Geophys Res Biogeosciences 124:537–55.

Hilker T, Coops NC, Wulder MA, Black TA, Guy RD. 2008. The use of remote sensing in light use efficiency based models of gross primary production: A review of current status and future requirements. Sci Total Environ 404:411–23.

Hill WR, Dimick SM. 2002. Effects of riparian leaf dynamics on periphyton photosynthesis and light utilisation efficiency. Freshw Biol 47:1245–56.

Hill WR, Mulholland PJ, Marzolf ER. 2001. Stream Ecosystem Responses to Forest Leaf Emergence in Spring. Ecology 82:2306–19.

Hilton J, O'Hare M, Bowes MJ, Jones JI. 2006. How green is my river? A new paradigm of eutrophication in rivers. Sci Total Environ 365:66–83.

Hoellein TJ, Bruesewitz DA, Richardson DC. 2013. Revisiting Odum (1956): A synthesis of aquatic ecosystem metabolism. Limnol Oceanogr 58:2089–100.

Hornberger GM, Kelly MG, Eller RM. 1976. The relationship between light and photosynthetic rate in a river community and implications for water quality modeling. Water Resour Res 12:723–30.

Hotchkiss ER, Hall Jr RO, Sponseller RA, Butman D, Klaminder J, Laudon H, Rosvall M, Karlsson J. 2015. Sources of and processes controlling CO2 emissions change with the size of streams and rivers. Nat Geosci 8:696–9.

Huxman TE, Smith MD, Fay PA, Knapp AK, Shaw MR, Lolk ME, Smith SD, Tissue DT, Zak JC, Weltzin JF, Pockman WT, Sala OE, Haddad BM, Harte J, Koch GW, Schwinning S, Small EE, Williams DG. 2004. Convergence across biomes to a common rain-use efficiency. Nature 429:651–4.

Hvorslev MJ. 1951. Time lag and soil permeability in ground-water observations. US Army Corps Eng Waterw Exp Stn Bull 36:1–50.

Inventory FNA, Resources FD of N. 1990. Guide to the natural communities of Florida.

Jenerette GD, Lal R. 2005. Hydrologic sources of carbon cycling uncertainty throughout the terrestrial-aquatic continuum. Glob Chang Biol 11:1873–82.

Johnson MS, Billett MF, Dinsmore KJ, Wallin M, Dyson KE, Jassal RS. 2010. Direct and continuous measurement of dissolved carbon dioxide in freshwater aquatic systems -- method and applications. Ecohydrology 3:68–78.

Johnson MS, Lehmann J, Riha SJ, Krusche A V, Richey JE, Ometto JPHB, Guimara E. 2008. CO2 efflux from Amazonian headwater streams represents a significant fate for deep soil respiration. Geophys Res Lett 35:1–5.

Julian JP, Doyle MW, Stanley EH. 2008a. Empirical modeling of light availability in rivers. J Geophys Res 113:1–16.

Julian JP, Stanley EH, Doyle MW. 2008b. Basin-scale consequences of agricultural land use on benthic light availability and primary production along a sixth-order temperate river. Ecosystems 11:1091–105.

Kalbus E, Reinstorf F, Schirmer M. 2006. Measuring methods for groundwater-surface water interactions: a review. Hydrol Earth Syst Sci 10:873–87.

Kaplan LA, Cory RM. 2016. Dissolved Organic Matter in Stream Ecosystems: Forms, Functions, and Fluxes of Watershed Tea. In: Stream Ecosystems in a Changing Environment. pp 241–320.

Khadka MB, Martin JB, Jin J. 2014. Transport of dissolved carbon and CO2 degassing from a river system in a mixed silicate and carbonate catchment. J Hydrol 513:391–402.

Khadka MB, Martin JB, Kurz MJ. 2017. Synoptic estimates of diffuse groundwater seepage to a spring-fed karst river at high spatial resolution using an automated radon measurement technique. J Hydrol 544:86–96.

King SA, Heffernan JB, Cohen MJ. 2014. Nutrient flux, uptake, and autotrophic limitation in streams and rivers. Freshw Sci 33:85–98.

Kirk JTO. 1983. Light and photosynthesis in aquatic ecosystems.

Kirk L, Hensley RT, Savoy P, Heffernan JB, Cohen MJ. *In review*. Benthic light regimes predict primary production and constrain light use efficiency in streams and rivers. Ecosystems.

Kolber Z, Wyman K V., Falkowski PG. 1990. Natural variability in photosynthetic energy conversion efficiency: A field study in the Gulf of Maine. Limnol Oceanogr 35:72–9.

Kurz MJ, Martin JB, Cohen MJ, Hensley RT. 2015. Diffusion and seepage-driven element fluxes from the hyporheic zone of a karst river. Freshw Sci 34:206–21.

Lamberti GA, Hauer R. 2017. Ecosystem Processes. In: Methods in stream ecology. 3rd ed. Academic Press

Lauerwald R, Laruelle GG, Hartmann J, Ciais P, Regnier P. 2015. Spatial patterns in CO2 evasion from the global river network. Global Biogeochem Cycles 29:534–54.

Leach J, Lidberg W, Kuglerova L, Peralta-Tapia A, Agren A, Laudon H. 2017. Evaluating topography-based predictions of shallow lateral groundwater discharge zones for a boreal lake-stream system. Water Resour Res:5998–6017.

Ledesma JLJ, Grabs T, Bishop KH, Schiff SL, Köhler SJ. 2015. Potential for long-term transfer of dissolved organic carbon from riparian zones to streams in boreal catchments. Glob Chang Biol 21:2963–79.

Ledesma JLJ, Kothawala DN, Bastviken D, Maehder S, Grabs T, Futter MN. 2018. Stream Dissolved Organic Matter Composition Reflects the Riparian Zone, Not Upslope Soils in Boreal Forest Headwaters. Water Resour Res 54:3896–912.

Lefèvre D, Guigue C, Obernosterer I. 2008. The metabolic balance at two contrasting sites in the Southern Ocean: The iron-fertilized Kerguelen area and HNLC waters. Deep Res Part II Top Stud Oceanogr 55:766–76.

Leith FI, Dinsmore KJ, Wallin MB, Billett MF, Heal K V., Laudon H, Öquist MG, Bishop K. 2015. Carbon dioxide transport across the hillslope-riparian-stream continuum in a boreal headwater catchment. Biogeosciences 12:1881–902.

Leopold LB, Maddock T. 1953. The hydraulic geometry of stream channels and some physiographic implications.

Li G, Jackson CR, Kraseski KA. 2012. Modeled riparian stream shading : Agreement with field measurements and sensitivity to riparian conditions. J Hydrol 428–429:142–51.

Lidman F, Boily Å, Laudon H, Köhler SJ. 2017. From soil water to surface water-how the riparian zone controls element transport from a boreal forest to a stream. Biogeosciences 14:3001–14.

Lindeman RL. 1942. The trophic-dynamic aspect of ecology. Ecology 23:399–417.

Lupon A, Denfeld BA, Laudon H, Leach J, Karlsson J, Sponseller RA. 2019. Groundwater inflows control patterns and sources of greenhouse gas emissions from streams. Limnol Oceanogr:1–13.

Mäkelä A, Pulkkinen M, Kolari P, Lagergren F, Berbigier P, Lindroth A, Loustau D, Nikinmaa E, Vesala T, Hari P. 2008. Developing an empirical model of stand GPP with the LUE approach: Analysis of eddy covariance data at five contrasting conifer sites in Europe. Glob Chang Biol 14:92–108.

Masiello CA, Gallagher ME, Randerson JT, Deco RM, Chadwick OA. 2008. Evaluating two experimental approaches for measuring ecosystem carbon oxidation state and oxidative ratio. J Geophys Res Biogeosciences 113:1–9.

Mayorga E, Aufdenkampe AK, Masiello CA, Krusche A V, Hedges JI, Quay PD, Richey JE, Brown TA. 2005. Young organic matter as a source of carbon dioxide outgassing from Amazonian rivers. Nature 436:358–341.

McBride J, Cohen MJ. 2019. Controls on productivity of submerged aquatic vegetation in 2 spring-fed rivers. Freshw Sci 39:000–000.

McDowell MJ, Johnson MS. 2018. Gas Transfer Velocities Evaluated Using Carbon Dioxide as a Tracer Show High Streamflow to Be a Major Driver of Total CO2Evasion Flux for a Headwater Stream. J Geophys Res Biogeosciences 123:2183–97.

McGlynn BL, Seibert J. 2003. Distributed assessment of contributing area and riparian buffering along stream networks. Water Resour Res 39:1–7.

McKnight DM, Boyer EW, Westerhoff PK, Doran PT, Kulbe T, Andersen DT. 2001. Spectrofluorometric characterization of dissolved organic matter for indication of precursor organic material and aromaticity. Limnol Oceanogr 46:38–48.

Mcmurtrie RE, Gholz HL, Linder S, Gower ST. 1994. Climatic Factors Controlling the Productivity of Pine Stands : A Model-Based Analysis. Ecol Bull:173–88.

Medlyn BE. 1998. Physiological basis of the light use efficiency model. Tree Physiol 18:167–76.

Meyer JL. 1990. A Blackwater Perspective on Riverine Ecosystems. Bioscience 40:643.

Minshall GW. 1978. Autotrophy in Stream Ecosystems. Bioscience 28:767–71.

Mitra S, Wassmann R, Vlek PLG. 2005. An appraisal of global wetland area and its organic carbon stock. Curr Sci 88:25–35.

Monteith JL. 1972. Solar radiation and productivity in tropical ecosystems. J Appl Ecol 9:747–66.

Monteith JL, Moss CJ. 1977. Climate and the Efficiency of Crop Production in Britain. Philos Trans R Soc Biol Sci 281:277–94.

de Montety V, Martin JB, Cohen MJ, Foster C, Kurz MJ. 2011. Influence of diel biogeochemical cycles on carbonate equilibrium in a karst river. Chem Geol 283:31–43.

Mulholland PJ, Fellows CS, Grimm NB, Webster JR, Hamilton SK, Marti E, Ashkenas L, Bowden WB, Dodds WK, Mcdowell WH, Paul MJ, Peterson BJ. 2001. Inter-biome comparision of factors controlling stream metabolism. Freshw Biol 46:1503–17.

Munch DA, Toth DJ, Huang C, Davis JB, Fortich CM, Osburn WL, Phlips EJ, Allen MS, Knight RL. 2006. Fifty-year retrospecitve study of the ecology of Silver Springs, Florida.

Murray TE, Rich PH. 1995. Respiratory quotients predict increases in reducing products in the hypolimnion of a stratified lake. Can J Fish Aquat Sci 52:1183–9.

Naiman RJ, Décamps H. 1997. The ecology of interfaces: Riparian zones. Annu Rev Ecol Syst 28:621–58.

Naiman RJ, Sedell JR. 1980. Relationships between metabolic parameters and stream order in Oregon. Can J Fish Aquat Sci 37:834–47.

Nathan RJ, McMahon TA. 1990. Evaluation of automated techniques for base flow and recession analyses. Water Resour Res 26:1465–73.

Nemergut DR, Schmidt SK, Fukami T, O'Neill SP, Bilinski TM, Stanish LF, Knelman JE, Darcy JL, Lynch RC, Wickey P, Ferrenberg S. 2013. Patterns and Processes of Microbial Community Assembly. Microbiol Mol Biol Rev 77:342–56.

Odum EP. 1975. Ecology: Modern Biology Series.

Odum EP. 1984. The Mesocosm. Bioscience 34:558–62.

Odum HT. 1956a. Efficiencies, Size of Organisms, and Community Structure. Ecology 37:592–7.

Odum HT. 1956b. Primary Production in Flowing Waters. Limnol Oceanogr 1:102–17.

Odum HT. 1957a. Primary Production Measurements in Eleven Florida Springs and a Marine Turtle- Grass Community. Limnol Oceanogr 2:85–97.

Odum HT. 1957b. Trophic Structure and Productivity of Silver Springs. Ecol Monogr 27:55–112.

Oviatt CA, Rudnick DT, Keller AA, Sampou PA, Almquist GT. 1986. A comparision of system (O2 and CO2) and C-14 measurements of metabolism in estuarine mesocosms. Mar Ecol Prog Ser 28:57–67.

Peng D, Zhang B, Liu L, Fang H, Chen D, Hu Y, Liu L. 2012. Characteristics and drivers of global NDVI-based FPAR from 1982 to 2006. Global Biogeochem Cycles 26:1–15.

Phlips EJ, Cichra M, Aldridge FJ, Jembeck J, Hendrickson J, Brody R. 2000. Light availability and variations in phytoplankton standing crops in a nutrient-rich blackwater river. Limnol Oceanogr 45:916–29.

Rabinowitch EI. 1945. Photosynthesis and related processes. New York: Interscience Publishers

Raich AJW, Rastetter EB, Melillo JM, Kicklighter DW, Steudler PA, Peterson J, Grace BM, Vörösmarty CJ. 1991. Potential Net Primary Productivity in South America: Application of a Global Model. Ecol Appl 1:399–429.

Raymond PA, Zappa CJ, Butman D, Bott TL, Potter J, Mulholland P, Laursen AE, McDowell WH, Newbold D. 2012. Scaling the gas transfer velocity and hydraulic geometry in streams and small rivers. Limnol Oceanogr Fluids Environ 2:41–53.

Reijo CJ, Hensley RT, Cohen MJ. 2018. Isolating stream metabolism and nitrate processing at point-scales, and controls on heterogeneity. Freshw Sci 37:0.

Rich PH. 1975. Benthic metabolism of a soft-water lake. Int Vereinigung für Theor und Angew Limnol Verhandlungen 19.

Richardson DC, Newbold JD, Aufdenkampe AK, Taylor PG, Kaplan LA. 2013. Measuring heterotrophic respiration rates of suspended particulate organic carbon from stream ecosystems. Limnol Oceanogr Methods 11:247–61.

Riley GA. 1944. The carbon metabolism and photosynthetic efficiency of the earth as a whole. Am Sci 32:129–34.

Roberts BJ, Mulholland PJ, Hill WR. 2007. Multiple scales of temporal variability in ecosystem metabolism rates: Results from 2 years of continuous monitoring in a forested headwater stream. Ecosystems 10:588–606.

Robinson C, Serret P, Tilstone G, Teira E, Zubkov M V, Rees AP, Woodward EMS. 2002. Plankton respiration in the Eastern Atlantic Ocean. Deep Res 49:787–813.

Rosemond AD, Mulholland PJ, Brawley SH. 2000. Seasonally shifting limitation of stream periphyton: response of algal populations and assemblage biomass and productivity to variation in light, nutrients, and herbivores. Can J Fish Aquat Sci 57:66–75.

Ruimy A, Saugier B. 1994. Methodology for the estimation of terrestrial net primary production from remotely sensed data data. J Geophys Res 99:5263–83.

Saldarriaga JG, Luxmoore RJ, Calle N, Program T. 1991. Solar Energy Conversion Efficiencies During Succession of a Tropical Rain Forest in Amazonia. J Trop Ecol 7:233–42.

Sand-Jensen K. 1997. Broad-Scale Comparison of Photosynthesis in Terrestrial and Aquatic Plant Communities. Oikos 80:203–8.

Sand-Jensen K, Binzer T, Middelboe AL. 2007. Scaling of photosynthetic production of aquatic macrophytes - A review. Oikos 116:280–94.

Savoy P, Bernhardt E, Kirk L, Cohen MJ, Heffernan JB. *In review*. A seasonally dynamic model of light at the stream surface. Freshwater Science.

Sawall Y, Hochberg EJ. 2018. Diel versus time-integrated (daily) photosynthesis and irradiance relationships of coral reef organisms and communities. PLoS One 13:1–14.

Schwalm CR, Black TA, Amiro BD, Arain MA, Barr AG, Bourque CPA, Dunn AL, Flanagan LB, Giasson MA, Lafleur PM, Margolis HA, McCaughey JH, Orchansky AL, Wofsy SC. 2006. Photosynthetic light use efficiency of three biomes across an east-west continental-scale transect in Canada. Agric For Meteorol 140:269–86.

Scott TM, Means GH, Meegan RP, Means RC, Upchurch SB, Copeland RE, Jones J, Roberts T, Willet A. 2004. Springs of Florida.

Seibert J, Grabs T, Köhler S, Laudon H, Winterdahl M, Bishop K. 2009. Linking soil- and stream-water chemistry based on a Riparian Flow-Concentration Integration Model. Hydrol Earth Syst Sci 13:2287–97.

Siemens J. 2003. The European carbon budget: A gap. Science (80-) 302:1681.

Singsaas EL, Ort DR, DeLucia EH. 2001. Variation in measured values of photosynthetic quantum yield in ecophysiological studies. Oecologia 128:15–23.

Slattery RA, Ort DR. 2015. Photosynthetic energy conversion efficiency: Setting a baseline for gauging future improvements in important food and biofuel crops. Plant Physiol 168:383–92.

Sobek S, Gudasz C, Koehler B, Tranvik LJ, Bastviken D, Morales-Pineda M. 2017. Temperature Dependence of Apparent Respiratory Quotients and Oxygen Penetration Depth in Contrasting Lake Sediments. J Geophys Res Biogeosciences 122:3076–87.

Staehr PA, Testa JM, Kemp WM, Cole JJ, Sand-Jensen K, Smith S V. 2012. The metabolism of aquatic ecosystems: history, applications, and future challenges. Aquat Sci 74:15–29.

Stets EG, Butman D, McDonald CP, Stackpoole SM, DeGrandpre MD, Striegl RG. 2017. Carbonate buffering and metabolic controls on carbon dioxide in rivers. Global Biogeochem Cycles 31:663–77.

Strohmeier S, Knorr KH, Reichert M, Frei S, Fleckenstein JH, Peiffer S, Matzner E. 2013. Concentrations and fluxes of dissolved organic carbon in runoff from a forested catchment: Insights from high frequency measurements. Biogeosciences 10:905–16.

Suwanee River Water Management District. 2007. MFL establishment for the upper Santa Fe River.

Suwanee River Water Management District. 2019. Minimum flows and minimum water levels re-evaluation for the Lower Santa Fe and Ichetucknee Rivers and priority springs - Draft.

Taddei D, Cuet P, Frouin P, Esbelin C, Clavier J. 2008. Low community photosynthetic quotient in coral reef sediments. Comptes Rendus - Biol 331:668–77.

Tank SE, Fellman JB, Hood E, Kritzberg ES. 2018. Beyond respiration: Controls on lateral carbon fluxes across the terrestrial-aquatic interface. Limnol Oceanogr Lett 3:76–88.

Therkildsen MS, Lomstein BA. 1993. Seasonal variation in net benthic C-mineralization in a shallow estuary. 12:131–42.

Thompson CG, Kim RS, Aloe AM, Becker BJ. 2017. Extracting the Variance In flation Factor and Other Multicollinearity Diagnostics from Typical Regression Results. Basic Appl Soc Psych 39:81–90.

Turner DP, Urbanski S, Bremer D, Wofsy SC, Meyers T, Gower ST, Gregory M. 2003. A cross-biome comparison of daily light use efficiency for gross primary production. Glob Chang Biol 9:383–95.

Vannote RL, Minshall GW, Cummins KW, Sedell JR, Cushing CE. 1980. The River Continuum Concept. Can J Fish Aquat Sci 37:130–7.

Vidon P, Allan C, Burns D, Duval TP, Gurwick N, Inamdar S, Lowrance R, Okay J, Scott D, Sebestyen S. 2010. Hot spots and hot moments in riparian zones: Potential for improved water quality management. J Am Water Resour Assoc 46:278–98.

Villamizar SR, Pai H, Butler CA, Harmon TC. 2014. Transverse spatiotemporal variability of lowland river properties and effects on metabolic rate estimates. Water Resour Res 50:482–93.

Wagner R, Boulger R, Oblinger C, Smith B. 2006. Guidelines and standard procedures for continuous water-quality monitors: station operation, record computation, and data reporting.

Ward RC, Robinson M. 1990. Principles of hydrology. 3rd ed. New York, USA: McGraw-Hill Book Company

Wassink EC. 1959. Efficiency of light energy conversion in plant growth. Plant Physiol.

Wetzel RG, Rich PH, Millerf ; M C, Allena HL. 1972. Metabolism of Dissolved and Particulate Detrital Carbon in a Temperate Hard-water Lake. 58:1–106.

Weyer KM, Bush DR, Darzins A, Willson BD. 2010. Theoretical maximum algal oil production. Bioenergy Res 3:204–13.

Whittaker RH, Likens GE. 1973. Primary production: The biosphere and man. Hum Ecol 1:357–69.

Wofsy SC, Goulden ML, Munger JW, Fan SM, Bakwin PS, Daube BC, Bassow SL, Bazzaz FA. 1993. Net exchange of CO2 in a mid-latitude forest. Science (80-) 260:1314–7.

Young RG, Huryn AD. 1996. Interannual variation in discharge controls ecosystem metabolism along a grassland river continuum. Can J Fish Aquat Sci 53:2199–211.

Zhu XG, Long SP, Ort DR. 2008. What is the maximum efficiency with which photosynthesis can convert solar energy into biomass? Curr Opin Biotechnol 19:153–9.

BIOGRAPHICAL SKETCH

Lily Kirk graduated from the University of Florida (B.S in forest resources and conservation), spent a decade teaching environmental education and science and math in public schools (M.A. in curriculum and instruction from Ole Miss), and was delighted to return to Florida to study springs, blackwater rivers, and wetlands. Her dissertation work reaffirmed a love of exploring new ecosystems through fieldwork, but also uncovered a penchant for coding. She really values how the PhD process has taught her how to think. Lily's hardest tasks and greatest accomplishments to date are teaching in the Mississippi Delta, thru-hiking the Appalachian Trail, and becoming a mother.